Improving removal and monitoring of nanoplastics and microplastics in aggregation-based wastewater treatment systems

Sinan Abi Farraj

Department of Chemical Engineering

McGill University, Montreal

December 2023

A thesis submitted to McGill University in partial fulfillment of the requirements of the degree of Master of Science in Chemical Engineering

Preface

In accordance with the “McGill Guidelines for Thesis Preparation”, this thesis is presented in a manuscript-based format. Chapter 1 includes an introduction on the topic discussed in the thesis and Chapter 2 presents a brief overview on the recent literature in the field. Chapters 3 and 4 present two original research manuscripts, while the conclusion and suggestion for future work is included in Chapter 5.

Acknowledgments

I would first like to thank my supervisor Nathalie Tufenkji for her guidance and support throughout my degree. I will always be grateful for all your help, advice, and wisdom that made me a better researcher. I would also like to thank all members of the Biocolloids and Surfaces Laboratory. In particular, I would like to thank Mathieu Lapointe and Rafael Kurusu for their expertise and support that were vital for the completion of this project. I want to also thank Laura Hernandez, Jun-Ray Macairan, Heidi Jahandideh, and Guadalupe Santos that I had the pleasure of collaborating with. I am also grateful to our summer research students Caroline Kouri and Annamaria Zubieta who consistently went above and beyond our expectations. I would like to thank Prof. Benoit Barbeau for welcoming me into his lab and for offering his expertise. To Prof. Kirk Bevan, thank you for your continuous support and encouragement.

In addition, I would like to acknowledge McGill University (Faculty of Engineering, Graduate Excellence Fellowships) and the Natural Science and Engineering Research Council of Canada (PURE CREATE program, NSERC Strategic and Discovery programs) for their generous funding.

Lastly, I would like to thank my family for their love, understanding, and unwavering support through all the challenges and achievements.

Abstract

Over the past decade, concerns have emerged over the accumulation of plastic contaminants in water bodies and their potential impact on aquatic life. Although wastewater treatment plants were determined to be significant pathways for the release of microplastics and nanoplastics into the environment, these treatment plants can also serve as vital barriers to prevent the discharge of these contaminants into water bodies. Earlier studies have demonstrated that coagulation, flocculation and settling lead to high removal of nanoplastics and microplastics. However, researchers have been unable to validate these laboratory observations in large-scale primary wastewater treatment systems due to limitations of current analytical techniques in measuring nano and micro-sized plastic contaminants. Furthermore, the precise mechanism(s) behind the removal of nanoplastics and microplastics during this process remains unknown. This thesis aims to introduce innovative methods for monitoring and enhancing the removal of nanoplastics and microplastics during chemically enhanced primary wastewater treatment systems. By understanding the mechanisms driving the collisions of nanoplastics during aggregation-based wastewater treatment, a novel correlation was established between the removal of nanoplastics and total suspended solids (TSS). The established correlation was able to predict nanoplastic removal with high accuracy (R^2= 0.92) for 117 individual nanoplastic measurements removed during physicochemical, activated sludge, and aerated lagoon treatment conditions. To evaluate the correlation, various types of nanoplastics with different plastic compositions, functionalizations, concentrations, and aging histories were tested in eight distinct water types including four synthetic wastewater and four municipal wastewater samples. The feasibility of employing TSS as a metric for microsphere, microfiber and microfragments contaminant removal was also tested. Since TSS is an established indicator in the field, this correlation allows municipal treatment plants to employ existing metrics to estimate the release of plastic contaminants to the environment. Based on our correlation, the

predicted nanoplastic removal for typical water treatment effluent streams in North America was estimated to fall between 39-69% for wastewater treatment plants using conventional coagulant (alum) and flocculant (anionic polyacrylamide). Although alum showed high removal of polystyrene nanoplastics (76 ± 3%) and polyester microfibers (97 ± 1%) at pH 7, water conditions with higher pH are known to impact alum's coagulation performance. Our study assessed whether plastic contaminant removal can be improved in these challenging pH conditions using alternative coagulants including aluminum chlorohydrate (ACH) and cationic polyamines (pDADMAC). Our work revealed that ACH coagulant was able to improve polyester microfiber removal from 85 ± 3% when alum was used to 95 ± 1%. At pH 8.2, replacing alum with ACH+pDADMAC coagulant improved polystyrene nanoplastics removal from 5.8% to 71 ± 5%. Quartz crystal microbalance with dissipation (QCM-D) measurements revealed the mechanisms of attachment of the three aluminum-based coagulants on a silica sensor. Frequency and dissipation shift measurements showed that ACH and ACH+pDADMAC resulted in a faster deposition rate and formed a more rigid layer compared to alum on the surface of the negatively charged model contaminant. Overall, this work established a novel metric to track nanoplastic and microplastic removal, explored alternative coagulants to improve the removal of these contaminants, and enhanced the understanding of coagulant interactions with plastic contaminants in aggregation-based wastewater systems.

Résumé

Au cours de la dernière décennie, l'accumulation des contaminants plastiques dans les masses d'eau ont suscité des inquiétudes sur leur impact potentiel sur la vie aquatique. Bien que les stations d'épuration constituaient des moyens importants pour la libération des microplastiques et des nanoplastiques dans l'environnement, ces stations d'épuration peuvent également servir de barrières vitales pour empêcher le déversement de ces contaminants dans les masses d'eau. Des études antérieures ont démontré que la coagulation, la floculation et la décantation permettaient d'éliminer une grande partie des nanoplastiques et des microplastiques. Toutefois, les chercheurs n'ont pas été en mesure de valider ces observations expérimentales dans les systèmes de traitement primaire des eaux usées à grande échelle, car il n'y avait pas des techniques analytiques pour mesurer les contaminants plastiques des tailles nano et micro. En outre, les mécanismes précis derrière l'élimination des nanoplastiques et des microplastiques au cours de ce processus restent inconnus. Cette thèse vise à introduire des méthodes innovantes pour surveiller et améliorer l'élimination des nanoplastiques et des microplastiques dans les systèmes de traitement primaire des eaux usées. En comprenant les mécanismes à l'origine des collisions des nanoplastiques pendant le traitement des eaux usées par agrégation, une nouvelle corrélation a été établie entre l'élimination des nanoplastiques et la concentration des matières en suspension (MES). La corrélation établie a permis de prédire l'élimination des nanoplastiques avec une grande précision (R^2= 0.92) pour 117 mesures individuelles de nanoplastiques éliminés dans les conditions de traitement physico-chimique, par boues activées et par lagunage aéré. Pour évaluer la corrélation, divers types de nanoplastiques avec des compositions plastiques, des fonctionnalisations, des concentrations et des historiques de vieillissement différents ont été testés dans huit types d'eau distincts, dont quatre échantillons d'eaux usées synthétiques et quatre échantillons d'eaux usées municipales. La faisabilité de l'utilisation des MES comme mesure de l'élimination des contaminants des microsphères, des

microfibres et des microfragments a également été testée. Cette corrélation permet aux stations d'épuration municipales d'utiliser des mesures existantes pour estimer le rejet des contaminants plastiques dans l'environnement. Sur la base de notre corrélation, l'élimination prévue des nanoplastiques pour les flux d'effluents de traitement de l'eau typiques en Amérique du Nord a été estimée entre 39 et 70 % pour les usines de traitement des eaux usées utilisant un coagulant conventionnel (alun) et un floculant (polyacrylamide anionique). Bien que l'alun ait montré une forte élimination des nanoplastiques en polystyrène (76 ± 3 %) et des microfibres de polyester (97 ± 1 %) à un pH de 7, les conditions de l'eau avec un pH plus élevé sont connues pour avoir un impact sur la performance de coagulation de l'alun. Notre étude a évalué si l'élimination des contaminants plastiques pouvait être améliorée dans ces conditions de pH difficiles en utilisant des coagulants alternatifs, notamment le chlorhydrate d'aluminium (CHA) et les polyamines cationiques (pDADMAC). Nos travaux ont révélé que le coagulant CHA était capable d'améliorer l'élimination des microfibres de polyester de 85 ± 3 % lorsque l'alun était utilisé à 95 ± 1 %. Au pH de 8.2, le remplacement de l'alun par le coagulant CHA+pDADMAC a permis d'augmenter l'élimination des nanoplastiques de polystyrène de 5.8 % à 71 ± 5 %. Les résultats de mesure de microbalance ý quartz avec dissipation ont révélé les mécanismes de fixation des trois coagulants à base d'aluminium sur un capteur en silice. Les résultats de mesure de fréquence et de déplacement de la dissipation ont montré que le CHA et le CHA+pDADMAC entraînaient une vitesse de dépôt plus rapide et formaient une couche plus rigide que l'alun à la surface du contaminant. Dans l'ensemble, ce travail a permis d'établir une nouvelle méthode pour suivre l'élimination des nanoplastiques et des microplastiques, d'explorer d'autres coagulants pour améliorer l'élimination de ces contaminants et d'améliorer la compréhension des interactions entre les coagulants et les contaminants plastiques dans les systèmes d'assainissement à base d'agrégats.

Table of Contents

List of Figures

List of Tables

Chapter 1: Introduction

1.1 Motivations for research

The presence of plastic waste in water bodies has raised global concern over the last few decades. Due to various environmental stressors, larger plastic waste can fragment into smaller fractions, such as microplastics[1-4] and nanoparticles[5,6] that have potential adverse effects to aquatic biota. Wastewater treatment plants present an ideal opportunity to limit the release of micro- and nanoplastics into the aquatic environment. In particular, researchers have investigated the removal of these plastic contaminants during coagulation/flocculation/settling, which is considered to be the most common primary treatment process found in wastewater treatment plants.[7] Although these studies have reported promising removal of microplastics and nanoplastics in laboratory settings through jar test experiments, it remains difficult to rely on these findings to accurately assess the performance of large-scale primary wastewater treatment systems.

Most researchers tested water samples spiked with pristine microplastics and nanoplastics despite the known impact of environmental weathering on plastic properties. Microplastics and nanoplastics from primary origin are estimated to only represent between 15 and 31% of plastics in the environment.[8] Therefore, a majority of microplastics and nanoplastics are produced through degradation processes such as photooxidation, chemical oxidation, and biodegradation.[1,9-11] A recent review by Alimi et al.[5] revealed that only ~10% of published literature studying microplastics used weathered particles with 90% of these studies showing a significant difference in results between weathered and pristine microplastics. This discrepancy calls into question the environmental relevance of particle removal measurements obtained using pristine microplastics. Similarly, weathering protocols for nanoplastics in coagulation jar

tests are even more scarce due to challenges in measuring the concentrations of these small particles and separating the nanoplastics from background matrices.[12]

Microplastics and nanoplastics can interact with natural colloids, natural organic matter, and other chemicals while being transported to wastewater treatment plants resulting in a noticeable impact in their transport and surface interactions.[5] However, a significant number of studies were performed using oversimplified deionized water spiked with humic acid as a substitute for natural organic matter in the synthetic water.[13-15] Likewise, coagulation experiments that measured nanoplastic removal were conducted in pure deionized water matrices.[16,17] This type of experiment discounts interactions that may occur between contaminants in the water streams (such as natural colloids, NOM, biofilms) and microplastics prior to the coagulation process.

In addition, technical and economic restrictions of analytical tools prevent the continuous monitoring of micro-[18,19] and nanoplastics.[20] These challenges ultimately prevent wastewater treatment operators from assessing the performance of their local treatment process in removing plastic contaminants. Research in the field of wastewater treatment should consider methods to validate their experimentally determined contaminant removals in large-scale primary treatment systems.

Therefore, a knowledge gap in the research area of micro- and nanoplastic removal in aggregation-based treatment systems still exists regarding the monitoring and understanding of their removal in environmentally relevant systems. This study will first target understanding the underlying mechanism of nanoplastics and microplastics removal during primary treatment systems. Second, the removal of nanoplastics and microplastics will be assessed using alternative aluminum-based coagulants that offer enhanced treatment performance.

1.2 Research objectives

1. To investigate the flocculation mechanism governing nanoplastic and microplastic removal during physiochemical treatment including physicochemical, activated sludge, and aerated lagoons treatment processes.
2. To identify a metric that estimates nanoplastic and microplastic removal in physicochemical treatment systems based on the identified flocculation mechanism.
3. To compare the nanoplastic, microplastic, and phosphorus removal performance of conventional coagulants (alum) and flocculants (polyacrylamide polymers) used in wastewater treatment with two alternative commercial coagulants (aluminum chlorohydrate coagulants).
4. To characterize the interactions of selected conventional and alternative coagulants with model surfaces using quartz crystal microbalance with dissipation monitoring (QCM-D).

1.3 Thesis organization

- Chapter 2 provides a brief literature review of microplastics and nanoplastics, their sources, fate, and detection methods. An overview is provided on the current state of research for the removal of microplastics and nanoplastics during coagulation, flocculation, and settling process.
- In Chapter 3, we show that total suspended solids (TSS) removal can be used as an inexpensive and rapid indicator to quantify nanoplastic removal in the aggregation-based wastewater treatment process. The correlation between TSS removal and nanoplastic removal was first established through principles of flocculation kinetics and validated for 41 different wastewater treatment conditions including jar test experiments in synthetic wastewater, municipal wastewater, activated sludge-treated

water samples, and aerated lagoon water samples. The correlation equation established was able to accurately model the removal of nanoplastics (R^2=0.92; n=117) using conventional coagulant (alum) and flocculant (anionic polyacrylamide). TSS was also investigated as a potential indicator for microsphere, microfiber, and microfragment removal. The result of our work offers the potential for estimating removal of nanoplastic contaminants in conventional wastewater treatment plants.

- In Chapter 4, the removal of plastic contaminants using alternative coagulants, including aluminum chlorohydrate (ACH) and cationic polyamines (pDADMAC), was compared to the removal using conventional coagulant (alum). Jar test experiments were performed with synthetic wastewater spiked with polyester (PEST, length: 160–1500 μm) microfibers and carboxylate-modified polystyrene (PS, diameter: 28 nm). The results revealed improved microfiber and nanoplastic removal for coagulants containing highly cationic species. The addition of cationic polyamines to ACH coagulant resulted in a greater removal of nanoplastics after settling (30 s): 10% for alum alone, 52% for ACH, and 68% ACH+pDADMAC (pH 7.5–8.5). Meanwhile, ACH resulted in a greater microfiber removal compared to alum (94% versus 87% respectively) at pH values greater than 8. A comparison between pristine nanoplastics and nanoplastics incubated in synthetic wastewater revealed that the aging process led to improved removal of particles with alum at pH 7. A quartz crystal microbalance with dissipation monitoring was used to elucidate the surface interactions of the coagulants with plastic surfaces.

1.4 Contribution of the Authors

This thesis contains two manuscripts and the original contributions of the authors are included below.

1. “Targeting nanoplastic and microplastic removal in treated wastewater with a simple indicator”, *Nature Water* (accepted on November 29th, 2023)

Authors: Sinan Abi Farraj†, Mathieu Lapointe†, Rafael S. Kurusu, Zhen Liu, Benoit Barbeau, and Nathalie Tufenkji

†S. Abi Farraj and M. Lapointe are co-first authors

Contributions: S.A.F, M.L., and N.T. conceived and designed the project and prepared the manuscript. S.A.F., M.L. and R.K. performed the experiments with synthetic wastewater. S.A.F., Z.L., and B.B. sourced the municipal wastewater influents, activated sludge-treated samples, and aerated lagoon water samples and performed the relevant experiments. M.L. designed and constructed the reactor for pilot scale experiments. M.L. initiated the concept of the correlation between nanoplastics and TSS removal. S.A.F. derived the mathematical model and designed the modeling approach and visual elements of the paper.

2. “Microplastics and nanoplastics in water: Improving removal performance in wastewater treatment plants with alternative coagulants”, to be submitted to *Environmental Science & Technology Water*

Authors: Sinan Abi Farraj, Mathieu Lapointe, Rafael S. Kurusu, and Nathalie Tufenkji

Contributions: S.A.F, M.L., and N.T. conceived and designed the project and prepared the manuscript. S.A.F. performed experimental work and created all computational codes to analyze data and generate figures. R.K. assisted in nanoplastic concentration measurements and SEM imaging. S.A.F. performed QCM-D data acquisition and experimental preparation. M.L. and N.T. assisted with QCM-D data analysis. N.T. supervised the project and edited the manuscript.

Chapter 2: Literature review

2.1 Microplastic and nanoplastic origin

Microplastics can be broadly distinguished as primary and secondary microplastics. Primary microplastics refers to plastics that are industrially manufactured as particles smaller than ~ 5 mm in size but larger than ~ 1 micrometer in size. These types of microplastics are commonly found as microbeads and nurdles in personal care products, exfoliants, or sand-blast materials, and fragments from washing synthetic textile fibers.[2,8] On the other hand, secondary microplastics are generated from the degradation of plastic products in the environment and are considered the most abundant type of microplastics representing roughly 69-85% by weight of plastics in the environment.[8] The degradation process to form microplastics was observed to occur through photooxidation by UV light, mechanical fracture, or biological degradation.[21,22] An important degradation process for polyurethane and polyethylene terephthalate (PET) was hydrolysis reactions of plastics in water bodies.[21] However, the dominant mechanism that results in rapid degradation of plastics to microplastics in the environment was found to be UV light exposure.[23]

Similarly, nanoplastics can be classified as primary and secondary nanoplastics. Direct release of nanoplastics has been observed from products such as waterborne paints, adhesives, coatings, electronics, and 3D printing.[24] Secondary nanoplastics are produced from the degradation of macro- and microplastics due to environmental weathering.[6] Laboratory experiments have shown that nanoplastics can be produced following steeping of plastic teabags,[25] washing of synthetic textiles,[26] degradation of facial scrubs,[27] and the mechanical degradation of polystyrene disposable coffee cup lid.[28]

2.2 Microplastic and nanoplastic presence in water bodies

The presence of microplastics in marine and freshwater is a result of discharge from urban runoff, soil erosion and runoff, air settling, or effluent discharge from wastewater treatment plants.[3,8,29] From these sources, wastewater treatment plants were seen as a major pathway for microplastics. Recent studies have estimated that one wastewater treatment plant in Lower Saxony, Germany releases approximately 9×10^7 to 4×10^9 microplastics and microfibers per day,[30] while one wastewater treatment plant in Turkey was found to release 2.9×10^7 microplastic particles per day.[31] Additional studies reported the release of microplastics from over 17 wastewater treatment plants across the United States had a daily release of 5×10^3 to 1.5×10^7 microplastics.[32] In Canada, a wastewater treatment plant in Vancouver and a plant in Saskatoon were estimated to release 8.4×10^8 and 1.41×10^8 microplastics per day, respectively.[33,34] A report by the International Union for Conservation of Nature[8] calculated that approximately 37% of primary microplastics and microfibers from synthetic textiles released into the world oceans are being transported along wastewater effluent streams. This finding reveals the importance of wastewater treatment plants as a pathway for microplastic release. In addition, the extensive pumping and turbulence of water flow in water treatment plants results in high shear forces that can further degrade plastics into micro- and nanoplastics.[29,35] The turbulence experienced by mixing and pumping in wastewater treatment plants resulted in the breakdown of microplastics into nanoplastics less than 10 nm in size through crack propagation.[36] This shows that wastewater treatment plants are not merely pathways for microplastics and nanoplastics, but can potentially also be sources of these plastic contaminants.

2.3 Microplastic and nanoplastic removal in wastewater treatment plants

With the large quantity of microplastic and potential nanoplastic contaminants released by effluent streams in wastewater treatment plants, it is imperative to assess the current ability of these plants to remove microplastics and nanoplastics. Conventional wastewater treatment processes commonly include a pretreatment, primary, secondary, and tertiary treatment.[7]

A recent review by Liu et al.[37] analyzed 23 publications of microplastic removal in global wastewater treatment plants for a meta-analysis study on the removal efficiency of primary, secondary, and tertiary treatment processes. The analysis revealed that primary treatment processes through settling tanks can remove microplastics anywhere between 4-99%, while secondary treatment plants can result in microplastic removal between 20-95%. On average, the microplastic removal efficiency was estimated to be around 86% based on available published literature with final effluents showing a microplastic removal range between 50-100%.[37] The results of this study revealed that filter-based technologies resulted in the highest efficiency in removing microplastics followed by primary settling treatment (coagulation-flocculation-settling). On the other hand, advanced oxidation processes, particularly UV irradiation, resulted in a negative removal of microplastics due to the degradation of microplastics during the oxidation process.[29]

Although filtration methods, specifically through ultrafiltration membranes, have proven to result in almost complete removal of microplastics,[14] challenges remain for this treatment method. Filtration membranes are susceptible to fouling during operation as solutes and particulates adsorb on the membrane surface.[7] A study by Enfrin et al.[38] found that during a filtration process with a commercial ultrafiltration poly(sulfone) membrane, microplastics and nanoplastics adsorbed onto the surface resulting in a reduction of water flux by 38%. Meanwhile, primary settling tanks were seen to have total microplastic removal comparable to

filter membranes and resulted in the highest removal of microfibers and large microplastics with sizes between 0.5-5 mm.[37] Since primary settling tanks are the most common primary treatment process found in wastewater treatment plants,[7] coagulation, flocculation and settling process present an ideal treatment process to increase the removal of microplastics and nanoplastics.

2.4 Coagulation, flocculation, and settling process

Coagulation is commonly used in primary treatment as it serves as an effective primary treatment step, but can also be found in secondary treatment integrated with biological reactors.[39] This treatment process relies on adding chemicals into the water stream to promote the removal of suspended particles and phosphorus.[40] The mostly negative charges on these suspended particles, colloids, and natural organic material (NOM) causes a repulsive force between these contaminants preventing them from forming larger colloids that settle from the solution.[40] During coagulation, chemicals, known as coagulants, are added to promote the destabilization of these particles under rapid mixing conditions which results in the formation of aggregates. The coagulant acts through two mechanisms: first, species in the coagulant that are positively charged will adsorb on the negatively charged particles and reduce the charge repulsion between the particles. Second, coagulant species can precipitate from the wastewater stream leading to the enmeshment of colloids in the solid or amorphous precipitate formed due to the limited solubility of the coagulant in solution.[41] Third, coagulant species can remove phosphorus from solution by direct adsorption or (co)precipitation that form phosphorus precipitates that are settle out of suspension.[42] The most common coagulants used in industry include aluminum sulfate (alum), polyaluminum chloride (PAC), aluminum chlorohydrate (ACH), and ferric chloride.[41] Following coagulation, flocculation is required where a high molecular weight polymer (most commonly polyacrylamide) is added to aggregate the destabilized colloids and particles forming larger aggregates, referred to as flocs. The large size

of these flocs ensures rapid settling during the sedimentation stage.[43] The choice of coagulant and flocculant type depends on the water conditions and the contaminants to be removed.[7]

Experimental studies have employed jar tests that mimic the conditions of coagulation process in laboratory environments to reveal the effect of several parameters such as coagulant type and dose, microplastic type, size and shape, weathering conditions, and water pH on the removal of microplastics and nanoplastics during coagulation.[13-15,44,45] Although jar tests do not represent the conditions of full treatment plants, Desjardins et al. only found a 7% difference between results obtained from jar test procedures and full-scale plants.[46]

2.5 Microplastic removal during coagulation and flocculation

A summary of the major findings of microplastic removal from laboratory jar test experiments are included in Table 1. These experiments revealed a relationship between microplastic removal and microplastic size. Using $FeCl_3$ as a coagulant, the experimental study by Ma et al. showed that polyethylene microplastic removal increased with smaller microplastic sizes.[13] This finding was further supported by findings from Lapointe et al. where polyethylene microspheres 15 μm in diameter showed higher removal than larger 140 μm microspheres when using alum as a coagulant.[45] The effect of size on polyethylene microplastic removal was further validated by Zhou et al.[47] revealing that polyethylene microplastics were predominantly removed due to their incorporation into the flocs, highlighting the importance of floc size in the removal of large polyethylene microplastics. In the study by Lapointe et al., reducing the floc size by lowering the dose of flocculant resulted in a significant decrease in the removal of 140 μm microspheres, whereas the 15 μm microspheres were not affected. The role of floc size and morphology in microplastic removal can be seen in the effect played by the flocculant during coagulant.[45] Ma et al. showed that adding anionic polyacrylamide (PAM) to the coagulation process of $FeCl_3$ led to an increase of polyethylene removal from 13% to 91%.[13]

With the addition of anionic PAM, the loosely formed flocs produced during coagulation with $FeCl_3$ became much denser. Similar improvement was observed with PAM addition to $AlCl_3$ coagulation procedure.[14] In contrast, Zhou et al. showed that polystyrene microplastic exhibited better removal at larger size ranges (500-5000 μm) compared to smaller sizes (<500 μm).[47] This improved removal at larger size was attributed to the ability of larger polystyrene microplastics to overcome the surface tension during settling as well as the suggested chemisorption occurring between polystyrene microplastics and the $FeCl_3$ and polyaluminum chloride (PAC) species during coagulation. In addition, Zhang et al. observed that poly(ethylene terephthalate) (PET) microplastics between 100-400 μm had better removal than sizes below 100 μm when using PAC as a coagulant.[44]

The effect of the microplastic shape on total removal was examined by Shahi et al. on PET microplastics.[15] The elongated microplastics resulted in improved removal compared to spherical microplastics at all coagulant doses. This enhanced removal was attributed to the increased surface area of elongated microplastics that increases the likelihood that the microplastic is incorporated into the floc during settling. Lapointe et al. also found that polyester microfibers showed higher removal compared to polystyrene and polyethylene microspheres which was partly attributed to their elongated shape.[45]

The type of coagulant and the coagulation pH was also shown to impact microplastic removal. Ma et al. showed that increasing the pH from 6 to 8 increased the removal of polyethylene microplastics (<500 μm) using $FeCl_3$ coagulant.[13] This increase in microplastic removal was associated with the increase in floc sizes at higher pH values. On the other hand, microplastic removal decreased with $AlCl_3$ coagulant from pH 6 to 8 due to the formation of $Al(OH)_4^-$ species and the decrease of amorphous $Al(OH)_3$ precipitation at high pH.[14] These factors lead to a loss in effective charge neutralization and sweep flocculation for the coagulant and thus a

reduction in the removal of negatively charged microplastics.[14] On the other hand, polyaluminum coagulants such as aluminum chlorohydrate (ACH) and polyaluminum chloride (PAC) contain prehydrolyzed highly cationic aluminum species, Al_{13}^{7+}, that have high charge neutralization capability and stability in alkaline conditions.[48] Zhou et al observed a higher removal for both polyethylene and polystyrene microplastics (<500 μm) when using PAC as opposed to $FeCl_3$.[47] This improved microplastic removal is due to the strong positive charge of polyaluminum species. In contrast to $AlCl_3$, PAC maintained similar polystyrene and polyethylene removal with an initial pH of 9, showing the stability of the polyaluminum species at higher pH values.

Therefore, current literature has shown that the conditions of microplastic size, type and shape as well as coagulant and flocculant type influence microplastic removal during coagulation. Microplastic removal was observed to be significantly affected by the final floc size and morphology, which suggests that the dominant removal mechanism of microplastics is through sweep flocculation. Therefore, the selection of flocculant during flocculation, which has a major effect on floc size, is an important parameter to control during microplastic removal. In addition, the conventional mononuclear coagulants such as $FeCl_3$, $AlCl_3$ and alum showed a large decrease in microplastic removal in alkaline conditions due to ineffective coagulation. Polynuclear coagulants such as PAC and ACH that showed better stability at higher pH values also exhibited larger microplastic removal.

Table 2.1. Summary of key findings of microplastic removal through experimental jar tests.

Reference	Microplastic Type	Morphology	Water	Removal Measurement	Size	Coagulant	Flocculant	pH	Removal %
Ma et al. [13]	Polyethylene	Mechanically disintegrated from larger particles	DI with HA (2g/L)	Weighing method	< 500 µm	$FeCl_3 \cdot 6H_2O$ (2 mmol/L)	N/A	6 7 8	11.6% ± 1.0% 13.3% ± 2.2% 17.2% ± 1.7%
Ma et al. [14]	Polyethylene	Mechanically disintegrated from larger particles	DI with HA (2g/L)	Weighing method	< 500 µm	$AlCl_3 \cdot 6H2O$ (5 mmol/L)	N/A	6 7 8	27.5% ± 0.9% 25.8 ± 2.9% 22.2 ± 1.7%
Zhang et al. [44]	Polyethylene terephthalate (PET)	PET crushed and sieved into fragments	DI water with ions (Cl^-, SO_4^{2-}, HCO_3^-) and HA	Weighing method	100-400 µm	PAC (20 mg/L)	PAM (100 mg/L)	7	79.3%
Shahi et al. [15]	Polyethylene	Spherical Elongated	DI with HA and Kaolin	Nile red staining of microplastic	10-100 µm	Alum (30 mg/L)	Cationic polyamine	7	66.7% (spherical) 81.8% (elongated)
Lapointe et al. [45]	Polyester	Microspheres	Surface water from Pont-Viau drinking water treatment plant	Stereo-microscope counting (Fluorescent)	15 µm 140 µm	Alum (2.73 mg Al/L)	PAM (0.3 mg/L)	7	89% (15 µm) 82% (140 µm)
		Weathered microspheres		Stereo-microscope counting (Fluorescent)	140 µm	Alum (0.45 mg Al/L)	PAM (0.3 mg/L)	7 8	89% 69%

		Weathered microspheres	Surface water from Pont-Viau drinking water treatment plant	Stereo-microscope counting (Fluorescent)	140 µm	ACH (0.45 mg Al/L)	PAM (0.3 mg/L)	78	93% 85%
	Polystyrene	Microspheres		Stereo-microscope counting (Fluorescent)	140 µm	Alum (2.73 mg Al/L)	PAM (0.3 mg/L)	7	84%
	Polyester	Fibers (polyester textile blended and sieved)		Stereo-microscope counting	Width: 12-16 µm Length: 105-1325 µm				99%
Zhou et al. [47]	Polystyrene	Crushed microplastics	DI water with ions (Cl^-, SO_4^{2-} and CO_3^{2-})	Weighing method	< 500 µm	PAC (60 mg/L)	N/A	79	75.5% 81.0%
						$FeCl_3$ (60 mg/L)		79	62.5% 64.6%
	Polyethylene	Crushed microplastics		Weighing method	< 500 µm	PAC (90 mg/L)		79	29.7% 30.7%
						$FeCl_3$ (90 mg/L)		79	16.5% 20.3%

2.6 Nanoplastic removal during coagulation and flocculation

Several experimental studies on nanoplastic removal through coagulation and settling have emerged in the last few years as summarized in Table 2.[16,17,49,50] The removal of carboxylate-functionalized polystyrene nanoplastics (50 nm) through coagulation methods was measured by Gong et al.[49] For a sample with 50 mg/L of polystyrene nanoplastics, Gong et al. were able to achieve more than 95% removal using $AlCl_3$, $FeCl_3$, and PACl coagulants at a concentration of 10 mg/L.[49] The effect of pH on nanoplastic removal with $AlCl_3$ showed a similar trend to that observed for microplastic removal with mononuclear aluminum coagulants. As the initial pH of the jar test increased from pH 3 to 8.5, nanoplastic removal was shown to increase. This enhanced removal coincided with the increase in the surface charge of the nanoplastic after coagulation which indicates the role of charge neutralization during carboxylate-functionalized polystyrene nanoplastic removal. However, with an initial pH of 10, the zeta potential following $AlCl_3$ coagulation was more negative than that measured at pH 8.5 due to the loss of cationic Al species at high pH. This loss of cationic species resulted in a reduction of nanoplastic removal from 95% to 83%. The relationship between the zeta potential and the nanoplastic removal reveals the importance of charge neutralization for removing negatively charged nanoplastics.

The addition of other contaminant species during coagulation was also seen to affect nanoplastic removal. In the experimental work presented by Gong et al., the coagulation process in filtered surface water resulted in lower polystyrene nanoplastic removal compared to pure deionized (DI) water (90.2% versus 96.6%, respectively).[49] This decrease was attributed to the adsorption of total organic carbon (TOC) with the polystyrene surface thereby preventing the charge neutralization interaction between the coagulant species and the nanoparticles. Furthermore, the addition of positively charged Al_2O_3 particles (20 nm) resulted in 43.3% aggregation of polystyrene nanoplastics without the use of a coagulant compared to

0% aggregation observed with negatively charged SiO_2 (50 nm) addition. Therefore, electrostatic stabilization is seen to play an important role in the removal of negatively charged nanoplastics.

In an effort to study the micro- and nanoplastic removal in a Detroit drinking water treatment plant, Zhang et al. measured the removal of 180 nm non-functionalized polystyrene nanoplastics from raw water collected from the plant.[50] Following a coagulation process using alum (20 ppm) and flocculation with polyDADMAC (0.5 ppm), nanoplastics were not observed in the sludge. This result indicates that the high performance of nanoplastic removal observed in earlier studies was predominantly attributed to charge neutralization since coagulation of non-functionalized polystyrene nanoplastics did not result in any removal while negatively charged polystyrene nanoplastics showed removal above 85%. However, a recent study by Zhang et al. reported that non-functionalized polystyrene nanoparticles with 50, 100, 500 nm showed relatively high removal (>85%) using PAC (400 mg/L) as a coagulant.[17]

Based on the studies above, the nanoplastic removal is shown to depend on the surface properties of the nanoplastics. For nanoplastics with highly negative surfaces, such as carboxyl-functionalized polystyrene nanoplastics, the nanoplastic removal was affected by the presence of highly cationic species during coagulation. On the other hand, neutral nanoplastics required much larger coagulant dose to achieve similar removal. This shows that neutral and charged nanoplastics have different removal mechanisms during coagulation. Further studies are required to elucidate the removal mechanisms of nanoplastics based on changes in surface functionalization and coagulant type.

Table 2.2. Summary of key findings of nanoplastic removal through experimental jar tests.

Reference	Nanoplastic Type and Concentration	Surface	Size	Water	NP Removal Measurement	Coagulant	Flocculant	pH	Removal %
Gong et al. [49]	Polystyrene (PS) 50 mg/L	Carboxyl modified	50 nm	DI water	Total organic carbon analyzer	$AlCl_3 \cdot 6H_2O$ $FeCl_3 \cdot 6H_2O$ PACl	N/A	4.2 4.1 4.4	96.6% 95.8% 95.2%
						$AlCl_3 \cdot 6H_2O$	N/A	6.5* 8.5* 10.5*	96.6% 96.3% 83.4%
				Surface water		$AlCl_3 \cdot 6H_2O$ (10 mg/L)	N/A	6.5*	90.2%
Zhang et al. [50]	Polystyrene (PS) 9500 NP/L	N/A	180 nm	Raw water from Detroit water treatment plant	Fluorescent measurement of captured sediment in filter membrane	Alum (20 ppm)	PolyDADMAC (0.5 ppm)	7.5	0**
Zhang et al. [17]	Polystyrene (PS)	N/A	50 nm 100 nm 500 nm	DI water	Fluorescent measurement	PAC (400 mg/L)	N/A	8	86% 86% 91%

*initial pH (pH before coagulation) reported
**no fluorescence observed in final collected sediment

Chapter 3: Targeting nanoplastic and microplastic removal in treated wastewater with a simple indicator

Abstract

With growing concerns over plastic accumulation in the environment, it is imperative to quantify nanoplastic and microplastic release to water bodies via water treatment plant effluent streams. Current methodological limitations present a major challenge for continuous monitoring of nanosized pollutants in effluent streams. In this work, a novel correlation was established between removal of nanoplastics and total suspended solids (TSS) during aggregation-based wastewater treatment. The established correlation successfully predicted nanoplastic removal for a wide range of relevant nanoplastic properties, including polymer type, size, surface functionalization, and aging history, under 41 different physicochemical and activated sludge treatment conditions (R^2=0.92; n=117). The results of our correlation reveal a predicted nanoplastic removal between 39 – 69 % for typical water treatment effluent streams governed by current TSS regulations in North America. The study also reveals the potential of using TSS as a simple metric to estimate microfiber, microsphere, and microfragment removal.

3.1 Main Text

Understanding the fate of nanoplastics and microplastics in aquatic environments is a subject of increasing importance due to the potential adverse effects associated with these contaminants of emerging concern[1,2]. Municipal wastewater effluents are an important source of plastic in natural waters[3] and the extensive mixing/pumping and the addition of oxidants (e.g., ozone) in the treatment process can further fragment microplastics into nanoplastics[4]. Wastewater treatment plants have been identified as an opportune barrier to reduce plastic-based anthropogenic stressors before they enter the aquatic environment[3-5]. In particular, aggregation processes that occur through a physicochemical treatment followed by settling can lead to high removal of nanoplastic. Gong et al.[6] achieved more than 95% removal of carboxylated polystyrene nanoplastics (50 nm) using $AlCl_3$, $FeCl_3$, and polyaluminum chloride as coagulants following a 30 min settling time. Similarly, high removal rates (>85%) were reported for non-functionalized polystyrene nanoparticles (50, 100, 500 nm) using polyaluminum chloride as a coagulant with a settling time of 30 min[7]. Furthermore, the activated sludge process is commonly used for wastewater treatment. Although it has shown only moderate microplastic removal ranging from 41%[8] to 77%[9], there are no studies to date investigating the removal of nanoplastics in this system.

While studies[6,7] reveal that nanoplastics can be effectively removed by conventional coagulation-based treatment, validating nanoplastic removal rates in wastewater treatment plants remains a major challenge due to the methodological difficulties in quantifying nanosized pollutants in effluent streams. Indeed, few studies (~5) reported the detection of nanoplastics in environmental samples.[10]. Although microplastics can be detected in wastewater influent and effluent streams, the complexity of the wastewater matrix and lack of a standardized analytical methodology present challenges in sampling, quantifying, and validating microplastic removal[11,12]. These limitations prevent operators of wastewater

treatment plants from monitoring both nanoplastic and microplastic removal performance and impede the regulation of these contaminants. Therefore, it is imperative to identify simple indicators and metrics for estimating nanoplastic and microplastic removal in wastewater streams.

Total suspended solids (TSS) is an established indicator in a majority of governmental water quality guidelines and standards[13]. The results of our experiments – simulating more than 41 conditions during physicochemical treatment and activated sludge treatment – reveal a correlation between TSS and nanoplastic removal which is independent of coagulant type, plastic size and surface charge, aging of plastics, pH, separation method (settling or screening), and wastewater properties. In addition, TSS was revealed as a potential metric to estimate microfibers and microsphere removal. Our results will provide municipalities with a simple and novel method to estimate the removal of plastic particles through the rapid and routine measurement of TSS.

3.2 Correlation between the removal of nanoplastics and TSS

In a conventional coagulation/flocculation process, metal hydroxides are introduced by the addition of coagulants that interact with negatively charged colloids leading to their destabilization[14]. The addition of flocculants then results in the aggregation of coagulant species and destabilizes colloids to form flocs[15]. The removal of nanoplastics and other particulate contaminants from suspension is therefore attributed to the incorporation of these contaminants into flocs either through attachment or enmeshment. The results of coagulation/flocculation experiments using two coagulants, alum and aluminum chlorohydrate (ACH), reveal a positive relationship between nanoplastic removal and TSS removal for various nanoparticle size, charge and aging conditions (Fig. 3.1a). The relative amounts of cationic Al-species formed by alum addition vary with pH[15], which leads to variations in

contaminant removal[16]. On the other hand, ACH coagulant contains cationic polyaluminum species (e.g., Al_{30}) that are stable at a wider pH range than species formed via alum coagulation[17]. The correlation between nanoplastic and TSS removal using both coagulants can be understood by investigating the mechanisms of contaminant removal during the coagulation and flocculation process.

A major mechanism of contaminant attachment on flocs is fluid shear induced flocculation, also known as orthokinetic flocculation. With this mechanism, the mixing conditions in the coagulation and flocculation stages create large shear forces that lead to particle collisions[18] (Fig. 3.1b). The wide particle size distribution of flocs and rapid mixing conditions during conventional treatment create the required conditions for orthokinetic flocculation to be the dominant removal mechanism for both TSS and nanoplastics as previously noted by O'Melia et al. [18] and quantitatively shown in the SI. The removal of nanoplastic and TSS exhibited a similar trend with increasing flocculation time (Fig. 3.1c). In this work, we propose a novel equation to predict nanoplastic removal based on TSS removal. Assuming that both TSS and nanoplastics are predominantly removed from the solution via orthokinetic flocculation, a relationship between nanoplastic removal (R_{NP}) and TSS removal (R_{TSS}) can be derived (see Fig. S3.1, S3.2 for details) as shown in equation (1):

$$(1 - R_{NP}) = (1 - R_{TSS})^{\frac{\alpha_{NP}}{\alpha_{TSS}}} \quad (1)$$

The relationship is seen to exclusively depend on the ratio of collision efficiencies $\left(\frac{\alpha_{NP}}{\alpha_{TSS}}\right)$ thereby revealing the possibility of using TSS removal as a simple and direct indicator of nanoplastic removal. In the following sections, the correlation relating nanoplastic and TSS removal will be validated for various plastic properties and treatment process conditions.

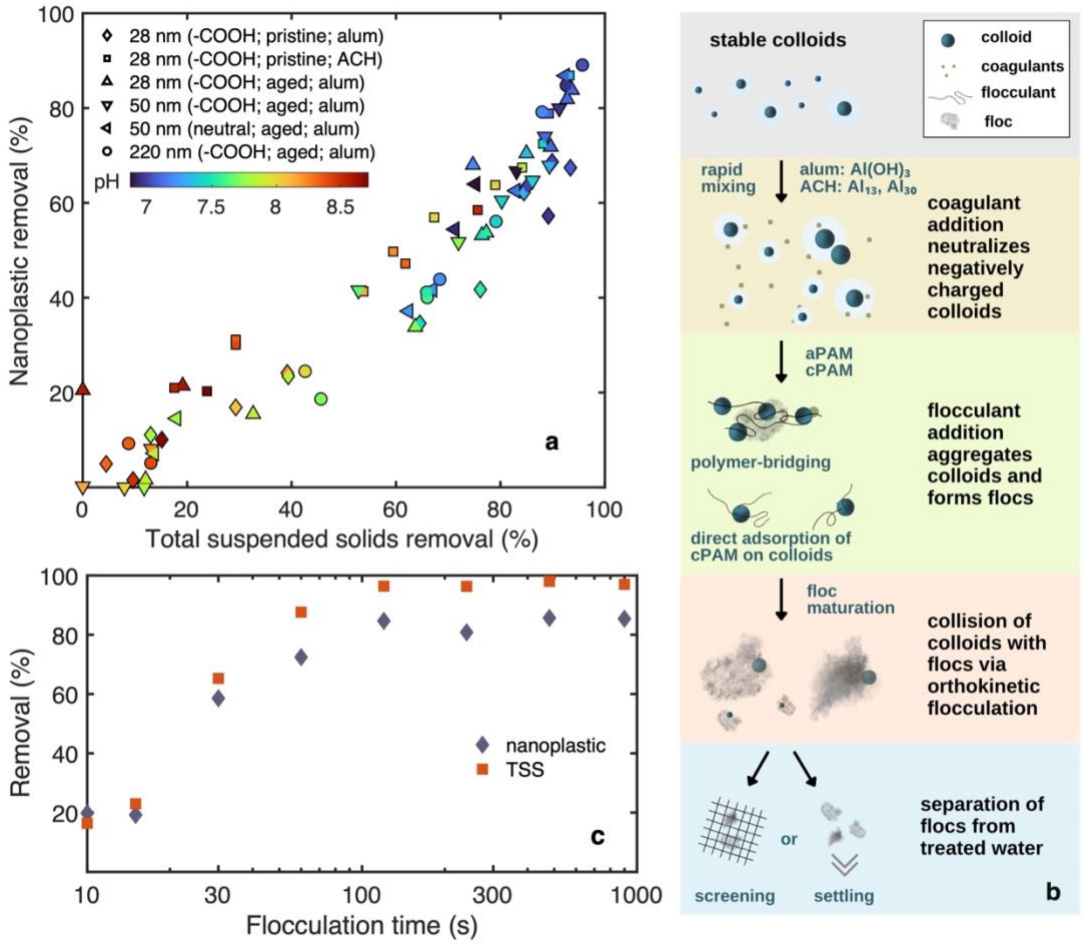

Figure 3.1. Total suspended solids and nanoplastic removal through physicochemical treatment in synthetic wastewater. a, Polystyrene nanoplastic removal as a function of total suspended solids (TSS) removal. Each data point represents a single jar test conducted in synthetic wastewater spiked with polystyrene nanoplastics of varying sizes (28, 50, and 220 nm), aging condition (pristine or aged), functionalization (carboxylate-modified or non-functionalized) and treated with alum or ACH as coagulant (5.45 mg Al/L). Conditions: aPAM1 used as flocculant (0.4 mg/L); 2 min coagulation time; 2 min flocculation time; 30 s of settling; final pH varied between 7.0-8.5; b, Schematic of contaminant destabilization and removal through incorporation in flocs following the addition of coagulants and flocculants; and c, Removal of nanoplastic (diamond) and TSS (square) as a function of flocculation time in synthetic wastewater. Conditions: alum used as coagulant (5.45 mg Al/L); aPAM1 used as flocculant (0.4 mg/L); 2 min coagulation time; 10-900 s flocculation time; 30 s of settling. Legend: aPAM: anionic polyacrylamide, cPAM: cationic polyacrylamide, aPAM1: very low anionic charge density polyacrylamide.

3.3 Validating the correlation in synthetic wastewater

The relationship between nanoplastic and TSS removal was first validated with pristine 28 nm nanoplastics for two coagulant types. Using alum as a coagulant, the nanoplastic removal is well fitted with the proposed eq. 1 (R^2 = 0.97; n=14) using an optimized collision efficiency

ratio of $\frac{\alpha_{NP}}{\alpha_{TSS}}$ = 0.46 as seen in Fig. 3.2a. The relationship between nanoplastic removal and TSS when using ACH as a coagulant also shows a high correlation with R^2= 0.98 ($\frac{\alpha_{NP}}{\alpha_{TSS}}$ = 0.70; n=14) validating the established model for different coagulants. In both cases, the ratios are below 1.0, indicating that nanoplastic removal is lower than TSS removal.

Exploring the effect of nanoplastic properties on the correlation of nanoplastic and TSS removal is critical since the physical and chemical properties of nanoplastics can considerably influence their interactions with coagulants and flocculants. The established relationship between TSS and nanoplastic removal was investigated for nanoplastics that were incubated in synthetic wastewater for 18 h to mimic the interactions occurring with nanoplastics in the sanitary sewer system. Following this incubation period, an eco-corona is expected to form at the surface of aged polystyrene nanoplastics due to adsorption of organic biomolecules[19-21]. The removal of TSS and aged 28 nm nanoplastics is well fitted with the proposed model, resulting in a R^2=0.90 (n=12) (Fig. 3.2b). Moreover, varying the nanoplastic size did not affect the established correlation with the combined removal data of aged 28 nm, 50 nm and 220 nm nanoplastics resulting in a R^2=0.95 ($\frac{\alpha_{NP}}{\alpha_{TSS}}$ = 0.58; n=35). To assess the impact of the particle surface charge on the proposed correlation, a similar aging procedure was conducted for non-functionalized 50 nm polystyrene nanoplastics which is expected to change the nanoplastic interaction with the coagulant and the formation of the eco-corona. The removal of aged non-functionalized nanoplastics followed the same trend as aged carboxylate-modified nanoplastics (Fig. 3.2c). In addition, lowering the initial concentration of 50 nm nanoplastics from 1,400 to 80 µg/L did not affect the relationship resulting in a combined R^2=0.98 ($\frac{\alpha_{NP}}{\alpha_{TSS}}$ = 0.59; n=28). Therefore, the established correlation equation with the optimized collision efficiency ratio describes well the removal of nanoplastics irrespective of size, concentration, or initial surface coating/functionalization. In addition to polystyrene, the removal of non-functionalized

polyvinyl chloride nanoplastics (250 nm) was well captured with the orthokinetic model that showed a combined R^2=0.97 ($\frac{\alpha_{NP}}{\alpha_{TSS}}$ = 0.56; n=12) (Fig. 3.2d). The results reveal that the orthokinetic model can accurately model the removal behavior of nanoplastics beyond polystyrene. Importantly, the collision efficiency ratio for 250 nm non-functionalized polyvinyl chloride nanoplastics ($\frac{\alpha_{PVC-NP}}{\alpha_{TSS}}$ = 0.56; n=12) is similar to that determined for comparably sized 220 nm polystyrene nanoplastics ($\frac{\alpha_{PS-NP}}{\alpha_{TSS}}$ = 0.56; n=11; Fig. S3.3a).

Particle properties (i.e., zeta potential and Hamaker constants) can play an important role in particle-particle interactions and the resulting collision efficiencies in orthokinetic aggregation[22]. However, in this work, the collision efficiency ratio was not significantly impacted by particle surface chemistry (Fig. S3.3b) including varying simulated aging history (aged: $\frac{\alpha_{50\ nm\ PS-COOH}}{\alpha_{TSS}}$ = 0.58; n=12 or pristine: $\frac{\alpha_{50\ nm\ PS-COOH}}{\alpha_{TSS}}$ = 0.58; n=8), initial functionalization (non-functionalized: $\frac{\alpha_{50\ nm\ PS-none}}{\alpha_{TSS}}$ = 0.60; n=8 or carboxylate-modified: $\frac{\alpha_{50\ nm\ PS-COOH}}{\alpha_{TSS}}$ = 0.58; n=12), or plastic type (polyvinyl chloride: $\frac{\alpha_{250\ nm\ PVC}}{\alpha_{TSS}}$ = 0.56; n=12 or polystyrene: $\frac{\alpha_{220\ nm\ PS}}{\alpha_{TSS}}$ = 0.56; n=11). Studies attempting to determine the effect of the surface chemistry on the orthokinetic collision efficiency of unequal sized particles have been limited to mathematical models conducted for relatively simple systems[23-25]. The study by Adler et al. [23] showed that electrostatic forces, that are influenced by surface chemistries, have limited effects during collisions between particles with a large size difference (as is the case with flocs with an average size of 541 µm and nanoplastics with the largest size of 250 nm; nanoplastic/floc size ratio = $5 \cdot 10^{-4}$). In addition, the presence of dissolved organic substances in the wastewater matrix leads to masking of the nanoplastic surface chemistry due to the formation of an eco-corona on the nanoplastic surface[21]. The presence of coagulants and flocculants results in further surface modifications and charge neutralization of the particle

surface charge driving particle destabilization and consequently rapid aggregation[14] despite differences in particle surface chemistry. These factors can result in the predicted collision efficiency ratio not being significantly affected by the nanoplastic surface charge and type as noted above.

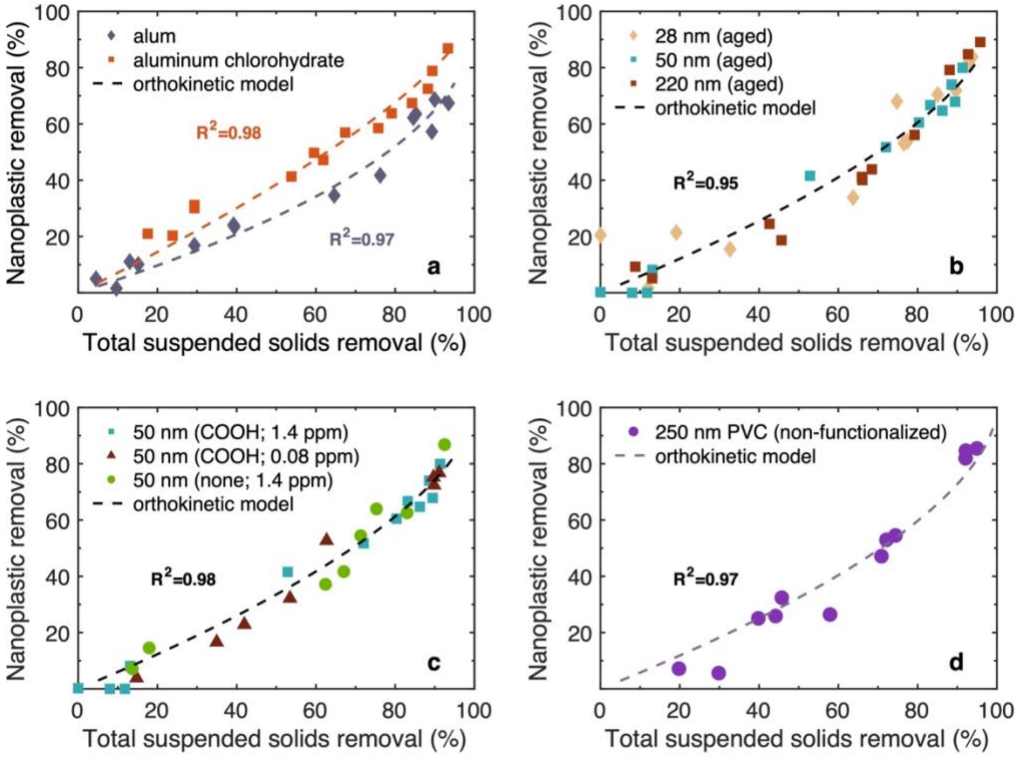

Figure 3.2. Relationship between the removal of nanoplastics and TSS for varying contaminant conditions. a, pristine carboxylate-functionalized 28 nm polystyrene nanoplastics coagulated with alum and ACH (5.45 mg Al/L); b, aged carboxylate-functionalized polystyrene nanoplastics with varying sizes (28 nm; 50 nm; 220 nm); c, aged 50 nm polystyrene nanoplastics with varying surface functionalization (carboxylate- and non-functionalized) and initial concentrations (1.4 and 0.08 ppm); and d, pristine non-functionalized 250 nm polyvinyl chloride nanoplastic. Conditions: alum (a-d) or ACH (a) used as coagulant (5.45 mg Al/L); aPAM1 used as flocculant (0.4 mg/L); 2 min coagulation time; 2 min flocculation time; 30 s of settling; final pH varied between 7.0-8.5. The data points shown in Fig. 3.2a-c are reproduced from Fig. 3.1a to optimize the orthokinetic model for specific experimental conditions in each subfigure. Legend: aPAM1: very low anionic charge density; COOH: carboxylate-modified nanoplastic; none: non-functionalized nanoplastic.

To study the impact of floc properties on the observed TSS-nanoplastic removal relationship, nanoplastic removal was measured using different flocculant charge densities and molecular weights as they are known to play a critical role in floc size[26]. Cationic flocculants resulted in a deviation from the correlation of nanoplastic and TSS removal observed for anionic PAM

(aPAM) (Fig. 3.3a). Earlier studies revealed that cationic PAM (cPAM) showed strong electrostatic interactions with polystyrene surfaces, while aPAM showed minimal deposition on the polymer surface[27]. The use of cPAM flocculant is therefore likely introducing additional removal pathways for nanoplastics through charge neutralization that result in deviations from the orthokinetic model. For samples collected at 3 min of settling, the improved nanoplastic removal by cPAM relative to aPAM is no longer evident. At 3 min of settling, most flocs are expected to settle, which suggests that longer settling times compensate for the difference in relative removal of TSS and nanoplastics. Increasing the molecular weight of the aPAM resulted in a nanoplastic and TSS removal that fit the curve modeled for aPAM1. At higher molecular weights (> 10^6) and low to moderate charge density, PAM acts by a bridging mechanism and charge neutralization is considered relatively insignificant[28]. Hence, the observed relationship between TSS and nanoplastic removal is relevant for flocs interacting with nanoplastics via bridging regardless of floc size and processes. Using flocculants that introduce attractive electrostatic interactions can also be described by the relationship at longer settling times. The nanoplastic-TSS removal relationship was also studied using fibrous super-bridging agents that have been shown to be an effective super-flocculant in water treatment as they form ultra-large flocs resulting in rapid settling time[29]. Despite the structural and charge differences between alum, alum + pristine fibers, and alum + Fe-grafted fibers, a strong correlation is observed between TSS and nanoplastic removal with a combined R^2 of 0.90 ($\frac{\alpha_{NP}}{\alpha_{TSS}}$ = 0.60; n=30) (Fig. 3.3b). In addition, the relationship between TSS and nanoplastic removal is maintained regardless of whether the floc is separated by settling (R^2=0.86 for $\frac{\alpha_{NP}}{\alpha_{TSS}}$ = 0.60; n=8) or screening (R^2=0.90 for $\frac{\alpha_{NP}}{\alpha_{TSS}}$ = 0.60; n=22).

Important sources of variability in coagulation-flocculation systems include local differences in shear rate due to turbulent conditions in the process[30] and non-idealities including improper

valve selection and hydraulic short-circuiting between flocculation and settling[31]. An increase in shear rate or the presence of local high-shearing zones in the aggregation tank can lead to floc breakage[32]. In the present study, the relationship between TSS removal and nanoplastic removal observed at 110 rpm is also respected at faster mixing conditions (150-300 rpm) (Fig. 3.3c). In addition, differences in nanoplastic removal were not statistically significant ($p>0.05$) when comparing all mixing conditions (Fig. S3.4). Such results were expected since polyacrylamide flocculant is known to form shear-resistant flocs which limits the effect of increasing velocity gradients on the correlation[15]. Furthermore, the orthokinetic model was seen to accurately predict the removal of 28 nm carboxylate-functionalized nanoplastics in a matrix containing a mixture of kaolinite/silica that constitutes a common type of inorganic suspended solid in influent wastewater[15] (R^2 = 0.99 for $\frac{\alpha_{NP}}{\alpha_{TSS}}$ = 0.51; n=14) (Fig. 3.3d). In addition, the orthokinetic model was able to describe the nanoplastic removal for a range of initial concentrations of TSS as a result of varying the inorganic particulate content of the synthetic wastewater with an R^2=0.96 ($\frac{\alpha_{NP}}{\alpha_{TSS}}$ = 0.51; n=41) (Fig. 3.3d). This result confirms that the final nanoplastic-TSS relationship is independent of initial contaminant concentration as predicted by the derived correlation (eq. 1). The removal of SiO_2 inorganic contaminants was further investigated through SEM and EDX which confirms the attachment of the inorganic contaminant to the floc and its interaction with aluminum-based coagulation species (Fig. 3.3e). This correlation demonstrates the validity of using TSS removal to predict nanoplastic removal regardless of wastewater conditions including inorganic content type, inorganic concentration, and varying shear rates.

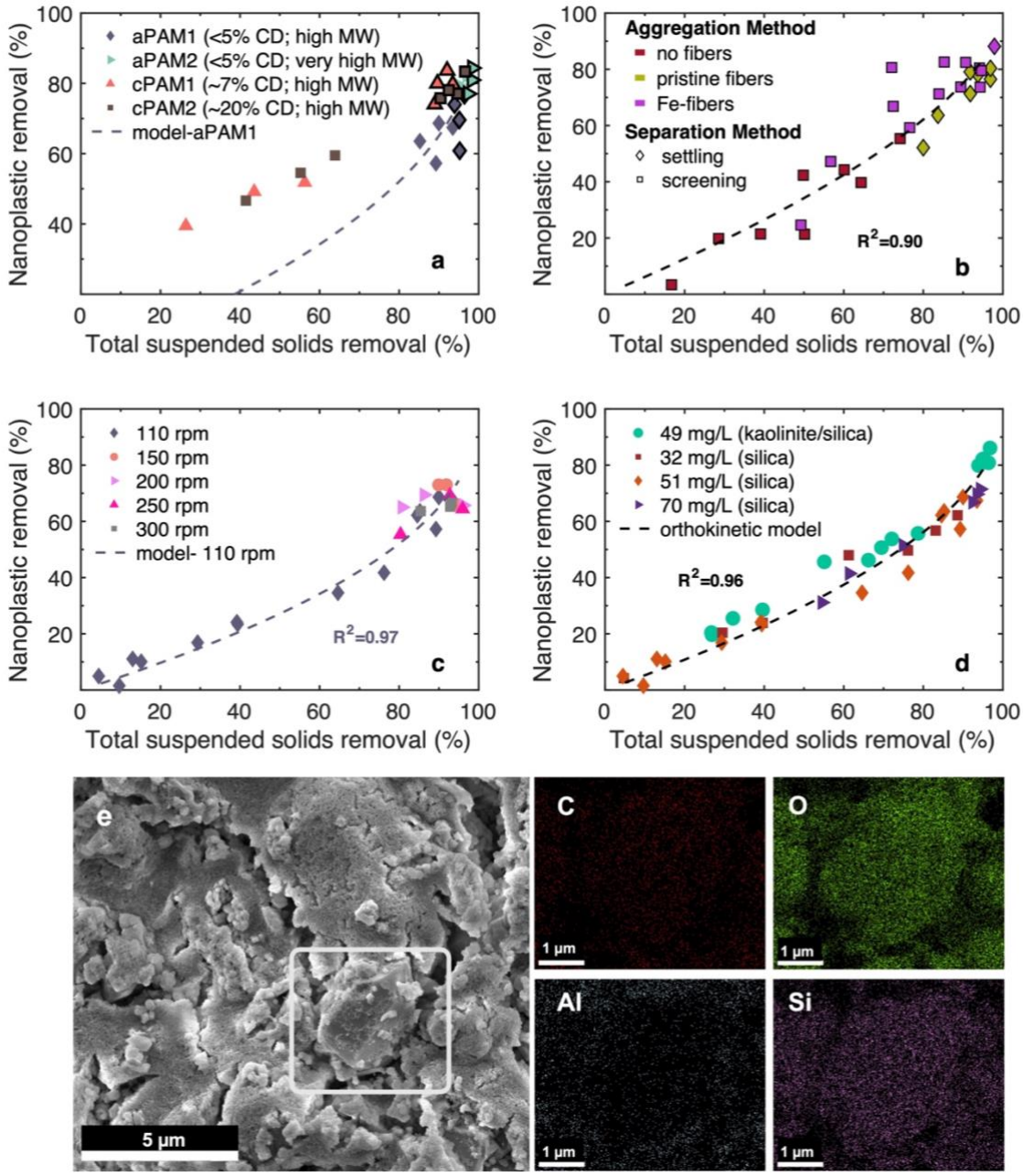

Figure 3.3. Correlation between polystyrene nanoplastic removal and total suspended solids for varying process conditions. a, pristine polystyrene carboxylate-functionalized 28 nm nanoplastics coagulated flocculated with varying polyacrylamide flocculant charge and molecular weight; b, pristine 28 nm polystyrene nanoplastics coagulated with a combination of alum and cellulose fibers (pristine fibers or Fe-grafted fibers) with two floc separation techniques; c, pristine polystyrene carboxylate-functionalized 28 nm nanoplastics undergoing coagulation and flocculation at varying shear mixing values (110-300 rpm); d, pristine carboxylate-functionalized polystyrene 28 nm nanoplastics spiked in synthetic wastewater with kaolinite/silica (initial TSS concentration of 49 mg/L) and silica (initial TSS concentration of 32, 51, and 70 mg/L) spiked as inorganic contaminants. Conditions: alum used as coagulant (5.45 mg Al/L); aPAM1 (a-d), aPAM2 (a), cPAM1(a), and cPAM2 (a) used as flocculant (0.4 mg/L); 2 min coagulation time; 2 min flocculation time; 30 s of settling (a-d) or 3 min of settling (a, shown with dark outlines); final pH varied between 7.0-8.5; initial TSS of 51 mg/L (a-c) and between 32-70 mg/L (d); and e, SEM images of settled flocs and the corresponding EDS elemental mapping showing the presence of carbon, oxygen, aluminum, and silicon. The

data points shown in Fig. 3.3(a, c, and d) are reproduced from Fig. 3.1a for 28 nm (-COOH; pristine; alum) to provide a comparison with nanoplastic removal when aPAM1 was used as a flocculant at a mixing speed of 110 rpm. Legend: CD: charge density, aPAM1: very low anionic charge density, high molecular weight; aPAM2: very low anionic charge density, very high molecular weight; cPAM1: very low cationic charge density, high molecular weight; cPAM2: low cationic charge density, high molecular weight.

3.4 Testing the nanoplastic-TSS correlation using wastewater samples

To validate the proposed correlation model, the nanoplastic and TSS removal was examined using real wastewater samples collected from two Canadian wastewater treatment plants (WWTP1 and WWTP2). The removal of spiked nanoplastics from wastewater influents is shown in Fig. 3.4a and 3.4b as a function of TSS removal using optimal and suboptimal coagulant doses (4.54 and 1.82 mg Al/L for WWTP1 influent, respectively and 5.45 and 4.54 mg Al/L for WWTP2 influent, respectively). The coagulant doses were selected to achieve a representative TSS range for treatment operations given the current regulatory effluent stream TSS limit of 25 mg TSS/L[33] (Fig. S3.5). Within this TSS range, the polystyrene nanoplastic removal results are well described by the orthokinetic model R^2=0.74 ($\frac{\alpha_{NP}}{\alpha_{TSS}}$=1.01; n=6) for influent from WWTP1. Similarly, the polyvinyl chloride nanoplastic removal can be accurately captured with the orthokinetic model with R^2=0.96 ($\frac{\alpha_{NP}}{\alpha_{TSS}}$=0.76; n=6). The optimized $\frac{\alpha_{NP}}{\alpha_{TSS}}$ for both municipal wastewater influent waters is larger than the maximum efficiency ratio obtained for synthetic wastewater experiments (0.60) which suggests that flocs in municipal wastewater have relatively greater efficiencies for removal of nanoplastic contaminants during flocculation.

The nanoplastic-TSS removal relationship was also examined in jar tests using water treated by activated sludge (WWTP1) and water samples collected from an aerated lagoon (WWTP2). The relationship between nanoplastic and TSS removal in samples treated with activated sludge is shown in Fig. 3.4c for optimal (100 s) and suboptimal (130 s) settling times following

aggregation. The observed trend of nanoplastic removal as a function of TSS is well captured by the orthokinetic equation with a collision efficiency ratio of 0.50. The optimized parameter is within the range determined for synthetic wastewater treated with aluminum-based coagulants ($\frac{\alpha_{NP}}{\alpha_{TSS}}$ ranging from 0.46 to 0.60) which suggests that the relative attachment efficiency of nanoplastics and TSS to biological flocs is similar to that of aluminum and PAM-based flocs. The nanoplastic-TSS removal relationship for aerated lagoon water samples treated with alum (1.82 mg Al/L) is shown in Fig. 3.4d for three different settling times. The optimized collision efficiency ratio of treated aerated lagoon water samples ($\frac{\alpha_{NP}}{\alpha_{TSS}}$ = 0.35) shows that flocs produced from biological oxidation and low doses of alum results in a lower attachment efficiency with nanoplastic contaminants. Although all experiments with real wastewater samples show a good fit with the orthokinetic model, the dependence of the collision efficiency on the types of flocs produced in the system highlights the need to tailor the orthokinetic model to the aggregation-based wastewater treatment system for more accurate nanoplastic tracking.

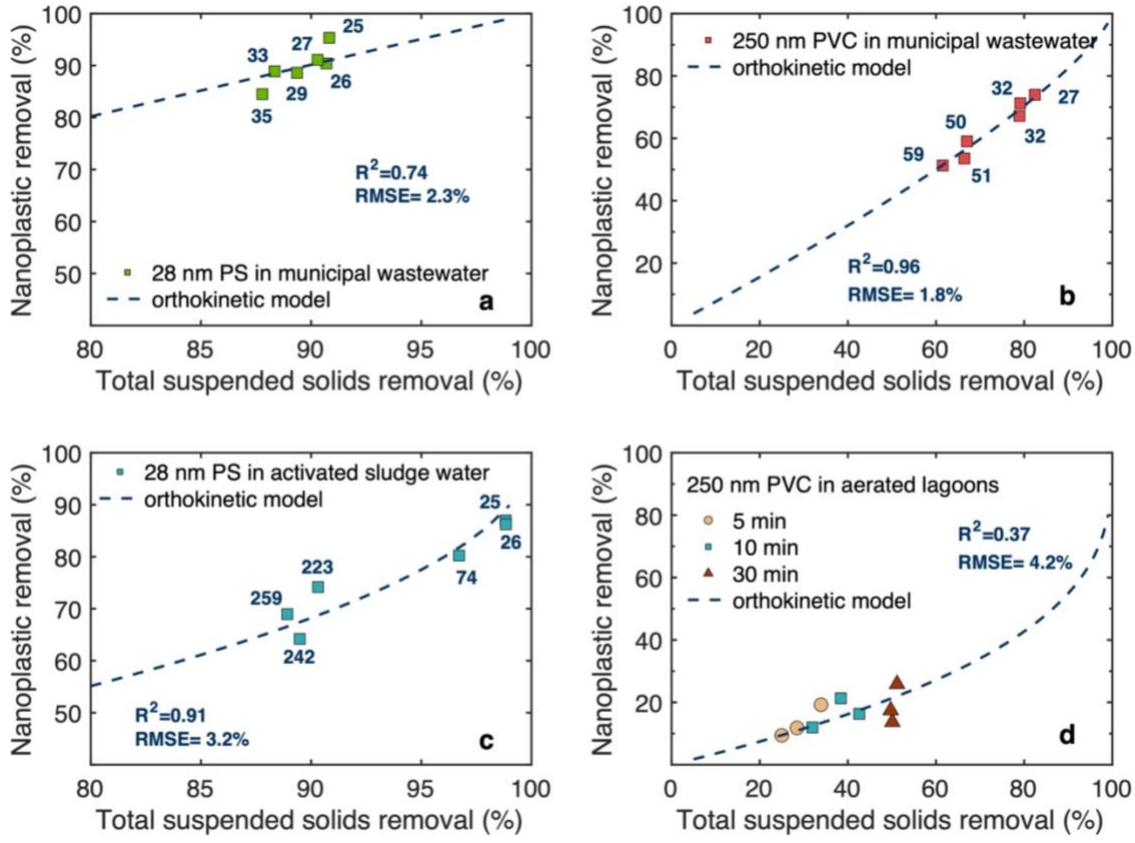

Figure 3.4. Nanoplastic removal as a function of TSS removal in samples of municipal wastewater influent, activated sludge treated water, and aerated lagoon water. a, wastewater influent collected from WWTP1 (pH = 8.2; initial TSS = 281 ± 13 mg/L). Conditions: alum used as coagulant (1.82 or 4.54 mg Al/L); aPAM1 used as flocculant (0.4 mg/L); 2 min coagulation time; 2 min flocculation time; 3 min settling; b, wastewater influent collected from WWTP2 (pH = 7.5; initial TSS = 157 ± 11 mg/L). Conditions: alum used as coagulant (4.54 or 5.45 mg Al/L); aPAM1 used as flocculant (0.4 mg/L); 2 min coagulation time; 2 min flocculation time; 3 min settling; c, water treated by activated sludge process collected from WWTP1 (pH = 7.1; initial TSS = 1,711 ± 57 mg/L). Conditions: no coagulant and flocculant added; 2 min aggregation time at 110 rpm, 100 or 130 s of settling, pH of 7.1; and d, aerated lagoon water samples collected from WWTP2 and treated with alum (pH = 7.8; initial TSS = 113 ± 13 mg/L). Conditions: alum used as coagulant (1.82 mg Al/L); no flocculant added; 10 min aggregation time at 110 rpm; 5, 10 and 30 min of settling. Each data point represents a single jar test and the numbers in blue font next to data points indicate the measured TSS (in mg/L) of the individual jar test after treatment (a-c).

3.5 Employing TSS removal as a metric for nanoplastic removal

The established correlation between nanoplastic and TSS removal (eq. 1) is shown to be valid regardless of coagulant type, nanoplastic size, type, surface charge, and simulated aging history, separation method, and wastewater properties (pH, solids content). Fig. 3.5a shows the results of all aggregation tests: without alum and polyacrylamide (for activated sludge-treated

water), treated with only alum (for aerated lagoon water sample) or using alum and anionic polyacrylamide (for synthetic and municipal wastewater influent). The orthokinetic model resulted in a combined R^2=0.92 for an optimized collision efficiency ratio $\frac{\alpha_{NP}}{\alpha_{TSS}}$ = 0.57 (0.54-0.60 at 95% confidence interval; p=5•10^{-66}; n=117). The high correlation coefficient shows the validity of the orthokinetic flocculation model in describing the relative removal of nanoplastics to TSS, despite the varying nanoplastic properties, water type, and aggregation process. Drawing on this strong correlation, we suggest implementing TSS removal measurements as an indicator for nanoplastic removal.

Indicators are commonly employed in water treatment plants to evaluate the effectiveness of treatment processes. For instance, turbidity measurements after filtration are used as an indicator of pathogen removal in drinking water quality monitoring[34-36]. Filtered turbidity targets are based on the relationship between turbidity and pathogen levels including *Cryptosporidium* oocysts, viruses, and *Giardia* cysts[15]. Similarly, we propose using TSS removal measurements as an indicator for nanoplastic removal after settling to aid wastewater treatment plants and regulatory agencies in assessing the treatment performance and making operational decisions. The estimation of nanoplastic removal established above can be used as an input to quantitively assess the risks posed by nanoplastics. This type of framework has been used to quantify risk related to contaminants that cannot be measured in a continuous mode such as assessing population health risk of waterborne pathogens through quantitative microbial risk assessment (QMRA) [35].

The results presented in this work reveal that nanoplastic removal through coagulation/flocculation/settling can be estimated for individual wastewater treatment plants by considering local conditions of wastewater treatment plants through TSS removal measurements. Such an assessment was conducted for water treatment systems in Québec

(Canada) where the current wastewater regulation typically limits the TSS effluent stream to less than 25 mg/L[33]. Fig. 3.5b reveals the predicted nanoplastic removal based on the collision efficiency parameter determined in this study for a TSS concentration in influent water ranging from 50 mg/L to 250 mg/L[37]. Based on the results of this study, using conventional coagulant (alum) and flocculant (anionic PAM) results in an estimated pristine nanoplastic removal of 39 ± 8% and 69 ± 8% (error range reflects root mean square error of the predicted model) for an influent TSS concentration of 60 mg/L and 200 mg/L, respectively. The combination of modeling parameters established in the literature and in-house monitoring can result in an accurate and locally relevant estimate of nanoplastics release in the aquatic ecosystem.

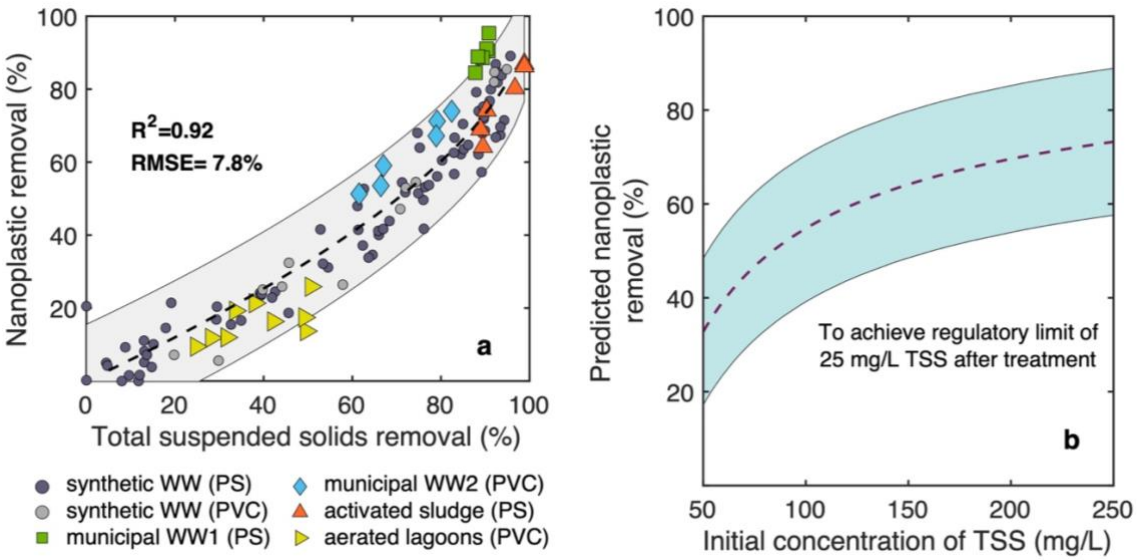

Figure 3.5. Correlation between TSS and nanoplastic removal for a typical physicochemical treatment process. a, correlation between TSS and nanoplastic removal where each data point represents a single jar test reproduced from earlier figures. Jar tests were conducted in synthetic wastewater (conditions: alum used as coagulant (5.45 mg Al/L); aPAM1 used as flocculant (0.4 mg PAM/L), 2 min of coagulation; 2 min of flocculation; 30 s of settling) spiked with polystyrene and polyvinyl chloride nanoplastics, municipal wastewater influent from WWTP1 spiked with polystyrene nanoplastics, municipal wastewater influent from WWTP2 spiked with polyvinyl chloride nanoplastics, water treated by activated sludge process and spiked with polystyrene nanoplastics, and aerated lagoon water treated with alum and spiked with polyvinyl chloride nanoplastics; and b, predicted nanoplastic removal based on targeted removal of TSS with varying initial concentration of influent wastewater to reach the regulatory limit of 25 mg/L. The dashed line represents the determined nanoplastic removal based on eq. (1) with the optimized collision efficiency ratio of 0.57 (0.54-0.60; 95% CI) determined in (a). The shaded region represents the observational prediction interval of the model with a 95% confidence level with the nanoplastic removal from eq. (1) as the centre of

the bands. Legend: WW: wastewater; WW1: wastewater from treatment plant 1; WW2: wastewater from treatment plant 2; PS: polystyrene; PVC: polyvinyl chloride.

3.6 Correlation of TSS and microplastics removal

Besides nanoplastics, microplastic contaminants are of growing concern with fibers estimated to be the dominant shape of microplastics (53%) in wastewater effluents[3]. Jar test experiments revealed polyester microfiber (length = 351-665 µm, Fig. S3.6) removals greater than 90% when TSS removal exceeded 60% (Fig. 3.6a). This result is in agreement with earlier reports that showed greater than 99% removal of blended polyester microfibers) using alum as a coagulant[38]. On the other hand, polyethylene microspheres (diameter = 45-53 µm) were not removed as effectively as microfibers with a maximum measured removal of 88%. This observation was also reported by Shahi et al. [39] who attributed the greater removal of elongated microplastics to their increased surface area that increases the likelihood that the microplastic is incorporated into the floc during settling. As evident in Fig. 3.6a, microfiber and microsphere removal cannot be correlated to TSS removal via the simple orthokinetic flocculation models that assume particle sphericity. Even though the microspheres are spherical, the large size of the microplastics influences the aggregation behavior since larger particles have a greater collision frequency with flocs. The difference in flocculation rates of microspheres is expected to impact the contaminant removal behavior due to varying hydrodynamic forces[40] and attachment behavior[41]. However, a linear relationship can be used to correlate the microfiber and TSS removal (R^2=0.87; n=9; Fig. S3.7a) as well as the microsphere and TSS removal (R^2 = 0.77; n=10; Fig. S3.7b) at low TSS removals (<65%). This finding is in agreement with previous studies that observed a high correlation coefficient between turbidity removal and pristine polyester fibers[38] as well as carboxylate-functionalized polystyrene microspheres[41,42] in physicochemical treatment systems.

To confirm the validity of the microplastic removal results in large scale coagulation/flocculation tanks, pilot-scale experiments were conducted using 20 L of synthetic wastewater in a reactor with an 80× scale-up factor compared to a jar tester. The microfiber removal is greater than 70% even after 30 s of settling while microsphere removal requires longer than 3 min to achieve similar removal (Fig. 3.6b). This result suggests that microfibers fully incorporate into the larger flocs that settle immediately while microspheres also attach to small flocs. Variability introduced by non-optimal local mixing conditions in the 20 L reactor was not seen to significantly affect the determined microfiber (93 ± 4%, p=0.12) and microsphere removals (86 ± 3%, p=0.54) after 3 min of settling when compared to jar test experiments with equivalent settling times (Fig. 3.6c). The average microfiber removal of 97 ± 3% is greater than microsphere removal (91 ± 3%; p=0.008) when treating municipal wastewater influent from WWTP1. A greater microfiber removal was also observed for treated municipal wastewater influent from WWTP2 (94 ± 2% versus 89 ± 3%) although not statistically significant (p=0.08). This finding confirms the improved removal of fiber-shaped microplastics relative to spherical particles. Since environmental microplastics in wastewater are dominated by fibrous and irregular morphologies[3], these contaminants are expected to exhibit aggregation behavior bound between that of microfiber and spherical microplastics. To confirm this hypothesis, synthetic wastewater samples were spiked with high-density polyethylene (HDPE) microfragments that contained fiber-shaped microfragments (length= 97-326 µm) and irregular-shaped microfragments (effective length= 66-106 µm, Fig. S3.8). The HDPE microfragment removals ranged between 56 and 84% when TSS removal exceeded 60% (Fig. 3.6d). This removal falls within the obtained range for polyethylene microspheres (66 to 88% removal) and below the removal of microfibers (92 to 99% removal) for the same TSS removal. It should also be noted that the removal of microfragments was observed to be greater (p=0.02) in municipal wastewater (90 ± 6%; n=3; average TSS removal of 80 ± 2%)

compared to synthetic wastewater (69 ± 11%; n=5; average TSS removal of 80 ± 2%). While no statistical significance is observed for microfibers between different water types, microsphere removal also showed an improved removal when spiked in municipal wastewater (91 ± 3% in municipal wastewater from WWTP1 versus 84 ± 4% in synthetic wastewater; p=0.008). Therefore, flocs produced in municipal wastewater can enmesh spherical and irregular-shaped microplastics to a greater extent than in synthetic wastewater. Optical images of settling flocs reveal the nature of microfiber and microsphere attachment during flocculation (Fig. 3.6e).

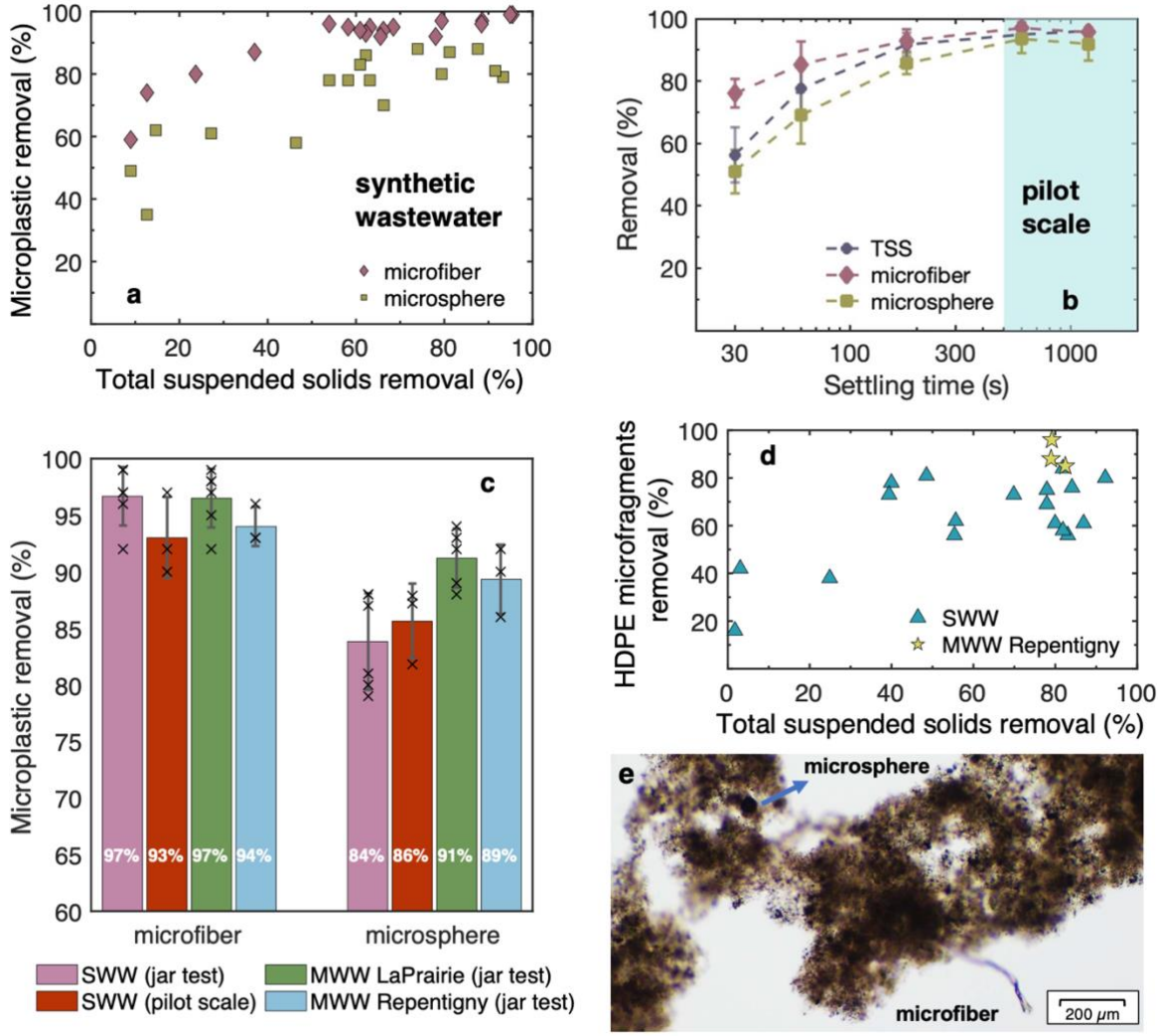

Figure 3.6. Microplastic and microfiber removal during physicochemical treatment. a, polyester microfibers (length = 351-665 µm; diamond) and polyethylene microspheres (diameter = 45-53 µm, square) removal as a function of TSS removal for jar test experiments with synthetic wastewater (250 mL). Conditions: alum used as coagulant (4.09-5.45 mg Al/L);

aPAM1 used as flocculant (0.4 mg/L); 2 min coagulation time; 30-120s flocculation time; 3 min settling; b. TSS, microfiber, and microsphere removal as a function of settling times for physicochemical treatment experiments in 20 L pilot scale studies with synthetic wastewater. Each data point is presented as the mean of three separate measurements (n=3) ± the standard deviation; c, average microfiber and microsphere removal in synthetic wastewater jar tests, synthetic wastewater pilot scale experiments, and municipal wastewater influent for all samples collected after 3 min of settling and resulting in a final TSS removal >70%. All tests contained an initial concentration of ~1000 microplastics/L treated with alum as a coagulant at a concentration between 4.09-5.45 mg Al/L (synthetic wastewater jar test; n=6), 5.45 mg Al/L (synthetic wastewater pilot scale; n=3), 1.82 or 4.54 mg Al/L (wastewater from WWTP1; $n_{microfiber}$=6 and $n_{microsphere}$=5), and 5.45 mg Al/L (wastewater from WWTP2; n=3) with aPAM1 (0.4 mg/L) used as a flocculant for all treatments. Samples for measuring TSS and microplastic removal were collected 3 min after settling following a 2 min coagulation and 2 min flocculation stage. Data are presented as mean values ± the standard deviation; d, high-density polyethylene microfragments as a function of TSS removal for jar test (250 mL) experiments with synthetic wastewater (triangle) and municipal wastewater influent from WWTP2 (star). Conditions: alum used as coagulant (4.09-5.45 mg Al/L for SWW and 5.45 mg Al/L for MWW); aPAM1 used as flocculant (0.4 mg/L); 2 min coagulation time; 30-120s flocculation time for SWW and 120 s for MWW; 3 min settling; and e, stereomicroscope images of flocs with microsphere and microfiber entrapped by the floc. Legend: SWW: synthetic wastewater; WW: wastewater; WW1: wastewater from treatment plant 1; WW2: wastewater from treatment plant 2; HDPE: high-density polyethylene.

3.7 Conclusion

In this work, we demonstrate the potential of employing total suspended solids (TSS) removal as a metric to estimate nanoplastic and microplastic removal during wastewater treatment. To correlate nanoplastic and TSS removal, an equation based on orthokinetic flocculation was derived and experimentally validated in 41 wastewater treatment conditions using eight different water types. The results of this work reveal a high correlation for different nanoplastics and treatment conditions (R^2=0.92). This is the first time an exposure assessment model has been demonstrated for nanoplastic contaminant removal in aggregation-based systems (physicochemical and biological). This work shows that for treatment procedures resulting in TSS removal below the regulatory limit of 25 mg/L, the estimated nanoplastic removal can be as low as 39 ± 8% which raises concern regarding the quantity of nanoplastics released in the treated effluent. The results of experiments using municipal wastewater reveal that aggregation-based systems achieve high average polyester microfiber removal (97 ± 3%),

polyethylene microsphere removal (91 ± 3%), and high-density polyethylene microfragments removal (90 ± 6%) for TSS removals greater than 70%. A linear relationship between TSS and microplastic removal is proposed for low TSS removals, however, more work is needed to confirm whether the linear relationship for microplastic removal is influenced by the size and type of plastic contaminant as well as weathering history. The significantly greater removal of microplastics compared to nanoplastics and the differences in their correlation with TSS removal further supports the growing body of literature calling to differentiate between these two forms of plastic contamination due to their unique physicochemical behaviors and environmental fate[43,44]. Based on these results, we recommend that indicators such as TSS and turbidity (for drinking water application) removal should be further explored and expanded to other nanoplastics as well as microplastic removal studies.

3.8 Methods

Chemicals and Materials

Fluorescent latex polystyrene nanoplastics used in this study included 28 nm (carboxylate-modified, FluoSpheres, ex/em: 365/415 nm), 50 nm (carboxylate-modified, FluoSpheres, ex/em: 580/605 nm), 50 nm (non-functionalized, Phosphorex, ex/em: 460/500 nm) and 220 nm (carboxylate-modified nanosphere, FluoSpheres, ex/em: 365/415 nm) as well as 250 nm fluorescent polyvinyl chloride (non-functionalized, Lab261, ex/em: 460/500 nm). Two coagulants, alum (ALS, Kemira Water Solutions Canada, Inc.) and aluminum chlorohydrate (ACH) (PAX XL1900, Kemira Water Solutions Canada, Inc.) and four polyacrylamide (PAM) flocculants with varying charge densities (CD) and molecular weight (MW) were tested in this study. The flocculants include: low MW anionic PAM (aPAM1, CD <5%, Veolia Water Technologies), high MW anionic PAM (aPAM2, CD <5%, Kemira Water Solutions Canada, Inc.), low MW cationic PAM (cPAM1, CD ≈ 7%, Kemira Water Solutions Canada, Inc.), low

MW cationic PAM (cPAM2, CD ≈ 20%, Kemira Water Solutions Canada, Inc.). Polyester microfibers were obtained following a procedure implemented in previous work[27]. Briefly, commercial polyester textile (SanMar Canada, ATC, ATC3600Y) was blended using a Ninja blender (~1200 rpm) for 5 min at 22 °C and sieved with a 250 µm mesh stainless steel sieve to produce PEST microfibers (length = 351-665 µm, average length = 530 µm, n=118, Fig. S3.6). Polyethylene microspheres were obtained with a diameter size of 43-50 µm (fluorescently labeled, Cospheric, ex/em: 607/575 nm, density 1.085-1.095 g/cc) to maintain an equivalent diameter to the blended microfibers. High-density polyethylene (HDPE) microfragments were obtained by first cutting HDPE sheets (48" 96" × 1/16", McMaster-Carr 8619K112) into 3 cm × 3 cm squares. A stainless steel spice grinder (2500 W; 36,000 rpm; Homend) was used to grind the HDPE squares for 2 min. The grinding process was repeated until the HDPE fragments reached the desired size. The fragments were then sieved with a 150 µm and then a 38 µm stainless steel sieve. The microfragments retained on the 38 µm sieve were then collected as HDPE microfragments containing irregular-shaped fragments (effective length= 66-106 µm, average effective length = 91 µm, n=51, Fig. S3.8) and fiber-shaped fragments (length= 97-326 µm, average length = 243 µm, n=54, Fig. S3.8). The length of the irregular-shaped fragments was calculated assuming an ellipsoid shape with an equivalent diameter = $(L \cdot W)^{0.5}$ where L and W are the length and width of the microfragments. All stock solutions were stored in the dark at 4 °C.

Jar test procedure with synthetic wastewater

Jar test experiments were conducted with 250 mL synthetic wastewater prepared according to the OECD guideline[45] and spiked with silica particles (~80% between 1-5 µm diameter, S5631, Sigma-Aldrich) to reach the desired final average TSS of 51 ± 1.5 mg/L. Nanoplastics were spiked in the synthetic wastewater at a concentration below 1 ppm for experiments measuring

removal of 28 nm nanoplastics (1 mL of 200 ppm concentrated stock). The concentration of larger nanoplastics were adjusted to ensure equivalent surface area resulting in a 50 nm and 220 nanoplastic concentration of 1.43 mg/L and 6.29 mg/L, respectively. For this study, aged nanoplastics were obtained by incubating nanoplastics (10 mg/L) in a 50 mL beaker containing synthetic wastewater that was placed on a shaker at a speed of 50 rpm for 18 h in the dark. polyethylene microspheres, polyester microfibers, and high-density polyethylene were spiked at a concentration of 1000 microplastics/L (1.38 mL of a 181 ± 11 microfiber/mL, 841 µL of a 297 ± 27 microsphere/mL, and 2.45 mL of a 102 ± 2 microfragments/mL stock solutions). The pH of the solution was then adjusted between 7.0-8.5 through the addition of 2 M NaOH and 1 M HCl. The coagulant was first added at a concentration of 5.45 mg Al/L to the 250 mL synthetic wastewater spiked with nanoplastics and mixed for 2 min at a speed of 110 rpm. Half the dosage of flocculant (total concentration of 0.4 mg PAM/L) was introduced at the beginning of flocculation, while the other half was added at mid-flocculation to ensure that the formed flocs do not break [38,46,47] and stirring was stopped after 2 min of flocculation. After 30 s and 180 s of settling, samples were collected from a depth of 3 cm below the water surface level for TSS and nanoplastic removal measurements. For jar test experiments that included cellulose fibers and Fe-grafted fibers, the fibers were added just before flocculation at concentrations of 20, 50, 100, 200, and 300 mg/L. The two-minute flocculation period included aPAM1 flocculant (0.3 mg/L) divided into two equal injections. Separation of treated water was based on settling after 30 s or 180 s of settling or through screening using baskets with different apertures (5000, 2000, 1000, 500, and 300 µm, Pentair). The synthesis of pristine fibers and Fe-grafted fibers were based on previous procedures established in the research group[29,48].

Jar tests spiked with polyester microfibers, polyethylene microspheres, and high-density polyethylene microfragments were conducted with a two-minute coagulation stage (4.09-5.45

mg Al/L) and a flocculation stage between 10 s to 2 min (0.4 mg aPAM1/L) at 110 rpm. Samples for measuring TSS and microplastic removal were collected 3 min after settling.

Municipal wastewater influent and activated sludge-treated water collection from wastewater treatment plant 1 and jar test procedure

Municipal wastewater influent and activated sludge samples were collected from a Canadian wastewater treatment plant (WWTP1). The influent wastewater stream had an average flowrate of 65,000 m^3/d, an average initial TSS concentration of 281 ± 13 mg/L, and a pH of 8.2. Water treated by activated sludge process was collected at the end of the aeration tank following the aeration process with an average initial TSS concentration of 1,711 ± 57 mg/L and a pH of 7.1. Each jar test experiment with municipal wastewater influent contained 250 mL wastewater spiked with 28 nm carboxylate-modified polystyrene nanoplastics (0.8 mg/L), polyester microfibers (1,000/L), and polyethylene microspheres (1,000/L). An identical initial concentration of each contaminant was spiked in jar tests containing 250 mL of activated sludge-treated water. The municipal wastewater influent jar test followed a similar procedure as synthetic wastewater. Briefly, alum was used as a coagulant at optimal and suboptimal concentrations (4.54 and 1.82 mg Al/L, respectively) with each condition measured in triplicates for a total of six jar tests. Following coagulation for 2 min at 110 rpm, aPAM1 flocculant (total concentration of 0.4 mg PAM/L) was added for a total flocculation time of 2 min. Samples for TSS and nanoplastic, microfiber, and microsphere removal measurements were collected after 3 min of settling. The jar test procedure for water samples treated by activated sludge process included flocculating the 250 mL sample for 2 min at 110 rpm followed by a settling time of 100 or 130 s. Each settling time condition was measured in triplicates for a total of six jar tests. Samples for TSS and contaminant removal was measured after the respective settling time.

Municipal wastewater influent and aerated lagoon water collection from wastewater treatment plant 2 and jar test procedure

Municipal wastewater influent and aerated lagoon water samples were collected from a second Canadian wastewater treatment plant (WWTP2). The wastewater influent had an average initial TSS concentration of 157 ± 11 mg/L, and a pH of 7.5. The water sample from the aerated lagoons was collected after coarse screening and prior to the first aerated lagoon. The average initial TSS concentration was 113 ± 13 mg/L while the pH was 7.8. Each jar test experiment with municipal wastewater influent contained 250 mL wastewater spiked with 250 nm non-functionalized polyvinyl chloride nanoplastics (0.8 mg/L), polyester microfibers (1,000/L), polyethylene microspheres (1,000/L), and high-density polyethylene microfragments (1,000/L). An identical initial concentration of each contaminant was spiked in jar tests containing 250 mL of aerated lagoon water. In the municipal wastewater influent jar tests, alum was used as a coagulant at optimal and suboptimal concentrations of 5.45 and 4.54 mg Al/L, respectively, with each condition measured in triplicates for a total of six jar tests. Following coagulation for 2 min at 110 rpm, aPAM1 flocculant (total concentration of 0.4 mg PAM/L) was added for a total flocculation time of 2 min. Samples for TSS and nanoplastic, microfiber, microsphere, and microfragments removal measurements were collected after 3 min of settling. On the other hand, 1.82 mg Al/L of alum was added to three jars containing 250 mL samples of aerated lagoon water. The jars were mixed for 10 min at 110 rpm and a 100 mL sample for TSS and nanoplastic, microfiber, microsphere, and microfragments removal measurement was collected after 30 min of sampling. Two additional 10 mL samples were taken after 5 and 10 min of settling for TSS and nanoplastic contaminant measurements.

Pilot scale tests

Pilot scale experiments were conducted with a 20 L batch reactor filled with synthetic wastewater for an 80× volume scale-up of lab-scale jar test experiments (250 mL). Microfibers were spiked at a concentration of ~1,000 microfibers/L (33.7 mL of a 593 ± 54 microfiber/mL stock solution) and microspheres at a concentration of ~1,500 microspheres/L (100 mL of a 297 ± 27 microsphere/mL stock solution). Three physicochemical treatments were conducted following similar procedure to jar tests with 2 min of coagulation (alum; 5.45 mg Al/L) and 2 min of flocculation (aPAM1; 0.4 mg/L) with a mixing speed of 300 rpm (BDC 2010 reversing digital stirrer, Caframo^{TM}). A 70 mm stainless steel square blade impeller was used for stirring (A150, Caframo^{TM}). The final pH of the three tests was measured to be 7.0 ± 0.2. 100 mL samples were taken from the top valve (Fig. S3.9) located 5 cm below the surface at varying settling times (30 s, 1 min, 3 min, 10 min and 20 min). The sample was used to measure the treated TSS, microfiber and microsphere concentrations.

Concentration measurements

The concentrations of pristine and aged nanoplastics were measured using fluorescence intensity (Spark microplate reader, Tecan) with a corresponding calibration curve in synthetic wastewater (linear relation, $R^2 > 0.99$, Fig. S3.10), treated municipal wastewater influent, activated sludge-treated water, and aerated lagoon water samples (linear relation, $R^2 > 0.99$, Fig. S3.11). The measured fluorescence intensity of each sample corresponds to the average of four measurements (sample equally distributed in four microplate wells). TSS values were determined from turbidity measurements based on a calibration curve in synthetic wastewater (linear relation, $R^2 > 0.99$, Fig. S3.12a), municipal wastewater influent from WWTP1 (linear relation, $R^2 > 0.99$, Fig. S3.12b), municipal wastewater influent from WWTP2 (linear relation, $R^2 = 0.98$, Fig. S3.12c), treated activated sludge (linear relation, $R^2 > 0.99$, Fig. S3.12d), and treated aerated lagoon water (linear relation, $R^2 = 0.96$, Fig. S3.12e). The contributions of the

220 nm nanoplastics to the measured turbidity were subtracted based on a calibration curve of distilled water turbidity and nanoplastic concentration (linear relation, $R^2 > 0.97$, Fig. S3.13). The 28 and 50 nm nanoplastics were not observed to affect the measured turbidity. TSS concentrations for calibration curves were measured based on the standard method of TSS measurement[49] with samples filtered through 1.2 µm glass-fiber filter (Cytiva Whatman™, Grade GF/C). Triplicate measurements were taken for each of the five conditions used for fitting the TSS-turbidity calibration curves. For microsphere and microfiber identification, 100 mL samples were collected following each jar test procedure and filtered on a 5 µm MCE membranes (MF-Millipore®, Membrane Filter). The microspheres and microfibers were then counted using a stereomicroscope (Olympus, model SZX16) to calculate the contaminant removal. Filtering the treated activated sludge samples resulted in a thick film of contaminants depositing on the MCE membranes which prevented the accurate identification of microfibers and microplastics from these samples.

Data reproducibility

Jar tests were performed for different coagulant doses (for municipal wastewater influent samples), settling times (for water samples from activated sludge and aerated lagoons), and water pH (for synthetic wastewater samples). Triplicate experiments were conducted for jar tests performed with municipal water samples where the variable quantity was the coagulant dose (municipal wastewater influent samples; standard errors reported in Table S1) or settling time (activated sludge and aerated lagoons samples; standard errors reported in Table S2). Similarly, jar tests in synthetic wastewater were performed for at least three separate pH conditions (within ± 0.2 pH units) and repeated in at least duplicate experiments (standard errors reported in Table S3 for $n \geq 3$).

Floc imaging

Flocs were collected 10 s before the end of the flocculation period at a distance of 3 cm below the water surface of the jar test for optical imaging. Images of the flocs for sizing were taken with brightfield imaging using an inverted fluorescence microscope (Olympus IX71). The length of the floc was calculated assuming an ellipsoid shape with an equivalent diameter = $(L \cdot W)^{0.5}$ where L and W are the length and width of the floc. For electron microscopy imaging, settled flocs were then collected and dried for 24 h and imaged using FEI Quanta 450 environmental scanning electron microscope. Samples were fixed on adhesive carbon tape and coated with a 3 nm layer of platinum (Leica Microsystems EM ACE600 Sputter Coater). Elemental mapping was analyzed using with EDAX Octane Super 60 mm^2 SDD and TEAM EDS Analysis System.

Orthokinetic flocculation modeling and statistical analysis

The derived orthokinetic flocculation relationship was used to fit the nanoplastic removal (R_{NP}) versus TSS removal (R_{TSS}) according to the derived equation:

$$(1 - R_{NP}) = (1 - R_{TSS})^{\frac{\alpha_{NP}}{\alpha_{TSS}}}$$

The collision efficiency ratio parameter $\left(\frac{\alpha_{NP}}{\alpha_{TSS}}\right)$ was optimized for a given data set using MATLAB Optimization Toolbox[50]. The selected parameter was optimized by minimizing the root mean square error (RMSE) of the model that can be calculated as:

$$RMSE = \sqrt{\frac{\sum\left(R_{NP,predicted} - R_{NP,actual}\right)^2}{n}}$$

Where $R_{NP,\ predicted}$ is the nanoplastic removal predicted by the orthokinetic model for a given $R_{TSS,\ actual}$ and n is the sample size. The optimized collision efficiency ratio parameter is then selected based on the lowest calculated RMSE value. Once the optimized collision efficiency

ratio is determined, other model parameters are calculated including p-values, correlation parameter (R^2), 95% confidence interval (CI_{95}) of the model:

$$R^2 = \left(\frac{n\sum\left(R_{NP,p} \cdot R_{NP,a}\right) - \sum R_{NP,p} \cdot \sum R_{NP,a}}{\sqrt{\left[n\sum R_{NP,p}^2 - \left(\sum R_{NP,p}\right)^2\right] \cdot \left[n\sum R_{NP,a}^2 - \left(\sum R_{NP,a}\right)^2\right]}} \right)^2$$

$$CI_{95} = \left(\frac{\alpha_{NP}}{\alpha_{TSS}}\right)_{optimal} \pm t_{crit,\alpha=0.95} \cdot \frac{\sigma}{\sqrt{n}}$$

The confidence interval and prediction interval used in the model were calculated using MATLAB Curve Fitting Toolbox[51]. Two-sample *t*-test with equal variance was conducted on MATLAB to compare the difference of means between nanoplastic removal at different mixing conditions values. The same analysis was conducted to compare means of microplastic and microfiber removal for different physicochemical treatment experiments. A *p*-value of less than 0.05 was considered statistically significant.

Data Availability

The data supporting the findings in this study are available within the paper and its Supplementary Information. Data collected and used to create the figures in this study are available in the figshare repository: https://doi.org/10.6084/m9.figshare.22082369.

Code Availability

The relevant code used for optimizing the collision efficiency ratio parameter and plotting the predicted nanoplastic removal can be accessed at repositories under the GitHub account in ref.[52].

3.9 References

1 Bouwmeester, H., Hollman, P. C. H. & Peters, R. J. B. Potential health impact of environmentally released micro-and nanoplastics in the human food production chain: experiences from nanotoxicology. *Environmental science & technology* **49**, 8932-8947 (2015).

2 Strungaru, S.-A., Jijie, R., Nicoara, M., Plavan, G. & Faggio, C. Micro-(nano) plastics in freshwater ecosystems: abundance, toxicological impact and quantification methodology. *TrAC trends in analytical chemistry* **110**, 116-128 (2019).

3 Sun, J., Dai, X., Wang, Q., van Loosdrecht, M. C. M. & Ni, B.-J. Microplastics in wastewater treatment plants: Detection, occurrence and removal. *Water research* **152**, 21-37 (2019).

4 Lv, X. *et al.* Microplastics in a municipal wastewater treatment plant: Fate, dynamic distribution, removal efficiencies, and control strategies. *Journal of Cleaner Production* **225**, 579-586 (2019). https://doi.org:https://doi.org/10.1016/j.jclepro.2019.03.321

5 Ngo, P. L., Pramanik, B. K., Shah, K. & Roychand, R. Pathway, classification and removal efficiency of microplastics in wastewater treatment plants. *Environmental Pollution* **255**, 113326 (2019).

6 Gong, Y., Bai, Y., Zhao, D. & Wang, Q. Aggregation of carboxyl-modified polystyrene nanoplastics in water with aluminum chloride: Structural characterization and theoretical calculation. *Water Research*, 117884 (2021). https://doi.org:https://doi.org/10.1016/j.watres.2021.117884

7 Zhang, Y. *et al.* Improving nanoplastic removal by coagulation: Impact mechanism of particle size and water chemical conditions. *Journal of Hazardous Materials*, 127962 (2021). https://doi.org:https://doi.org/10.1016/j.jhazmat.2021.127962

8 Liu, X., Yuan, W., Di, M., Li, Z. & Wang, J. Transfer and fate of microplastics during the conventional activated sludge process in one wastewater treatment plant of China. *Chemical Engineering Journal* **362**, 176-182 (2019).

9 Raju, S. *et al.* Improved methodology to determine the fate and transport of microplastics in a secondary wastewater treatment plant. *Water research* **173**, 115549 (2020).

10 Cai, H. *et al.* Analysis of environmental nanoplastics: Progress and challenges. *Chemical Engineering Journal* **410**, 128208 (2021). https://doi.org:https://doi.org/10.1016/j.cej.2020.128208

11 Nguyen, B. *et al.* Separation and analysis of microplastics and nanoplastics in complex environmental samples. *Accounts of Chemical Research* **52**, 858-866 (2019). https://doi.org:https://doi.org/10.1021/acs.accounts.8b00602

12 Silva, A. B. *et al.* Microplastics in the environment: Challenges in analytical chemistry-A review. *Analytica Chimica Acta* **1017**, 1-19 (2018). https://doi.org:https://doi.org/10.1016/j.aca.2018.02.043

13 Bilotta, G. S. & Brazier, R. E. Understanding the influence of suspended solids on water quality and aquatic biota. *Water research* **42**, 2849-2861 (2008).

14 Duan, J. & Gregory, J. Coagulation by hydrolysing metal salts. *Advances in colloid and interface science* **100**, 475-502 (2003).

15 Crittenden, J. C., Trussell, R. R., Hand, D. W., Howe, K. J. & Tchobanoglous, G. *MWH's water treatment: principles and design*. (John Wiley & Sons, 2012).

16 Pernitsky, D. J. & Edzwald, J. K. Solubility of polyaluminium coagulants. *Journal of Water Supply: Research and Technology—AQUA* **52**, 395-406 (2003).

17 Lapointe, M., Papineau, I., Peldszus, S., Peleato, N. & Barbeau, B. Identifying the best coagulant for simultaneous water treatment objectives: Interactions of mononuclear and polynuclear aluminum species with different natural organic matter fractions. *Journal of Water Process Engineering* **40**, 101829 (2021). https://doi.org:https://doi.org/10.1016/j.jwpe.2020.101829

18 O'Melia, C. R. in *The Scientific Basis of Flocculation* 219-268 (Springer, 1978).

19 Schür, C. *et al.* Incubation in wastewater reduces the multigenerational effects of microplastics in Daphnia magna. *Environmental science & technology* **55**, 2491-2499 (2021).

20 Fadare, O. O. *et al.* Humic acid alleviates the toxicity of polystyrene nanoplastic particles to Daphnia magna. *Environmental Science: Nano* **6**, 1466-1477 (2019).

21 Wheeler, K. E. *et al.* Environmental dimensions of the protein corona. *Nature Nanotechnology* **16**, 617-629 (2021).

22 Elimelech, M., Gregory, J. & Jia, X. *Particle deposition and aggregation: measurement, modelling and simulation*. (Butterworth-Heinemann, 2013).

23 Adler, P. M. Heterocoagulation in shear flow. *Journal of Colloid and Interface Science* **83**, 106-115 (1981).

24 Kusters, K. A. The influence of turbulence on aggregation of small particles in agitated vessels. (1991).

25 Balakin, B., Hoffmann, A. C. & Kosinski, P. The collision efficiency in a shear flow. *Chemical engineering science* **68**, 305-312 (2012).

26 Nasser, M. S. & James, A. E. The effect of polyacrylamide charge density and molecular weight on the flocculation and sedimentation behaviour of kaolinite suspensions. *Separation and purification technology* **52**, 241-252 (2006).

27 Lapointe, M. & Barbeau, B. Understanding the roles and characterizing the intrinsic properties of synthetic vs. natural polymers to improve clarification through interparticle Bridging: A review. *Separation and Purification Technology* **231**, 115893 (2020).

28 Patience, M., Addai-Menash, J. & Ralston, J. Investigation of the effect of polymer type on flocculation, rheology and dewatering behaviour of kaolinite dispersions. *International Journal of Mineral Processing* **71**, 247-268 (2003).

29 Lapointe, M., Jahandideh, H., Farner, J. M. & Tufenkji, N. Super-bridging fibrous materials for water treatment. *npj Clean Water* **5**, 11 (2022). https://doi.org:10.1038/s41545-022-00155-4

30 Logan, B. E. Coagulation in Natural and Engineered Systems. *Environ. Transp. Process*, 362-407 (2012).

31 Kawamura, S. *Integrated design and operation of water treatment facilities*. (John Wiley & Sons, 2000).

32 Jarvis, P., Jefferson, B. & Parsons, S. A. Floc structural characteristics using conventional coagulation for a high doc, low alkalinity surface water source. *Water research* **40**, 2727-2737 (2006).

33 Ministère de l'Environnement et de la Lutte contre les changements climatiques. Règlement sur les ouvrages municipaux d'assainissement des eaux usées chapitre Q-2, r. 34.1. (MELCC, 2013).

34 Health Canada. Guidelines for Canadian Drinking Water Quality: Guideline Technical Document—Turbidity. (Water and Air Quality Bureau, Healthy Environments and Consumer Safety Branch, Health Canada, Ottawa, Ontario, 2013).

35 World Health Organization. Quantitative microbial risk assessment: application for water safety management. Report No. 9241565373, (World Health Organization, 2016).

36 U.S. Environmental Protection Agency. Distribution system indicators of drinking water quality. (Office of Water, Office of Ground Water and Drinking Water, Washington, D.C., 2006).

37 Metcalf & Eddy. *Wastewater Engineering: Treatment and Reuse*. (McGraw-Hill Education, 2003).

38 Lapointe, M., Farner, J. M., Hernandez, L. M. & Tufenkji, N. Understanding and improving microplastic removal during water treatment: Impact of coagulation and flocculation. *Environmental Science & Technology* **54**, 8719-8727 (2020). https://doi.org:https://doi.org/10.1021/acs.est.0c00712

39 Shahi, N. K., Maeng, M., Kim, D. & Dockko, S. Removal behavior of microplastics using alum coagulant and its enhancement using polyamine-coated sand. *Process Safety and Environmental Protection* **141**, 9-17 (2020). https://doi.org:https://doi.org/10.1016/j.psep.2020.05.020

40 Thomas, D. N., Judd, S. J. & Fawcett, N. Flocculation modelling: a review. *Water research* **33**, 1579-1592 (1999).

41 Xue, J., Peldszus, S., Van Dyke, M. I. & Huck, P. M. Removal of polystyrene microplastic spheres by alum-based coagulation-flocculation-sedimentation (CFS) treatment of surface waters. *Chemical Engineering Journal* **422**, 130023 (2021).

42 Rajala, K., Grönfors, O., Hesampour, M. & Mikola, A. Removal of microplastics from secondary wastewater treatment plant effluent by coagulation/flocculation with iron, aluminum and polyamine-based chemicals. *Water Research* **183**, 116045 (2020).

43 Ter Halle, A. & Ghiglione, J. F. Nanoplastics: A Complex, Polluting Terra Incognita. *Environmental Science & Technology* **55**, 14466-14469 (2021).

44 Gigault, J. *et al.* Nanoplastics are neither microplastics nor engineered nanoparticles. *Nature nanotechnology* **16**, 501-507 (2021).

45 Organisation for Economic Cooperation & Development. *Test No. 303: Simulation Test-Aerobic Sewage Treatment--A: Activated Sludge Units; B: Biofilms*. (OECD Publishing, 2001).

46 Lapointe, M. & Barbeau, B. Evaluation of activated starch as an alternative to polyacrylamide polymers for drinking water flocculation. *Journal of Water Supply: Research and Technology-Aqua* **64**, 333-343 (2014). https://doi.org:10.2166/aqua.2014.114

47 Lapointe, M. & Barbeau, B. Dual starch–polyacrylamide polymer system for improved flocculation. *Water Research* **124**, 202-209 (2017). https://doi.org:https://doi.org/10.1016/j.watres.2017.07.044

48 Kurusu, R. S., Lapointe, M. & Tufenkji, N. Sustainable iron-grafted cellulose fibers enable coagulant recycling and improve contaminant removal in water treatment. *Chemical Engineering Journal* **430**, 132927 (2022).

49 Rice, E. W., Baird, R. B., Eaton, A. D. & Clesceri, L. S. *Standard methods for the examination of water and wastewater*. Vol. 10 (American public health association Washington, DC, 2012).

50 MATLAB and Optimization Toolbox Release 2022b (Natick, Massachusetts, United States).

51 MATLAB and Curve Fitting Toolbox Release 2022b (Natick, Massachusetts, United States).

52 Sinanaf. *GitHub*, <https://github.com/Sinanaf> (2023).

3.10 Acknowledgements

The authors acknowledge the Canada Research Chairs Program (CRC-2016-00205, NT), the Natural Sciences and Engineering Research Council of Canada (RGPIN/04519-2019, NT), the Killam Research Fellowship (7025-19-0049, NT), and the Canada Foundation for Innovation (36368, 40070, NT). S.A.F. was supported by a Graduate Excellence Fellowship at McGill, M.L. was supported by a NSERC Postdoctoral Fellowship, R.S.K. was supported by NSERC and FRQNT Postdoctoral Fellowships, and Z.L. was supported by NSERC CREATE. The authors thank Dr. Laura Hernandez (McGill University, Montreal, Canada) for assistance with electron microscopy imaging and Qi Zheng for assistance with synthetic wastewater jar test experiments.

3.11 Supplementary Information

Mechanisms and Modeling of Flocculation

In a heterogenous suspension, the rate constant of collisions between particle (i) with size d_i and particle (j) with size d_j are as follows:

Perikinetic flocculation: $$k_{peri} = \left(\frac{2kT}{3\mu}\right)\left(\frac{1}{d_i}+\frac{1}{d_j}\right)\left(d_i + d_j\right) \quad \text{(S1)}$$

Orthokinetic flocculation: $$k_{ortho} = \left(\frac{G}{6}\right)\left(d_i + d_j\right)^3 \quad \text{(S2)}$$

Differential settling: $$k_{DS} = \left(\frac{g\pi}{72v}\right)(S-1)\left(d_i + d_j\right)^3\left|d_i - d_j\right| \quad \text{(S3)}$$

where k is the Boltzmann's constant, T is the temperature, μ is the absolute viscosity, v is the kinematic viscosity, G is the mean velocity gradient, S is the specific gravity of the solids, and g is the gravitational acceleration[1]. To assess the relative contribution of orthokinetic and perikinetic flocculation, the ratio of orthokinetic to perikinetic collision constants can be calculated:

$$\frac{K_{ortho}}{K_{peri}} = \frac{\mu G}{4kT} \cdot d_i \cdot d_j \cdot \left(d_i + d_j\right) \quad \text{(S4)}$$

Using the mean velocity gradient and water conditions typically observed for coagulation and flocculation in water treatment systems, Fig. S3.1 reveals the relative contribution of orthokinetic and perikinetic flocculation based on Equation (S4).

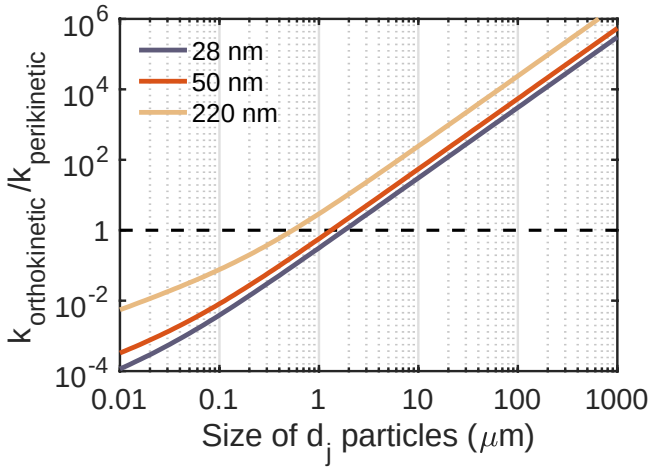

Figure S3.1. Relative contribution of orthokinetic and perikinetic flocculation for polydisperse suspension. Ratio of orthokinetic to perikinetic collision frequency is plotted for particles of size (d_i) of 28 nm (blue), 50 nm (orange) and 220 nm (grey) as a function of particle size d_j ranging from 0.01-1000 µm. The following conditions were assumed: G = 200 s^{-1}; T = 298 K and µ =0.89 x 10^{-3} Pa•s.

As seen in Figure S1, perikinetic flocculation is dominant $\left(\frac{K_{ortho}}{K_{peri}} \ll 1\right)$ when the 28 nm particle is interacting with particles that are smaller in size than ~500 nm. On the other hand, orthokinetic flocculation is dominant $\left(\frac{K_{ortho}}{K_{peri}} \gg 1\right)$ when the 28 nm particle is colliding with particles larger than ~10 µm in size. Coagulation with alum is expected to produce flocs that are large enough to allow for orthokinetic flocculation[1]. This conclusion was confirmed during coagulation experiments in this study with flocs measured to have an average size of 541 µm and a median of 427 µm (N = 73 flocs) as shown in Fig. S3.2. Since over 90% of the measured flocs are larger than 100 µm, the 28 nm particles are expected to flocculate predominantly through orthokinetic flocculation $\left(\frac{K_{ortho}}{K_{peri}} > 10^3\right)$. As the primary particles increase, the orthokinetic flocculation becomes more dominant at lower size ranges of secondary particles as seen for 50 and 220 nm nanoplastics. Therefore, orthokinetic flocculation is expected to dominate collision interactions of all nanoparticles (larger than 28 nm) and inorganic solids (1-10 µm) when interacting with flocs larger than 10 µm.

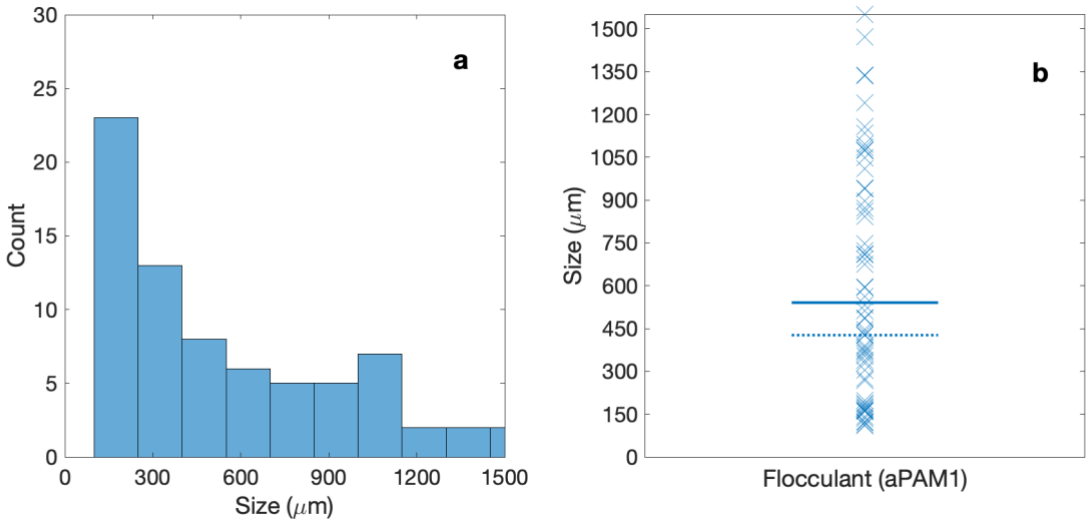

Figure S3.2. Floc size distribution with alum as coagulant and anionic polyacrylamide as flocculant. a, Histogram and **b,** size distribution of flocs formed with alum (5.45 mg/L) as coagulant and anionic polyacrylamide (aPAM1; 0.4 mg/L) as flocculant under a constant mixing rate of 110 rpm and 2 minutes of coagulation followed by 2 minutes of flocculation. Solid line shows the mean size and the dashed line represents the median. Full analysis of floc sizes was conducted with ImageJ software for at least 20 representative flocs from each triplicate measurements (N=73; pH 7 ± 0.2). The length of the floc was calculated based on assuming an ellipsoid shape with an equivalent diameter. The total length of the floc was approximated as the equivalent diameter of the ellipsoidal shape = $(L \cdot W)^{0.5}$ where *L* and *W* are the length and width of the floc.

Derivation of orthokinetic flocculation expression

The rate of change of total particle concentration due to orthokinetic flocculation can be expressed by:

$$\frac{dN_t}{dt} = \frac{16\alpha G r_i^{\,3}}{3} \sum_{k=1}^{p} N_k^{\,2} k \qquad (S5)$$

where N_k is the number of floc particles and the sum term refers to the size-distribution of flocs[2]. If the primary particles including nanoplastic and inorganic material with size (r_i) are significantly smaller than suspended floc particles (r_j) and the relative number of floc particles remains the same ($N_k \approx$ constant), then:

$$\frac{\mathrm{d}\sum_{\mathrm{k}=1}^{\infty}\mathrm{N_k}}{\mathrm{dt}} \approx \frac{\mathrm{dN_i}}{\mathrm{dt}} \tag{S6}$$

The floc volume concentration (ϕ) is equal to the number of flocs per volume and is invariant since it only depends on the number of particles initially present during flocculation[2]:

$$\phi = \frac{4}{3}\pi \mathrm{r_j}^3 N_j \tag{S7}$$

Combining Equations (S5) and (S7):

$$\int_{\mathrm{N_0}}^{\mathrm{N_t}} \frac{d\mathrm{N_i}}{\mathrm{N_i}} = -\int_0^t \frac{\alpha G \phi}{2\pi} \cdot dt \tag{S8}$$

$$\frac{\mathrm{N_t}}{\mathrm{N_0}} = \exp\left(-\frac{4}{\pi} \cdot \alpha G t \cdot \phi\right) \tag{S9}$$

Applying the final expression to the concentration of TSS and nanoplastics remaining in suspension:

$$\frac{\mathrm{N_{TSS}}}{\mathrm{N_0}} = \exp\left(-\frac{4}{\pi} \cdot \alpha G t \cdot \phi\right) \tag{S10}$$

$$\frac{\mathrm{N_{NP}}}{\mathrm{N_0}} = \exp\left(-\frac{4}{\pi} \cdot \alpha G t \cdot \phi\right) \tag{S11}$$

Assuming removal of contaminants is achieved by orthokinetic flocculation:

$$R_{TSS} = \text{TSS Removal (\%)} = 1 - \frac{\mathrm{N_{TSS}}}{\mathrm{N_0}} \tag{S12}$$

$$R_{NP} = \text{NP Removal (\%)} = 1 - \frac{\mathrm{N_{NP}}}{\mathrm{N_0}} \tag{S13}$$

Dividing the two expressions above results in the following relationship:

$$(1 - R_{NP}) = (1 - R_{TSS})^{\frac{\alpha_{NP}}{\alpha_{TSS}}} \tag{S14}$$

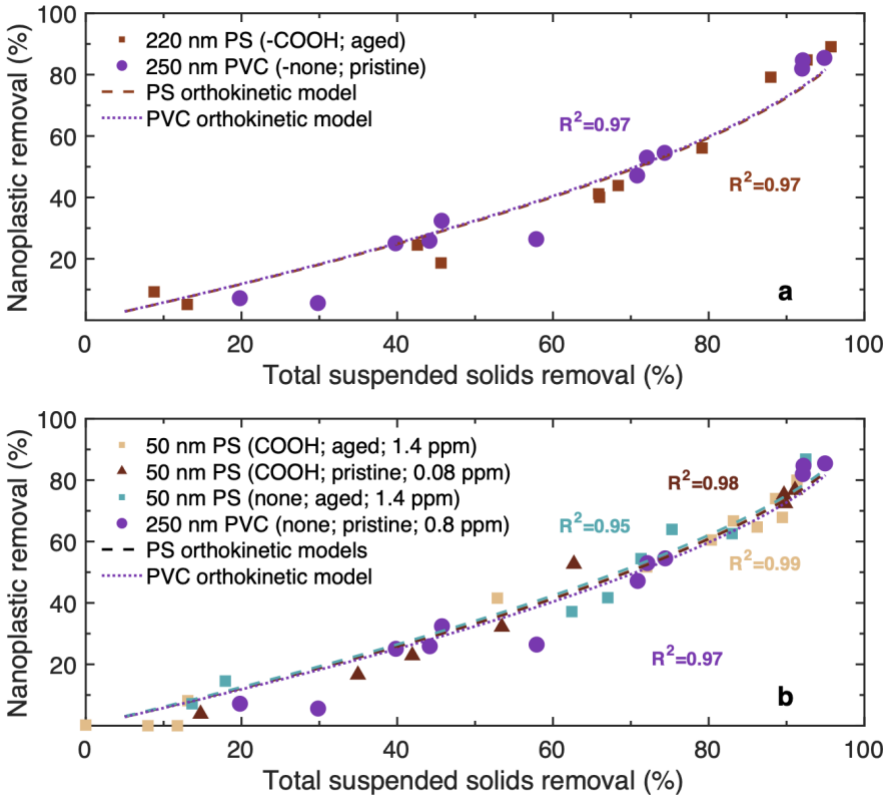

Figure S3.3. The relationship between the removal of nanoplastic and TSS for varying nanoplastic surface conditions. **a,** aged carboxylate-functionalized 220 nm polystyrene nanoplastics and pristine non-functionalized 250 nm polyvinyl chloride nanoplastic; **b,** 50 nm polystyrene nanoplastics and 250 nm polyvinyl chloride nanoplastic with varying surface functionalizations (carboxylate-modified or non-functionalized) and aging condition (pristine or aged). Each data point represents a single jar test conducted in synthetic wastewater. Dashed lines plot the orthokinetic models optimized for each nanoplastic contaminant. Conditions: alum used as coagulant (5.45 mg Al/L); aPAM1 used as flocculant (0.4 mg/L); 2 min coagulation time; 2 min flocculation time; 30 s of settling; final pH varied between 7.0-8.5. Legend: aPAM1: very low anionic charge density; COOH: carboxylate-modified nanoplastic; none: non-functionalized nanoplastic.

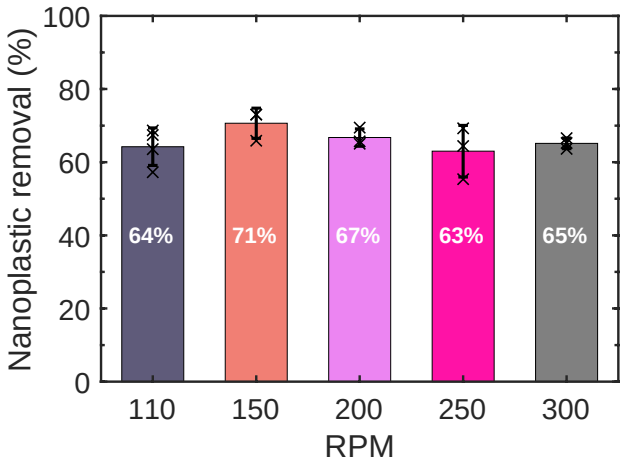

Figure S3.4. Nanoplastic removal measurement for varying rpm. Pristine carboxylate-functionalized 28 nm nanoplastics undergoing coagulation and flocculation at varying shear mixing values: 110 rpm (n=4), 150 rpm (n=3), 200 rpm (n=3), 250 rpm (n=3), and 300 rpm (n=3). Samples for measuring TSS and nanoplastic removal were collected 30 s after settling. Alum (5.45 mg Al/L) and aPAM1 (0.4 mg/L) were used as coagulant and flocculant respectively and the final pH was 7.0 ± 0.2. Data are presented as mean values ± the standard deviation.

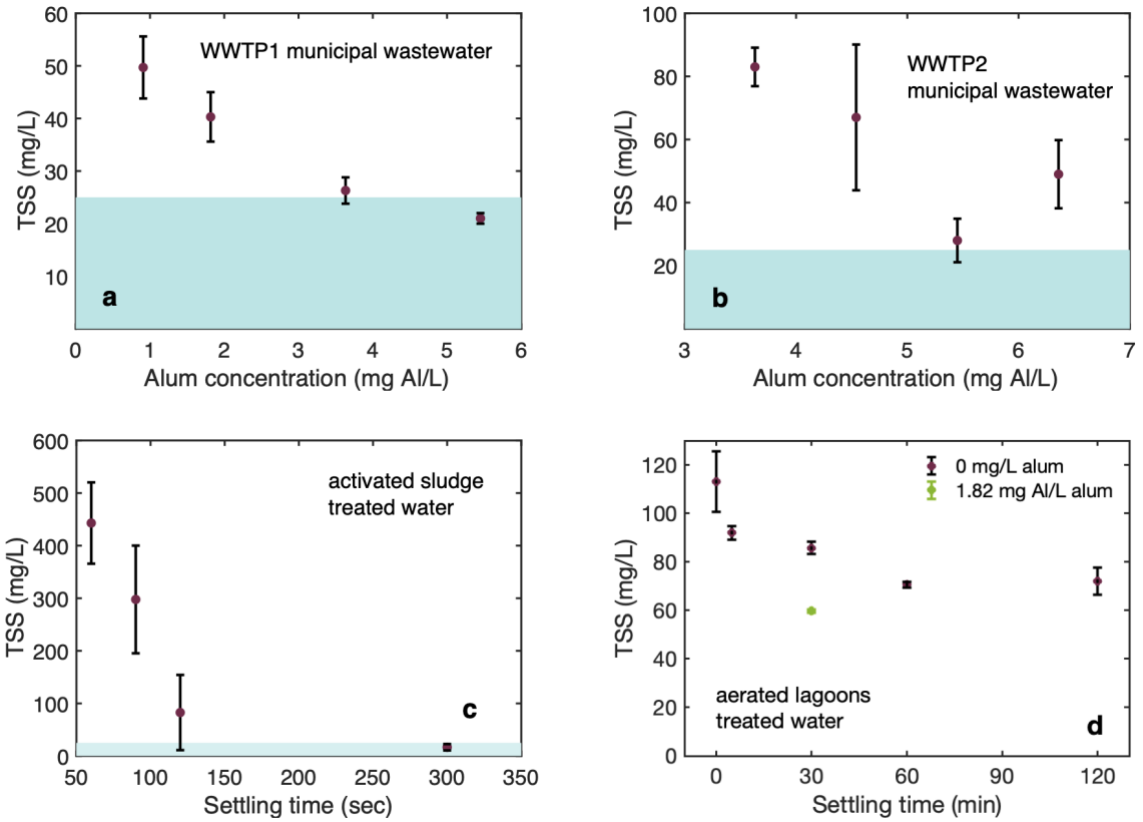

Figure S3.5. Final TSS measurement following treatment in wastewater samples. a, WWTP1 and b, WWTP2 municipal wastewater influent treated with varying concentration of alum for a 2 min coagulation stage followed by 2 min of flocculation (0.4 mg aPAM1/L) with

samples collected after a total settling time of 3 min. c, activated sludge-treated water samples after 2 min of flocculation at 110 rpm and varying settling times; and d, treated aerated lagoon water samples after 10 min of flocculation at 110 rpm and varying settling times with alum added at the beginning of the flocculation time. All experiments were conducted in triplicates (n=3). Data are presented as mean values ± the standard deviation and the rectangle in blue reveals the region of TSS below the regulatory limit of 25 mg TSS/L.

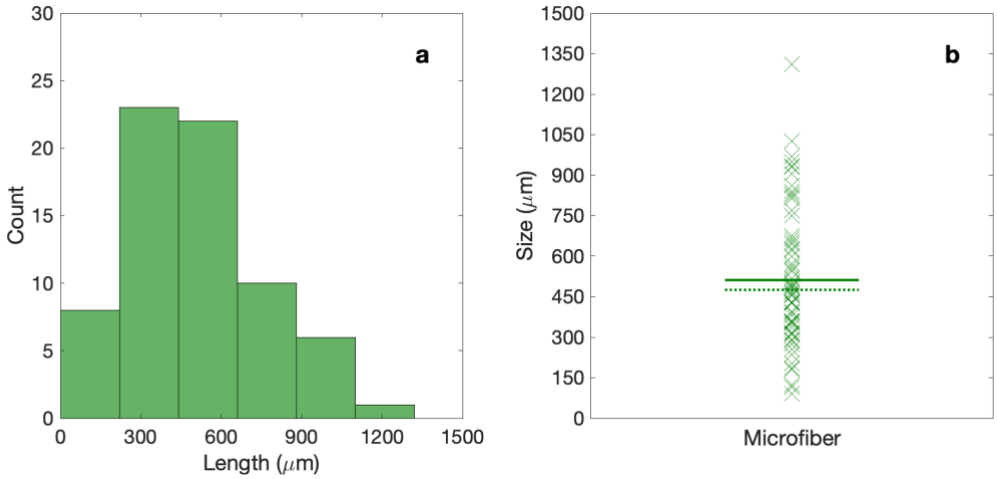

Figure S3.6. Blended polyester microfiber length. a, Histogram and b, size distribution of polyester microfibers obtained following blending polyester fibers and sieving with a 250 µm mesh stainless steel. Solid line shows the mean size and the dashed line represents the median. Full analysis of microfibers was conducted with ImageJ for N=70 representative microfibers from five separate samples taken from the stock suspension.

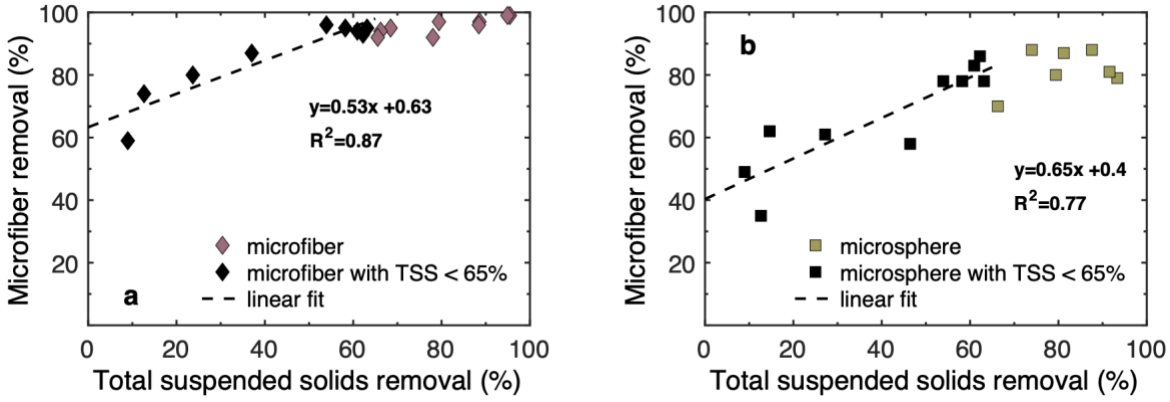

Figure S3.7. Linear fitting for microfiber and microsphere removal as a function of TSS removal. a, microfiber and b, microsphere removal as a function of TSS removal for jar test experiments with synthetic wastewater (250 mL). Conditions: alum used as coagulant (4.09-5.45 mg Al/L); aPAM1 used as flocculant (0.4 mg/L); 2 min coagulation time; 30-120s flocculation time; 3 min settling. Dashed line shows the linear line of best fit for all results with a TSS removal below 65% (data points used for the linear correlation are shown in black).

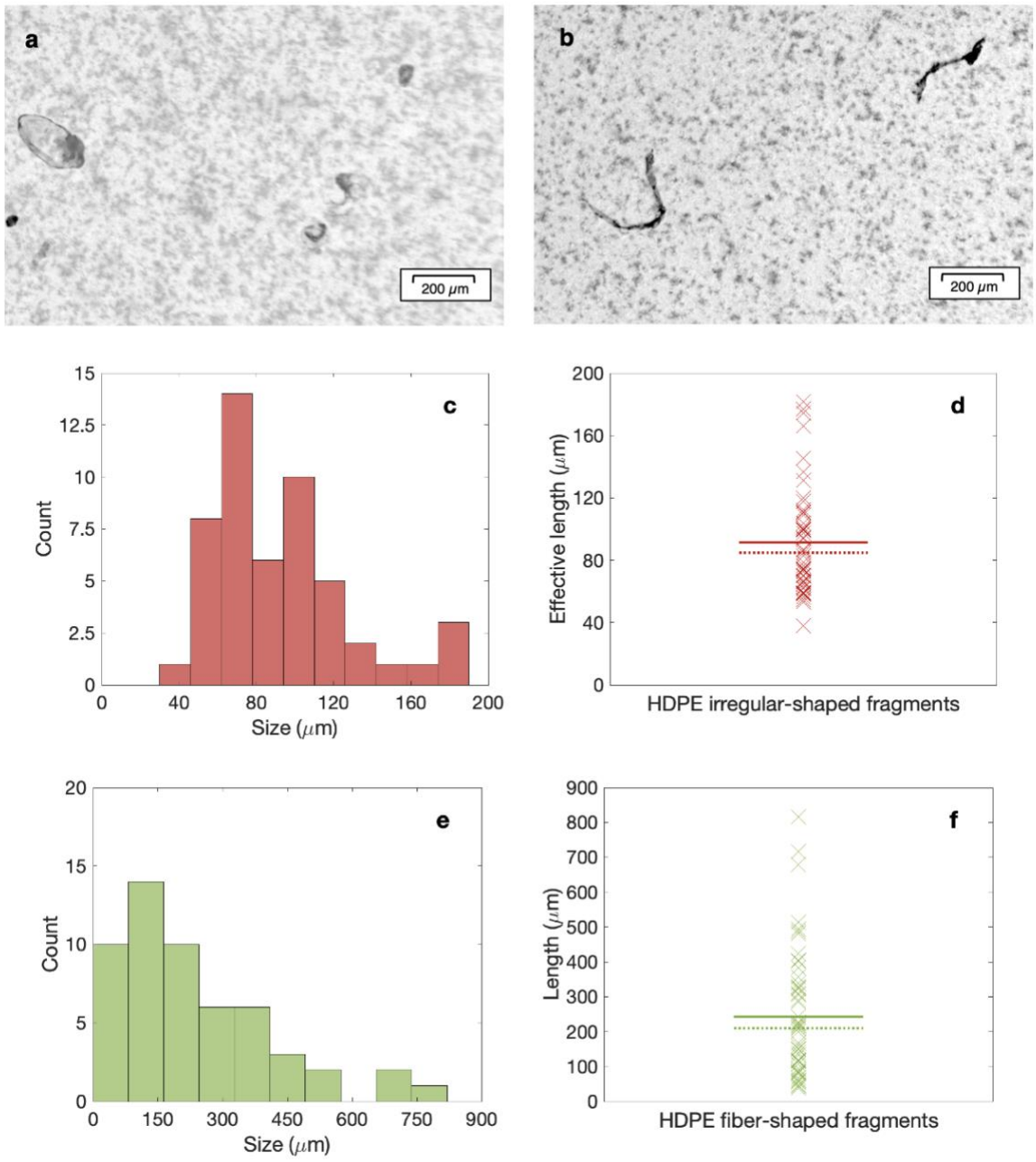

Figure S3.8. Ground high density polyethylene (HDPE) microfragments. Stereomicroscope images of a, irregular-shaped microfragments and b, fiber-shaped microfragments obtained after blending HDPE sheets and collecting the microfragments sieved between 38 and 150 μm mesh stainless steel. Histogram and size distribution of HDPE irregular-shaped fragments (c, d) and fiber-shaped fragments (e, f). Solid line shows the mean size and the dashed line represents the median. Full analysis of HDPE microfragments was conducted with ImageJ for N=54 and N=51 representative fiber-shaped and irregular shaped HDPE microfragments respectively taken from eight separate samples taken from the stock suspension.

Figure S3.9. Pilot scale setup that can hold up to 20 L of synthetic wastewater. To measure TSS, microfiber, and microsphere removal, 100 mL samples were collected from the top valve approximately 3 cm from the surface of the water.

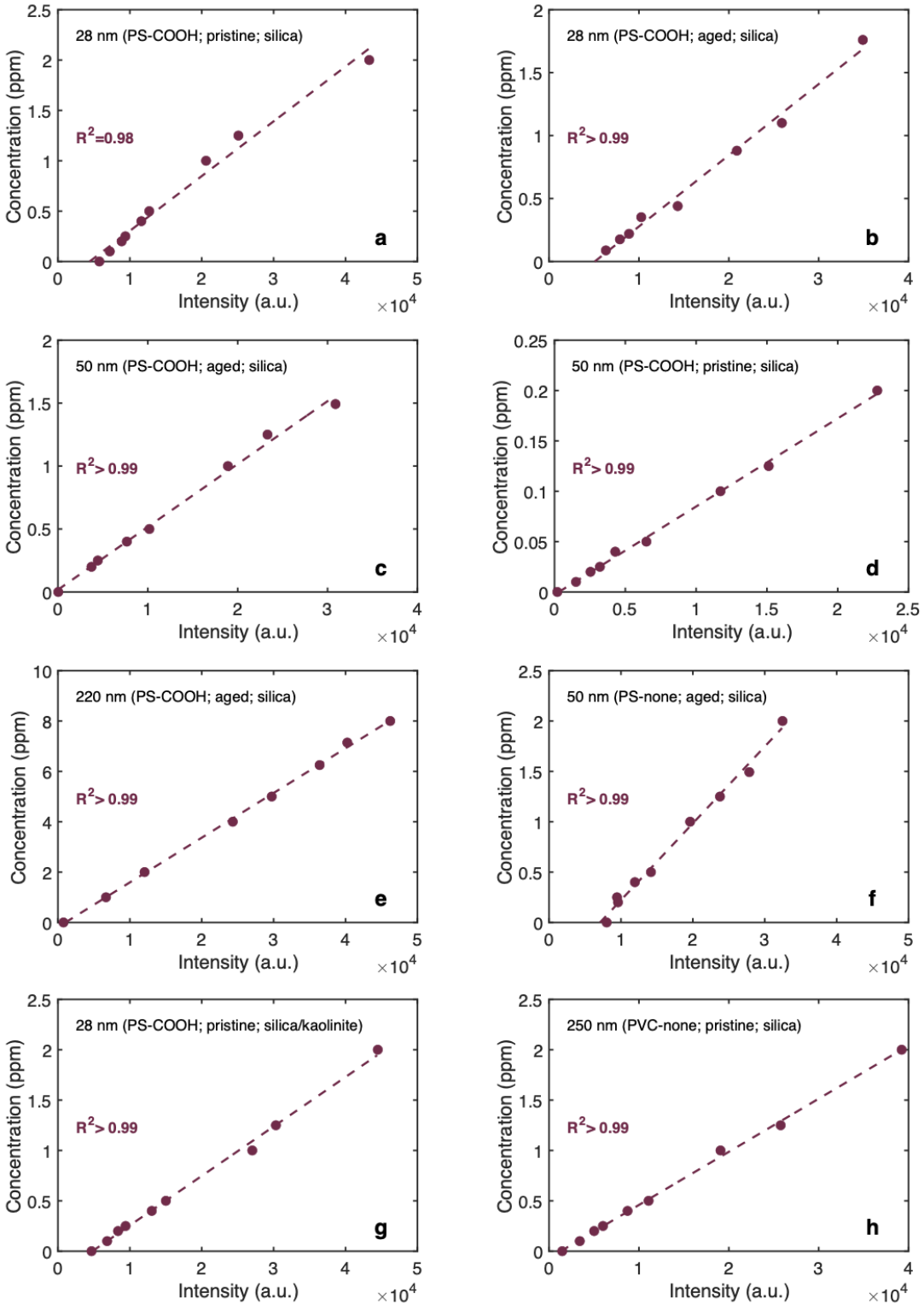

Figure S3.10. Calibration curves for fluorescent polystyrene nanoplastics in synthetic wastewater. Calibration curves of polystyrene and polyvinyl chloride nanoplastics of varying sizes in synthetic wastewater. The text in the figure indicates, the type of plastic (polystyrene or polyvinyl chloride), a given functionalization (carboxylate modified or non-functionalized), aging condition (pristine or aged), and inorganic content type (SiO_2 or mixture of silica and kaolinite).

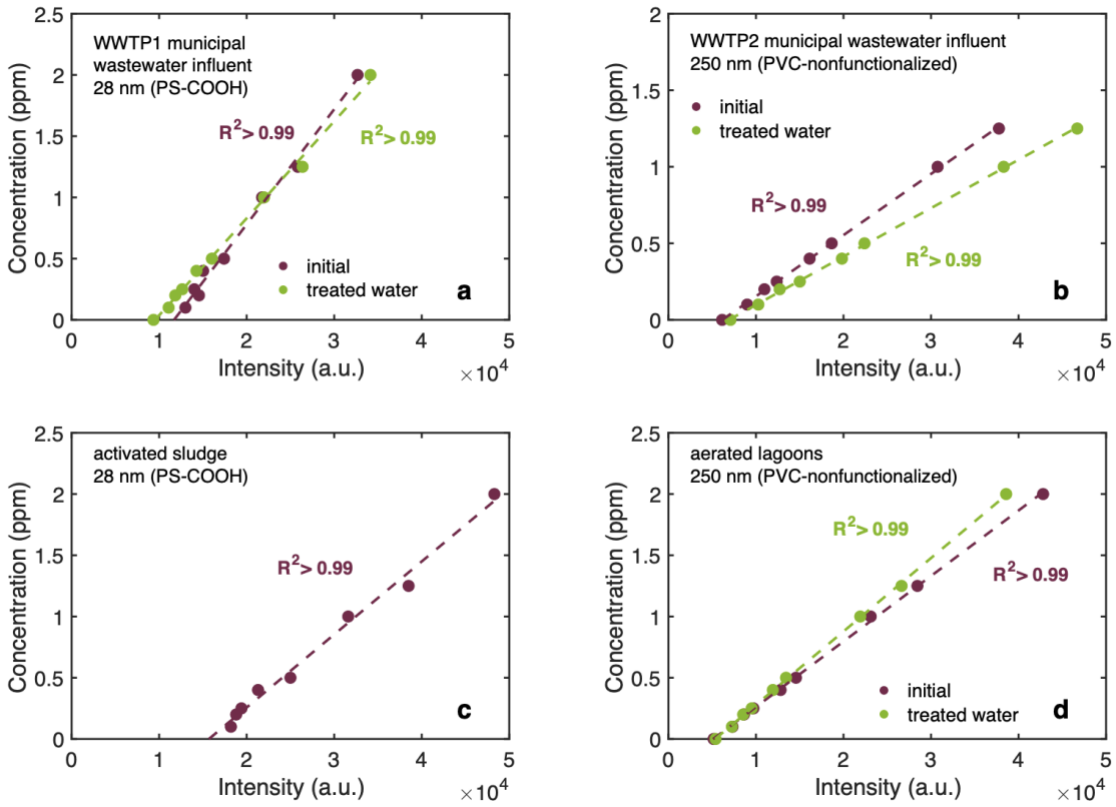

Figure S3.11. Calibration curves for fluorescent polystyrene nanoplastics in municipal wastewater. Calibration curves of pristine carboxylated 28 nm polystyrene nanoplastics or non-functionalized 250 nm PVC nanoplastics in a, initial and treated municipal wastewater influent from WWTP1, b, initial and treated wastewater influent from WWTP2, c, activated sludge treated waters, and d, initial and treated aerated lagoon water samples.

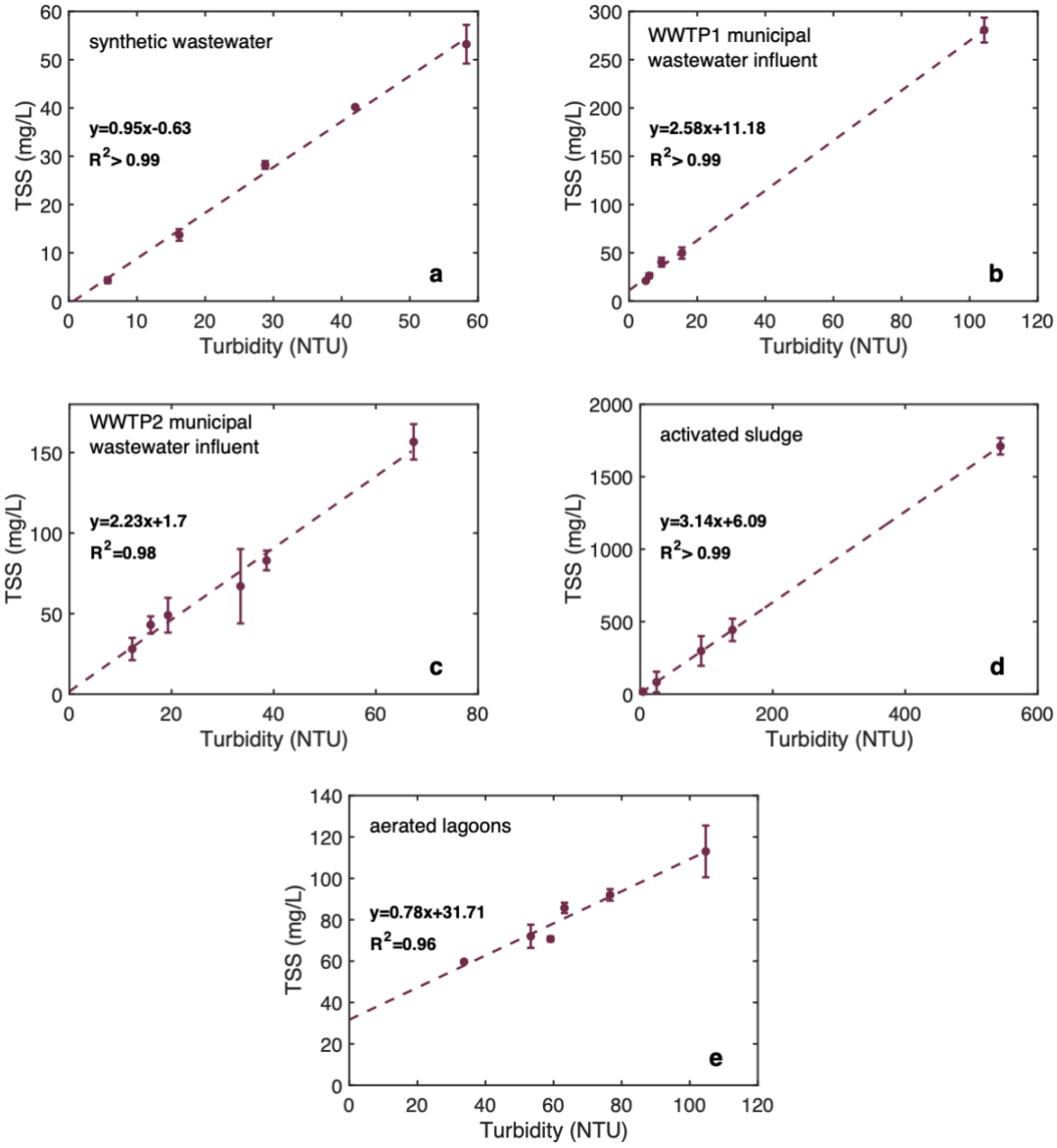

Figure S3.12. Calibration curves for TSS as a function of turbidity. Calibration curves of TSS and Turbidity for a, synthetic wastewater, b, municipal wastewater from WWTP1, c, municipal wastewater influent from WWTP2, d, activated sludge-treated water, and, e, aerated lagoons water samples. All experiments were conducted in triplicates and data are presented as mean values ± the standard deviation.

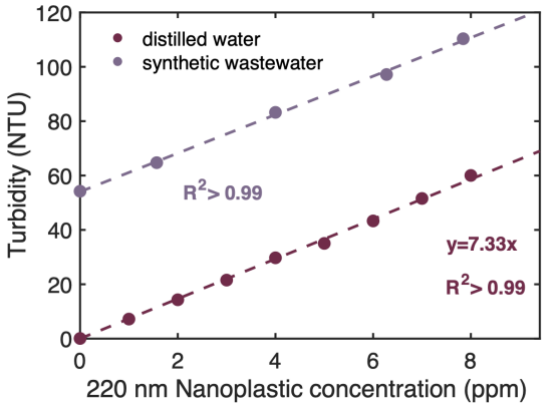

Figure S3.13. Calibration curve for turbidity as a function of 220 nm nanoplastic concentration. Correlation of 220 nm nanoplastic concentration with measured turbidity in distilled water and synthetic wastewater.

Table S3.1. Standard error of TSS removal and nanoplastic removal for jar test replicates performed with municipal wastewater influent. Legend: NP: nanoplastic; PS: polystyrene; PVC: polyvinyl chloride; COOH: carboxylate-modified nanoplastic; none: non-functionalized nanoplastic; aPAM1: polyacrylamide with very low anionic charge density, high molecular weight.

Nanoplastic	Waste-water sample	pH	Flocculant	Settling time (s)	Jar test replicates	Alum dose (mg/L)	TSS removal standard error (%)	NP removal standard error (%)
PS (28 nm; COOH; pristine)	influent (WWTP 1)	8.2	aPAM1 (0.4 mg/L)	180	3	4.54	0.2	1.5
					3	1.82	0.5	1.4
PVC (250 nm; none; pristine)	influent (WWTP 2)	7.5	aPAM1 (0.4 mg/L)	180	3	5.45	1.1	2.0
					3	4.54	1.7	2.3

Table S3.2. Standard error of TSS removal and nanoplastic removal for jar tests performed with water samples from municipal wastewater treatment plant. Legend: NP: nanoplastic; PS: polystyrene; PVC: polyvinyl chloride; COOH: carboxylate-modified nanoplastic; none: non-functionalized nanoplastic.

Nanoplastic	Waste-water sample	pH	Alum dose (mg Al/L)	Jar test replicates	Settling time	TSS removal standard error (%)	NP removal standard error (%)
PS (28 nm; COOH; pristine)	Activated sludge (WWTP 1)	7.1	0	3	130 s	0.7	2.1
				3	100 s	0.4	2.9
PVC (250 nm; none; pristine)	Aerated lagoons (WWTP 2)	7.8	1.82	3	5 min	2.6	3.0
				3	10 min	3.1	2.7
				3	30 min	0.4	3.6

Table S3.3. Standard error of TSS removal and nanoplastic removal for jar tests performed with synthetic wastewater matrix. Legend: NP: nanoplastic; PS: polystyrene; PVC: polyvinyl chloride; COOH: carboxylate-modified nanoplastic; none: non-functionalized nanoplastic; aPAM1: polyacrylamide with very low anionic charge density, high molecular weight; ACH: aluminum chlorohydrate.

Nano-plastic	Synthetic water matrix	Coagulant	Flocculant	Settling time (s)	Jar test replicates	pH	TSS removal standard error (%)	NP removal standard error (%)
PS (28 nm; COOH; pristine)	silica (51 mg/L)	alum (5.45 mg Al/L)	aPAM1 (0.4 mg/L)	30	4	7.0	1.7	2.6
					3	7.4	5.8	8.3
					3	7.8	7.7	3.6
					2	8.2	(39.2, 4.5)[a,b]	(24.1, 5.0)[a,b]
					2	8.6	(9.6, 15.1)[a]	(1.5, 10.1)[a]
PS (28 nm; COOH; pristine)	silica (51 mg/L)	ACH (5.45 mg Al/L)	aPAM1 (0.4 mg/L)	30	3	7.3	1.5	4.2
					3	7.8	5.0	3.1
					4	8.2	7.5	4.1
					4	8.6	13.2	9.0
PS (28 nm; COOH; aged)	silica (51 mg/L)	alum (5.45 mg Al/L)	aPAM1 (0.4 mg/L)	30	4	7.0	4.4	3.8
					3	7.4	2.7	5.7
					3	7.8	15.0	9.3
					2	8.6	(0.0, 19.1)[a]	(20.5, 21.4)[a]
PS (50 nm; COOH; aged)	Silica (51 mg/L)	alum (5.45 mg Al/L)	aPAM1 (0.4 mg/L)	30	3	7.0	2.4	3.8
					3	7.4	2.7	2.1
					3	7.8	17.8	15.8
					3	8.2	3.8	2.7
PS	silica	alum	aPAM1	30	4	7.0	4.7	7.0

(50 nm; none; aged)	(51 mg/L)	(5.45 mg Al/L)	(0.4 mg/L)		2	7.4	(67.0, 62.4)[a]	(41.7, 37.2)[a]
					2	7.8	(17.9, 13.6)[a]	(14.5, 7.2)[a]
PS (220 nm; COOH; aged)	silica (51 mg/L)	alum (5.45 mg Al/L)	aPAM1 (0.4 mg/L)	30	3	7.0	2.2	2.9
					3	7.4	4.1	4.6
					3	7.8	7.3	6.4
					2	8.2	(8.8, 13.0)[a]	(9.3, 5.1)[a]
PVC (250 nm; none; pristine)	silica (51 mg/L)	alum (5.45 mg Al/L)	aPAM1 (0.4 mg/L)	30	3	7.0	0.9	1.1
					3	7.4	9.2	7.1
					6	7.8	7.6	6.2
PS (28 nm; COOH; pristine)	silica (32 mg/L)	alum (5.45 mg Al/L)	aPAM1 (0.4 mg/L)	30	3	7.0	3.6	3.6
					4	7.7	11.7	9.0
PS (28 nm; COOH; pristine)	silica (70 mg/L)	alum (5.45 mg Al/L)	aPAM1 (0.4 mg/L)	30	3	7.0	0.5	1.4
					3	7.6	6.0	5.9
PS (28 nm; COOH; pristine)	kaolinite /silica (51 mg/L)	alum (5.45 mg Al/L)	aPAM1 (0.4 mg/L)	30	4	7.0	0.5	0.5
					7	7.4	9.5	8.2
					3	7.8	8.2	7.6

[a] Where only duplicate jar tests were conducted, the values of TSS removal and NP removal are reported instead of the SE.
[b] As expected, larger variability is observed for sub-optimal coagulation conditions[3].

3.12 Reference

1 O'Melia, C. R. in *The Scientific Basis of Flocculation* 219-268 (Springer, 1978).

2 Ives, K. J. in *The Scientific Basis of Flocculation* 37-61 (Springer, 1978).

3 Duan, J. & Gregory, J. Coagulation by hydrolysing metal salts. *Advances in colloid and interface science* **100**, 475-502 (2003).

Preface to Chapter 4:

As seen in Chapter 3, coagulation, flocculation, and settling systems in typical North American wastewater treatment plants were estimated to remove between 39-70% of nanoplastic contaminants in plants using conventional coagulant (alum) and flocculant (anionic PAM). Similarly, microfiber removal showed greater than 90% removal under optimal wastewater treatment conditions. However, the pH of the water sample was identified as an important parameter that can impact alum's coagulation performance leading to suboptimal treatment conditions. In the following chapter, alum's ability to remove micro- and nanoplastics was systemically assessed in synthetic wastewater with pH values of 7, 7.4, 7.8, 8.2 and 8.6. Additional experiments were then conducted with alternative coagulants, including aluminum chlorohydrate (ACH) and cationic polyamines (pDADMAC), to improve alum's performance during challenging pH conditions. We hypothesized that the addition of cationic coagulants can improve the removal of negatively charged plastic contaminants. This study also included a quartz crystal microbalance with dissipation monitoring to investigate the interactions between the three coagulants (alum, ACH, and ACH+pDADMAC) with a model negatively charged surface. The importance of this study was to offer municipalities alternative solutions to alum that can improve plastic contaminant removal during challenging treatment conditions. In addition, this study serves to further enhance the understanding of plastic interactions with coagulants during the physicochemical treatment process.

Chapter 4: Microplastics and nanoplastics in water: Improving removal in wastewater treatment plants with alternative coagulants

Abstract

Due to the growing concerns of plastic pollution release into water bodies, it is imperative to understand and assess the removal of nanoplastics and microplastics during wastewater treatment processes. Although earlier studies have shown high removal of plastic contaminants during coagulation, flocculation and settling, a limited number of experiments have examined the removal of nanoplastics in relevant water chemistries including higher pH values and in the presence of organics. In this study, the removal of nanoplastics and microfibers is assessed using conventional (alum) and alternative coagulants including aluminum chlorohydrate (ACH) and cationic polyamines (pDADMAC) in a synthetic wastewater matrix for pH conditions between 7 and 8.6. Our results show that plastic removal is considerably reduced at higher pH values when alum is used as a coagulant. At the shorter settling time of 30 s, removal of pristine and aged nanoplastics declined from 64 ± 3% and 76 ± 3% respectively (pH 7) to less than 20% at pH values greater than 7.8. Similarly, polyester microfiber removal was observed to decline from 97 ± 1% at pH 7 to 85 ± 3% at pH 8.6 for samples collected after 3 min of settling. Replacing alum with polynuclear aluminum coagulants resulted in greater plastic contaminant removal at pH values above 8 with a maximum observed microfiber removal of 95 ± 1% (ACH; pH 8.6; 3 min settling time) and a maximum observed nanoplastic removal of 71 ± 5% (ACH+pDADMAC; pH 8.2; 30 s settling time). Quartz crystal microbalance with dissipation (QCM-D) measurements revealed that ACH coagulant species results in a thicker deposition layer on negatively charged surfaces compared to alum. The addition of pDADMAC to ACH led to a more favorable interaction with a model negatively

charged surface, indicated by a faster and more rigid deposition of the alternative coagulant. Taken together, these results show that environmental conditions, including water pH and presence of wastewater colloids, affect plastic contaminant removal during primary wastewater treatment. Alternative coagulants, particularly ones that contain stable cationic species, offer municipalities improved removal of plastic contaminants under these challenging treatment conditions.

4.1 Introduction

The presence of microplastics and nanoplastics in water bodies is expected to increase with the continuous rise in global plastic production. Several studies have already reported the presence of microplastics in various water bodies including oceans[1,2], estuaries[3], freshwater[4], urban rivers[5], lakes[6], and groundwater[7]. Of these plastic contaminants, microfibers were found to be the dominant shape of microplastics in wastewater effluents[8] likely originating from washing machine discharges that contain synthetic textile material[9-12]. Degradation of single-use polypropylene facemasks is also expected to introduce plastic microfibers to natural waters[13]. Recent estimates show that synthetic textiles account for approximately 35% of all primary microplastic release into the environment and constitute the main source of microplastic release in developing countries[14]. Bulk plastic and microplastic litter can further degrade into nanoplastics due to environmental weathering[15,16]. Nanoplastics can be produced following washing and abrasion of synthetic textiles[17], degradation of polyethylene and polypropylene plastic debris[18], and mechanical degradation of polystyrene coffee cup lids and expanded polystyrene foam[19]. Nanoplastics are also expected to be released into domestic wastewaters from the use of microbead-containing personal care products[20].

To limit the release of microfibers and nanoplastics into the aquatic environment, it is imperative to assess and improve the ability of existing water treatment plants to remove these

contaminants. Since primary settling tanks represent the most common primary treatment process found in wastewater treatment plants[21], coagulation, flocculation and settling processes present an ideal treatment stage to remove microfibers and nanoplastics. Using alum as a coagulant, Lapointe *et al.*[22] were able to successfully remove more than 99% of polyester microfibers (105 – 1325 µm in length) at pH 7. Li *et al.*[23] showed microfiber removal greater than 90% with 30 mg/L of ferric chloride ($FeCl_3$) from real laundry wastewater and up to 99% microfiber removal with 3 mg/L of polyaluminum chloride. Similarly, Gong *et al.*[24] were able to achieve more than 95% removal of carboxyl-modified polystyrene nanoplastics using $AlCl_3$, $FeCl_3$, and polyaluminum chloride coagulants at a concentration of 10 mg/L. More than 85% of non-functionalized 50, 100, and 500 nm polystyrene nanoparticles were also removed when polyaluminum chloride was used as a coagulant[25].

Although these results show high microfiber and nanoplastic removal, it is important to study the effect of water conditions such as pH and organic content on treatment performance since conventional coagulants are known to be influenced by these conditions. Final pH values can range from 6-9.5 according to regulatory standards of wastewater effluent in Québec[26]. Such a change in pH will affect coagulation behaviour as seen with the decline in the removal of polyester microplastics (140 µm) from 89% at pH 7 to 69% at pH 8 when treated with alum[22]. A decrease in polyethylene microplastic removal was also observed by Ma *et al.* using $AlCl_3$ as a coagulant when the pH was increased from 6 to 8 (27% to 22% removal)[27]. The effect of pH on nanoplastic removal with $AlCl_3$ showed a similar behavior where an increase of initial pH from 8 to 10 resulted in a reduction of nanoplastic removal from 95% to 83.4% [24]. The importance of water type is also shown to impact removal as seen in the experimental work presented by Gong *et al.*[24] where the coagulation process in filtered surface water resulted in significantly lower polystyrene nanoplastic removal compared to pure deionized (DI) water (90.2% versus 96.6% nanoplastic removal). Therefore, to improve the treatment performance

of physicochemical processes for microfibers and nanoplastics, it is essential to understand the removal of these contaminants under varying environmental conditions.

In this study, the removal of microfibers and nanoplastics was explored through coagulation, flocculation and settling experiments under environmentally relevant conditions for conventional alum coagulant. All experiments were conducted in synthetic wastewater with a final pH range of 7-8.6. In addition, the removal of microfibers and nanoplastics was tested using alternative coagulants, including aluminum chlorohydrate (ACH) and a mixture of ACH and pDADMAC as well as alternative flocculants including anionic and cationic polyacrylamide flocculants. Quartz crystal microbalance with dissipation monitoring (QCM-D) was employed in this study to investigate the underlying interactions of coagulants with negatively-charged contaminants.

4.2 Materials and Methods

Chemicals and materials

Plastic contaminants tested in this study included fluorescent 28 nm carboxylate-modified polystyrene nanoplastics (FluoSpheres, ex/em: 365/415 nm) and microfibers obtained from blended polyester (PEST) textile implemented in previous work[28]. To produce the microfibers, a Ninja blender (~1200 rpm) was used to blend commercial polyester textile (SanMar Canada, ATC, ATC3600Y) for 5 min at 22 °C. The blended fibers were sieved with a 250 µm mesh stainless steel sieve resulting in PEST microfibers with a length between 105 and 1325 µm[28]. For experiments with aged nanoplastics, pristine nanoplastics (1 mL of a 200 mg/L stock suspension) were incubated in a 50 mL centrifuge tube containing 20 mL of synthetic wastewater to reach a concentration of 9.5 mg/L. The incubated nanoplastics were left on a shaker at a speed of 50 rpm for 18 h in the dark. Three aluminum-based coagulants, alum (ALS, Kemira Water Solutions Canada, Inc.), aluminum chlorohydrate (ACH) (PAX XL1900,

Kemira Water Solutions Canada, Inc.), and ACH+pDADMAC (PAX XL 3932J, Kemira Water Solutions Canada, Inc.) were used in this study. Four polyacrylamide (PAM) flocculants were tested including: low MW anionic PAM (aPAM1, charge density <5%, Veolia Water Technologies), high MW anionic PAM (aPAM2, charge density <5%, Kemira Water Solutions Canada, Inc.), low MW cationic PAM (cPAM1, charge density ≈ 7%, Kemira Water Solutions Canada, Inc.), low MW cationic PAM (cPAM2, charge density ≈ 20%, Kemira Water Solutions Canada, Inc.). All stock solutions were stored in the dark at 4 °C.

Jar test procedure

Jar test experiments were conducted in synthetic wastewater adapted from the synthetic sewage wastewater recipe from the OECD[29]. Briefly, a synthetic wastewater concentrate was prepared using 0.8 g of peptone, 0.55 g of meat extract, 0.15 g of urea, 35 mg of sodium chloride (NaCl), 20 mg of calcium chloride ($CaCl_2$), 1 mg of magnesium sulfate heptahydrate ($MgSO_4 \cdot 7H_2O$), and 0.14 g of dipotassium phosphate (K_2HPO_4) dissolved in 500 mL of deionized water. To adjust the pH to 8, 300 µL of a 2 M NaOH solution was added to the concentrate. Each jar test contained 20 mL of the synthetic wastewater concentrate and 230 mL of tap water that was then spiked with 350 µL of a 40 g/L silica particle suspension (~80% between 1-5 µm diameter, S5631, Sigma-Aldrich) to reach an average TSS concentration of 51 ± 1.5 mg/L. Pristine nanoplastics were then added to 250 mL of synthetic wastewater to achieve a concentration of 0.8 mg/L (1 mL of a 200 mg/L stock suspension). Microfibers were also added to the jar to achieve a number concentration of 1000 microfibers/L (2.31 mL of a stock solution of 108 ± 11 microfibers/mL). For experiments with aged nanoplastics, 20 mL of synthetic wastewater containing the incubated nanoplastics (9.5 mg/L) were added to 230 mL of synthetic wastewater to achieve a nanoplastic concentration of 0.8 mg/L. The pH of the solution was adjusted by adding 2 M NaOH and 1 M HCl before the onset of the jar test procedure to achieve the target pH. After spiking the synthetic wastewater with the plastic contaminants, the

coagulant was added at a concentration of 5.45 mg Al/L and mixed for 2 min at a speed of 110 rpm. The concentration of alum was optimized to reach a turbidity value less than 10 NTU after 3 min of settling in jar tests containing synthetic wastewater spiked with polyester microfibers at a concentration of 1000 microfibers/L (Fig. S4.1). This was followed by a 2 min flocculation period with the addition of 0.4 mg PAM/L at the same speed of 110 rpm. Half of the total dosage of PAM (0.2 mg PAM/L) was added at the onset of flocculation, while the other half was added at mid-flocculation to avoid floc breakage[22,30,31]. Stirring was stopped after the flocculation period and samples were collected at 30 s and 3 min of settling from a depth of 3 cm below the water surface level. Results obtained after 30 s of settling reveal the ability of the coagulation-flocculation process to remove contaminants rapidly and effectively which can impact the operating cost of the process. Meanwhile, results after 3 min of settling reveal the removal of contaminants when the majority of flocs have been settled.

The concentrations of pristine and aged nanoplastics were determined by measuring fluorescence intensity (Spark microplate reader, Tecan) with a corresponding calibration curve in synthetic wastewater (linear relation, $R^2 > 0.98$, Fig. S4.2). To measure microfiber removal, 100 mL samples were collected from each jar test after 3 min of settling. The sample was then filtered with a 5 µm mixed cellulose ester membrane (MF-Millipore®, membrane filter) and the number of microfibers on the membranes were counted using a stereomicroscope (Olympus, model SZX16).

To measure the phosphorus concentration after treatment, 50 mL of treated water from each jar was filtered with a 0.45 µm mixed cellulose ester membrane (MF-Millipore®, membrane filter). The concentration of phosphorus was measured in triplicates by Eurofins Environex (Québec, Canada) using inductively coupled plasma mass spectrometry (ICP-MS, ICAP, Thermo Fisher Scientific). The initial concentration of soluble phosphorus in untreated synthetic wastewater is 5.0 ± 0.5 mg/L based on the recipe implemented in this study[32,33].

Floc imaging and sizing

To measure floc sizes, samples were collected 10 s before the end of the flocculation period at a distance of 3 cm below the water surface. An inverted fluorescence microscope (Olympus, model IX71) with brightfield imaging was then used to take optical images of the flocs. Analysis of floc sizes was performed with ImageJ software for at least 20 representative flocs from three separate jar tests. The length of the floc was calculated assuming an ellipse shape with an equivalent diameter = $(L \cdot W)^{0.5}$ where L and W are the length and width of the floc[34]. For SEM images, settled flocs were collected and placed on carbon tape, dried for 24 h, and coated with 4 nm of platinum (Leica Microsystems, EM ACE600 High Resolution Sputter Coater). The electron microscopy images (FEI Quanta 450 environmental scanning electron microscope) were obtained at 5 kV (secondary electrons), while the elemental analysis obtained by energy-dispersive X-ray spectroscopy was performed at 10 kV. Elemental mapping was analyzed with EDAX Octane Super 60 mm^2 SDD and TEAM EDS Analysis System.

Quartz Crystal Microbalance with Dissipation Monitoring (QCM-D) measurements

QSense Explorer was used to study the affinity of the three coagulants to a 5 MHz AT-cut crystal with silica-coated surface (QSX 303, QSense). All three coagulant samples were prepared to reach a final concentration of 5.45 mg Al/L in 250 mL of pre-filtered (0.2 µm) DI water. To control the pH of the coagulant sample, NaOH (0.5 mol/L) and HCl (1 mol/L) were added to reach a pH of 7 ± 0.2 for alum and 8.5 ± 0.2 for ACH and ACH+pDADMAC. A peristaltic pump was used to flow pre-filtered DI water with the same pH as the selected coagulant at a rate of 100 µL/min. The changes in frequency shifts (Δf) and dissipation (ΔD) were measured for five min using the filtered DI water at an identical pH to establish a baseline. The coagulant sample (5.45 mg Al/L) was then pumped into the flow module at an identical

flowrate of 100 µL/min. The Δf and ΔD responses of the crystal to the coagulant were reported for the third overtone (n=3). It should be noted that the frequency shift obtained from the QCM-D (Q-Sense) is already normalized when using standard software settings such that $\Delta f_{(n)} = \Delta f_n/n$. Three separate experiments were conducted for each coagulant to measure frequency shift and dissipation shift as a function of time (Fig. S4.3).

Before each measurement, the silica-coated sensor (QSX 303, QSense) was cleaned three times in 0.2 µm pre-filtered DI water, soaked in 0.2 µm pre-filtered Hellmanex (1%) and bath sonicated for 20 min[35]. Following sonication, the sensor was rinsed 10 times with DI water, 3 times with ethanol and dried under nitrogen gas. Finally, the sensor was exposed to UV/ozone treatment for 45 min (UV chamber, Bioforce Nanosciences). To clean the crystal, chamber, and tubing after each measurement, pre-filtered DI water was pumped into the chamber for five min, followed by 1% Hellmanex for one min, and then DI water for five additional min.

4.3 Results and Discussion

Microfiber and nanoplastic removal using alum as a coagulant

A maximum observed nanoplastic removal of 64 ± 3% was reached at pH 7 with an alum concentration of 5.45 mg/L for samples collected after 30 s of settling (Fig. 4.1a). Nanoplastic removal was observed to be largely impacted by increasing pH with a measured nanoplastic removal below 10% for all pH values greater than 8. To study the effect of nanoplastic aging on their behaviour during physicochemical treatment, nanoplastics were incubated in synthetic wastewater for 18 h. The incubation period is introduced in this study to mimic the potential interactions between wastewater colloids and nanoplastics that occur during nanoplastic transport in sanitary sewer systems. Following coagulation with alum, nanoplastic removal at pH 7 is seen to be significantly greater for aged nanoplastics compared to pristine nanoplastics (76 ± 4% versus 64 ± 3% respectively, Fig. 4.1b). At higher pH values, the aged nanoplastics

showed the same decline in removal to reach values lower than 20% at all pH values above 8 as noted previously for pristine nanoplastics.

The lower nanoplastic removal in more alkaline conditions can be explained by the effect of pH on the behaviour of alum during coagulation. When alum is used as a coagulant, colloid destabilization can occur through charge neutralization or sweep flocculation. Given the alum dose of 60 mg/L used in this study, sweep flocculation is expected to be the dominant removal mechanism across the pH range of 7–9.[36] In this flocculation regime, the concentration of the added alum is beyond the solubility limit which results in excess alum hydrolyzing to amorphous $Al(OH)_3$ that entraps the colloids within the precipitating aluminum hydroxide[36]. In alkaline conditions, hydrolyzed alum species are known to be negatively charged. Although the charge of $Al(OH)_3$ is positive at a pH of 7–8, the charge of $Al(OH)_3$ becomes weakly negative at pH values greater than 8.[37] In addition, the concentration of negatively charged $Al(OH)_4^-$ increases with pH[36]. The excess of negatively charged soluble and insoluble alum species is expected to impact their affinity to negatively charged colloids in the wastewater as well as the anionic polyacrylamide used in the flocculation stage[38]. This increase in electrostatic repulsion between coagulation species and flocculants and contaminants can possibly explain the smaller flocs formed at higher pH values. Floc images revealed that flocs formed at pH 7 had an average size of 541 µm compared to 296 µm for flocs formed at pH 8 (Fig. S4.4). In addition, roughly 26% of flocs produced at pH 7 were larger than 750 µm compared to only 1% for pH 8. Therefore, nanoplastic removal in samples measured after 30 s of settling at pH 8 is expected to be lower since these smaller flocs require a longer time to settle.

Nanoplastic removal after 3 min of settling takes into account any nanoplastics removed with smaller flocs that take longer to settle (Fig. 4.1c). Although a significant decline in pristine nanoplastics removal was observed at the lower settling time (30 s) with alum, the results after

3 min show no significant difference in removal between pH 7 and higher pH levels ($p>0.05$, two sample *t*-test). This result shows that nanoplastics are entrapped in the smaller flocs produced at higher pH. Interestingly, the lowest nanoplastic removal for both pristine and aged nanoplastics after 3 min of settling is seen at pH 7.8. Removal of aged nanoplastics at pH 7.8 is significantly lower than removal at pH 7 and 8.6 ($p=0.002$ and 0.004 respectively). Zeta potential and DLS measurements reveal that the polystyrene nanoplastics maintain a negative surface charge (< -30 mV) with minimal aggregation across the pH range of 7.0-8.5 (Fig. S4.5). Therefore, the improved removal at pH values greater than 8 can be due to the high quantity of smaller flocs produced based on $Al(OH)_3$ precipitates that possibly induces more collisions between nanoplastics and flocs thereby enhancing sweep flocculation. Even with the excess of anionic species at high pH, a high concentration of alum can lead to high nanoplastic removal after the longer settling time. The similar removal of pristine and aged nanoplastics shows that the behaviour of nanoplastics in coagulation, flocculation and settling is comparable when sweep flocculation dominates[39].

On the other hand, microfibers showed a significant difference in removal at varying pH conditions after 3 min of settling. At an optimal pH of 7, coagulation with alum achieves high removal of polyester microfibers (97 ± 1%) (Fig. 4.1d). This result agrees with earlier coagulation studies that showed a 99% polyester fiber removal (mean floc diameter of 977 ± 36 µm) when alum (2.73 mg Al/L) and PAM (0.3 mg/L) were added as a coagulant and flocculant, respectively[22]. Similarly, Shahi et al.[40] observed a 81.8% removal of elongated polyethylene (10-100 µm) with alum (30 mg/L). The high fiber removal was attributed to the shape of microplastics with a recent meta-analysis revealing that microplastics shaped like fibers have the highest removal in the coagulation and sedimentation process[41]. However, increasing the pH of wastewater in this study showed a decrease of microfiber removal reaching 85 ± 3% removal at a pH of 8.6. A similar decline in removal was also reported for

polyester microspheres (140 µm) with a reduced removal of 69% at pH 8 when alum was used as a coagulant [22].

The different effects of pH conditions on nanoplastic and microfiber removal after 3 min of settling can be explained by the attachment process of each contaminant. In the sweep coagulation regime, the removal of microfibers is expected to be dominated by the attachment of microfibers to flocs[13,22]. As can be seen in the SEM image (Fig. 4.2), the microfiber appears to be enmeshed in the aluminum-based floc along with silica particles that constitute the inorganic colloids in the synthetic wastewater. The effect of pH on the removal of microfibers can be attributed to the size and charge of the produced flocs. Due to the length of microfibers (160 – 1500 µm), it is expected that microfibers are less likely to enmesh with smaller flocs produced at pH > 8 than the larger flocs produced at pH < 8. The effect of floc size on microplastic removal was also shown in the study by Lapointe et al.[22]. When the floc size was reduced by lowering the dose of flocculant, a significant decrease in the removal of 140 µm microspheres was observed, while the removal of smaller 15 µm microspheres was not affected. Similarly in this study, the smaller flocs impacted the removal of microfibers but not the smaller-sized nanoplastics. The different removal behaviour between microfibers and nanoplastics further supports the need to differentiate between the unique physicochemical behaviors of nanoplastics and microplastics[42,43]. In addition, the weakly negative charge of $Al(OH)_3$ that precipitates at pH values greater than 8 can result in electrostatic repulsion with the negatively-charged polyester microfibers resulting in a lower likelihood of microfiber enmeshment in the aluminum hydroxide based flocs.

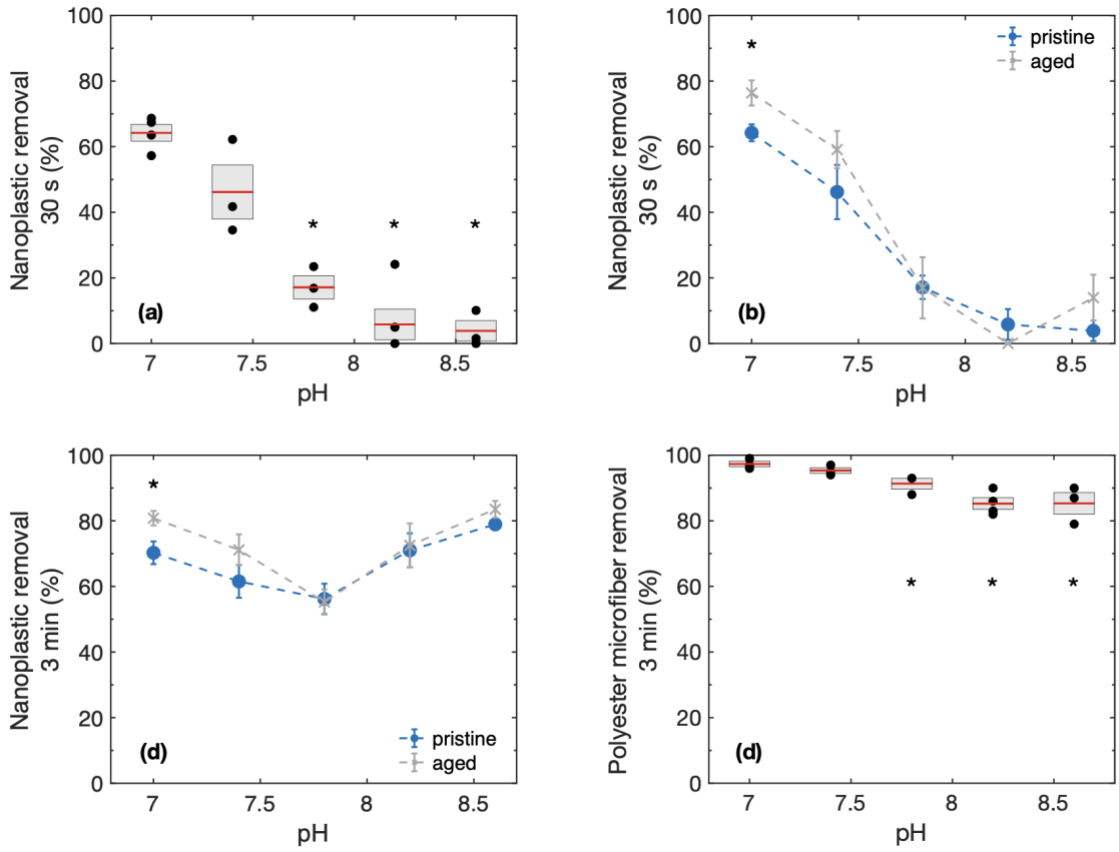

Figure 4.1. (a) Removal of pristine nanoplastics as a function of final pH conditions of water after 30 s of settling. Removal of pristine (circle) and aged (star) nanoplastics after (c) 30 s of settling and (d) 3 min of settling. (d) Removal of polyester microfibers after 3 min of settling. Conditions: 5.45 mg Al/L of alum, 0.4 mg/L of anionic PAM; 2 min of coagulation and 2 min of flocculation at 110 rpm. Legend: * indicates statistically significant difference ($p < 0.05$; two sample *t*-test) with respect to contaminant removal with alum at pH 7. The data shown in Fig. 4.1a and b shows nanoplastic removal as a function of pH, sourced from the same dataset as Abi Farraj et al.[39].

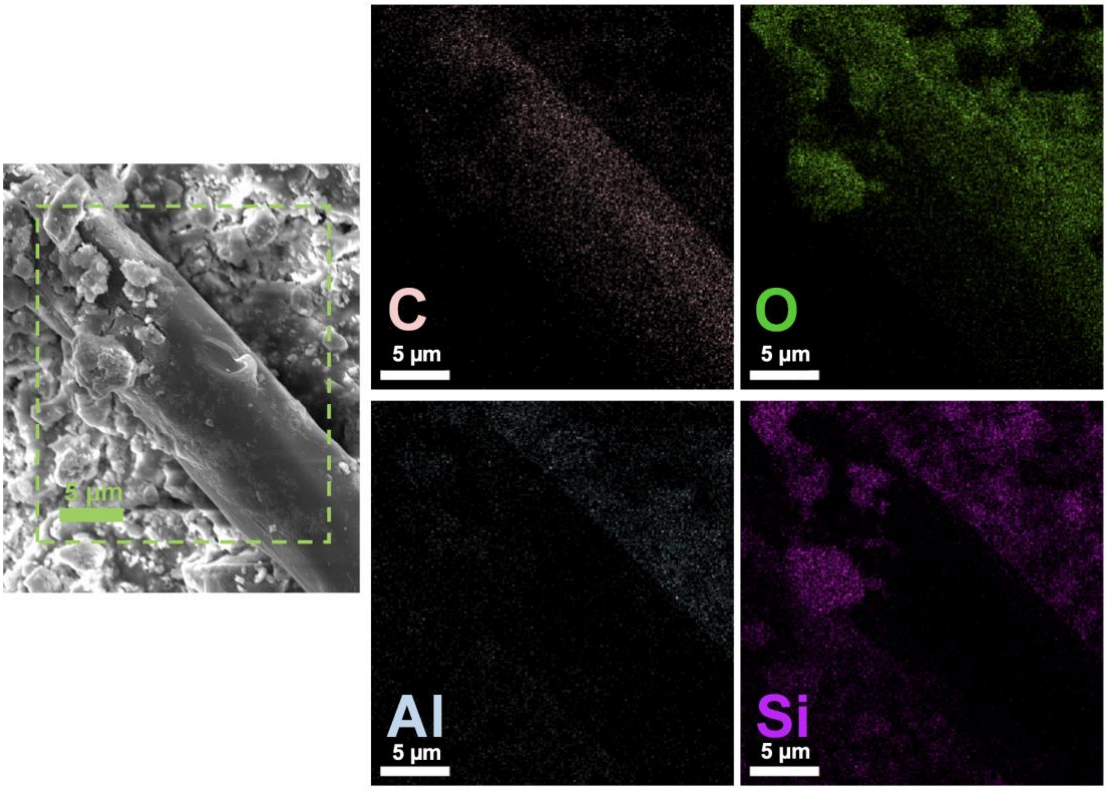

Figure 4.2. Scanning electron microscope image of polyester microfiber embedded in a settled floc and the corresponding EDS elemental mapping showing the presence of carbon, oxygen, aluminum (as Al hydroxides obtained from alum), and silicon (scale bars = 5 µm).

Microfiber and nanoplastic removal with alternative coagulants in alkaline conditions

Aluminum chlorohydrate (ACH) is a prehydrolyzed aluminum-based coagulant containing positively charged polymeric aluminum species including $AlO_4Al_{12}(OH)_{24}(H_2O)_{12}^{7+}$ and $[Al_{30}O_8(OH)_{56}(H_2O)_{24}]^{18+}$, known as Al_{13} and Al_{30}, respectively[44]. In contrast to monomeric Al hydroxide species from alum, the hydrolyzed cationic species formed from ACH are stable at a wider pH range[45]. Using ACH as a coagulant resulted in a significantly greater nanoplastic removal compared to alum at all pH values greater than 7.8 ($p<0.05$) for samples collected after 30 s of settling (Fig. 4.3a). The introduction of cationic polyaluminum species is seen to improve the removal of nanoplastics due to the stable flocs produced at that pH range as well as a possible enhanced charge neutralization of colloids. It is worth noting that the nanoplastic removal significantly decreased for ACH at higher pH conditions ($p<0.05$ for data points

compared to pH 7.8). Al_{13} and Al_{30} species show lower zeta potential at high pH which can explain the decrease of nanoplastics removal with ACH[46]. The role of the cationic species in improving nanoplastic removal at short settling times is further supported when pDADMAC is introduced with ACH. Nanoplastic removal at pH 8.2 is seen to be significantly greater for ACH+pDADMAC at 75 ± 3% removal compared to ACH at 42 ± 4% ($p<0.05$). Therefore, the addition of cationic pDADMAC is seen to compensate for the loss of cationic charge on the polyaluminum nuclear species to ensure the rapid removal of nanoplastics.

For samples collected after 3 min of settling, ACH as well as ACH added in combination with pDADMAC significantly improves nanoplastic removal compared to alum at pH 7.8 ($p=0.035$ and $p=0.002$ respectively; Fig. 4.3b). In addition, nanoplastic removal with ACH+pDADMAC is seen to be significantly greater than ACH alone ($p=0.046$ at pH 7.8). Therefore, at pH conditions of 7.8, the cationic pDADMAC species play an important role in contaminant removal particularly through destabilizing the nanoplastic contaminants. For pH values greater than 8.2, there was no significant difference in nanoplastic removal between alum, ACH, and ACH+pDADMAC. This finding supports the hypothesis that in highly alkaline conditions, sweep flocculation by alum compensates for the loss in cationic species and results in similarly high nanoplastic removal given enough settling time.

Microfiber removal also revealed significant improvement when polynuclear aluminum coagulants are added. Jar test experiments show that ACH maintains high removal of microfibers in alkaline conditions and offers a significantly greater removal than alum (Fig. 4.3c). This result shows that cationic species that are stable at higher pH values can improve removal of negatively charged colloids and microfibers. However, introducing additional cationic species to the coagulant via pDADMAC addition resulted in a wide variation in microfiber removal at high pH values. Microscopy images reveal that the low microfiber removal can be attributed to small flocs that are floating on the surface of the water (Fig. S4.6).

These small flocs are suspected to form due to the strong cationic nature of pDADMAC as was later confirmed in the QCM-D analysis. As mentioned earlier, microfiber removal was determined by counting the number of microfibers left in suspension after the prescribed settling time. Since this concentration measurement includes any flocs suspended near the surface, the incorporation of microfibers into these smaller floating flocs can explain the lower observed removal.

Although alkaline conditions did not appear to affect nanoplastic removal with alum at long settling times, there was observed decline in phosphorus removal (Fig. 4.3d). Final phosphorus concentration with alum achieved a concentration less than 1 mg/L at pH 7 (initial concentration = 5.0 ± 0.5 mg/L). As the pH increased, the phosphorus removal declined with final concentrations reaching 1.17 ± 0.27 mg/L (removal of 77%) at pH 8.2 and 1.75 ± 0.03 mg/L (removal of 65%) at pH 8.6. Orthophosphate is known to be removed through direct adsorption on coagulant species or (co)precipitation with Al^{3+}.[47] At pH values above 8, phosphorus forms PO_3^{4-} and the lack of cationic aluminum-based species results in ineffective removal of phosphorus[48]. Therefore, the loss of cationic species at high pH conditions is seen to affect phosphorus and microfiber removal but does not impact nanoplastic removal at a longer settling time. Although ACH-based coagulants were seen to improve contaminant removal at higher pH, ACH and ACH+pDADMAC showed poor phosphorus removal regardless of pH when compared to alum. The improved phosphorus removal with alum compared to ACH can be attributed to the high basicity of pre-hydrolyzed aluminum coagulants. ACH coagulant species contain hydroxyl groups that are strongly bound to Al which prevents them from forming inner-sphere complexes with phosphates[49]. In contrast to alum, the lowest phosphorus concentration for these coagulants was achieved at the highest pH condition of 8.6 with a final concentration of 2.87 ± 0.09 mg/L (removal of 43%) and 2.56 ± 0.22 mg/L (removal of 49%) for ACH and ACH+pDADMAC, respectively. The improved

removal of phosphorus at higher pH with ACH was also observed in previous work[50] which was attributed to the lower overall alkalinity at high pH which can improve precipitation efficiency of phosphate salts[51].

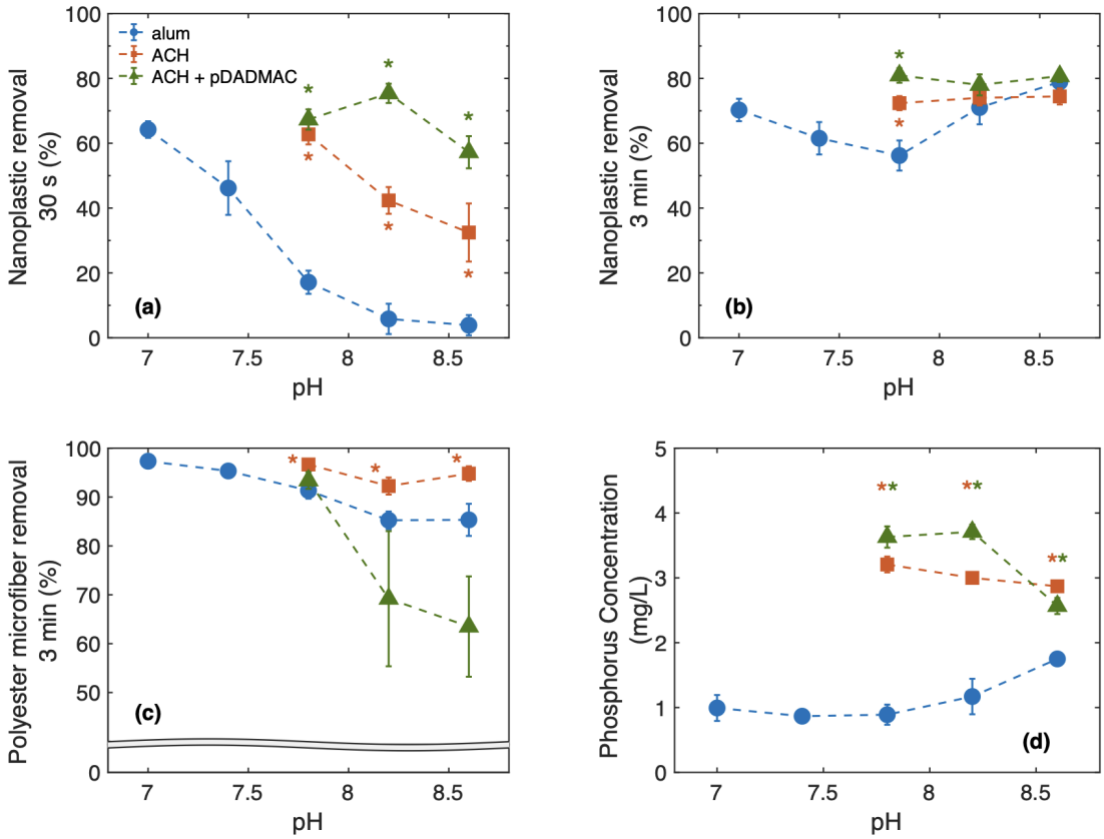

Figure 4.3. Comparison between alum (circle), ACH (square) and ACH+pDADMAC (triangle) coagulants on the (a) removal of pristine nanoplastics after 30 s of settling, (b) removal of pristine nanoplastics after 3 min of settling, (c) removal of polyester microfibers after 3 min of settling, and (d) final phosphorus concentrations. Conditions: 5.45 mg Al/L of coagulant; 0.4 mg/L of anionic PAM; 2 min of coagulation and 2 min of flocculation at 110 rpm with a final pH between 7 and 8.6 ± 0.2; initial concentration of 5.0 ± 0.5 mg/L mg phosphorus/L [32,33]. Each data point represents an average of at least three measurements and the error bar indicates standard error. Legend: * indicates statistically significant difference ($p<0.05$; two sample *t*-test) of contaminant removal when comparing ACH (orange) or ACH+pDADMAC (green) to alum. The data points for alum and ACH shown in Fig. 4.3a and b are sourced from the same dataset as Abi Farraj et al.[39].

Quartz crystal microbalance with dissipation monitoring study

Quartz crystal microbalance with dissipation monitoring (QCM-D) was used to investigate the differences in interactions of the three coagulants with a model negatively-charged

contaminant surface in wastewater. In the field of water treatment, QCM-D has recently provided useful insights into the mechanisms of coagulation and flocculation observed during primary treatment stages[22,52,53]. As an aqueous solution is flown over the sensor, QCM-D can provide valuable quantitative and qualitative information of species deposition on the sensor surface and properties of the deposited film. Silica was selected as the sensor coating in these experiments as a representative negatively charged surface to enable us to better understand the nature of interaction between the coagulant with negatively-charged Si-based colloids, nanoplastics, and microfibers.

In QCM-D measurements, deposition on the crystal can be measured through monitoring the shifts of the crystal resonance frequency (Δf) allowing nanoscale mass to be detected[54,55]. Within the first 15 min of QCM-D measurements, alum shows minimal decrease in frequency shift (Fig. 4.4a). This result indicates the alum hydrolyzed products at pH 7 do not yield large deposition on the sensor surface suggesting weak interactions between alum species and negatively charged SiO_2 surface. At pH 7, alum hydrolyses mostly into amorphous $Al(OH)_3$,[44] thus any deposition on the surface is likely due to the interaction of these amorphous products. On the other hand, ACH hydrolysis species at pH 8.5 showed a large negative frequency shift reaching an average value of approximately -80 Hz before the 15 min mark. The ACH species therefore resulted in large deposition on the sensor surface, indicating significantly stronger interactions with the sensor surface compared to alum. Nuclear magnetic resonance (NMR) spectra measurements showed that this ACH coagulant contains roughly 88% of polynuclear Al_{30}.[45] The positively charged aluminum species are stable at wide ranges of pH[44], and therefore are expected to experience strong electrostatic interactions with the surface at pH 8.5. This result is in agreement with QCM-D measurements by Zhang al.[52] where Al_{30} deposition was mainly formed through particulate aluminum deposition resulting in a viscoelastic hydrated film. Similarly, Lapointe et al.[22] showed that alum species (containing $Al(OH)_3$),

resulted in the lowest deposition rate while ACH (containing Al_{30} species) resulted in greater deposition on weathered polystyrene surface. The addition of cationic pDADMAC with ACH resulted in the fastest deposition rate with a frequency shift rate of -18.8 ± 0.4 Hz/min compared to -10.9 ± 0.5 Hz/min and -0.269 ± 0.076 Hz/min for ACH and alum, respectively (Fig. 4.4a). The deposition rate of ACH was still found to be 100× larger than that of alum when the calculated slopes were normalized with the theoretical deposition rate of the respective coagulation species according to the Smoluchowski-Levich approximation for a parallel-plate flow chamber[56]. Moreover, ACH+pDADMAC was the only coagulant to reach full surface saturation within 15 min of measurement. This result shows that the addition of pDADMAC significantly strengthens interaction between the coagulant and the negatively charged SiO_2 surface.

The viscoelastic properties of the deposited layer can be further evaluated by plotting the change in dissipation (ΔD) versus the change in frequency shift (Δf)[57]. A flat ΔD-Δf slope indicates a rigid film with low energy dissipation per coupled-mass change, while a steep slope indicates a loosely bound film with high energy dissipation as the quantity of deposited material increases. The least steep ΔD-Δf slope (smallest slope magnitude) was measured for ACH+pDADMAC (Fig. 4.4b) with a value of -6.29 ± $0.38 \cdot 10^{-8}$ Hz^{-1} showing that ACH+pDADMAC forms a more rigid film than both ACH ($\Delta D_{(3)}$-$\Delta f_{(3)}$ slope of -1.78 ± $0.24 \cdot 10^{-7}$ Hz^{-1}) and alum ($\Delta D_{(3)}$-$\Delta f_{(3)}$ slope of -3.20 ± $0.61 \cdot 10^{-7}$ Hz^{-1}). Therefore, the film of ACH+pDADMAC can be considered to have minimal dissipative losses and thus forms the most rigid layer out of the three coagulants. This result shows that the addition of pDADMAC results in the fast formation of a rigid layer at the surface of the negatively charged model contaminant at pH 8.5. This quick adsorption can explain the small flocs produced when ACH+pDADMAC is used as a coagulant at pH values above 8. The cationic pDADMAC can rapidly saturate negatively charged contaminants and flocculant loops preventing the bridging

mechanism. It has previously been shown that strong electrostatic interactions between flocculants and cationic species result in smaller floc sizes[28]. It should be noted that the average value of $\Delta D_n/(-\Delta f_n/n)$ obtained for all coagulants is below the empirical stiff-viscoelastic film limit ($4 \cdot 10^{-7}$ Hz^{-1})[58] which implies that all the tested coagulants form a rigid film. In addition, frequency shifts at high overtones $\Delta f_{(n)}$ for all the tested coagulants are negative which serves as further evidence that all coagulants result in rigidly adsorbed films[59,60] (Fig. S4.7).

The ΔD–Δf plots for ACH and ACH+pDADMAC are linear throughout the measured frequency shifts which indicates that the conformation of both deposited layers did not change during deposition. On the other hand, the measurements of ΔD–Δf for alum reveal a nearly flat slope at the initial frequency shifts followed by an increase in the slope to reach an average of $-3.2 \pm 0.61 \cdot 10^{-7}$ Hz^{-1} (Fig. 4.4b). The increase in slope indicates that the deposited layer became more loosely bound as the deposited material increases. This increase in ΔD–Δf slope was also observed by Zhang et al.[52] for monomeric Al_0 species. Using the dissipation shift measurements, the ACH+pDADMAC deposited film was concluded to be rigid and uniform, while both ACH and alum resulted in less rigid films.

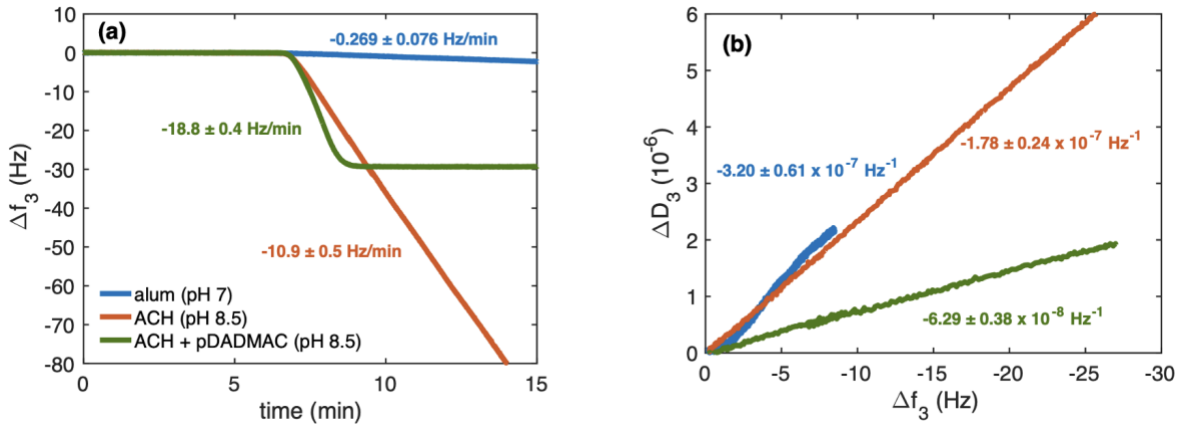

Figure 4.4. (a) Average frequency shift (Δf_3) versus time and (b) average change in dissipation (ΔD_3) versus frequency shift (Δf_3) for the deposition of alum (pH 7 ± 0.2), ACH (pH 8.5 ± 0.2), and ACH+pDADMAC (pH 8.5 ± 0.2) with a concentration of 5.45 mg Al/L on crystals with silica-coated surfaces. Each line shows the average of three distinct measurement and the

slopes are calculated based on the average slope of the three measurements with standard error shown.

Testing nanoplastic removal with alternative flocculants

Flocculant properties, including molecular weight and charge density, are known to affect the formed flocs in a physicochemical treatment process[61]. Jar tests with anionic flocculants resulted in significantly larger floc sizes compared to cationic flocculants ($p<0.005$ for aPAM1 and $p<10^{-7}$ for aPAM2; Fig. 4.5). Earlier studies have shown that electrostatic repulsion between anionic PAM and the negatively charged colloids in wastewater generally lead to the expansion of the polymer and consequently forms open-structure flocs that are larger than those produced by cationic flocculants[61]. A higher molecular weight of anionic polyacrylamide (aPAM2) also resulted in significantly larger average floc sizes ($p<0.05$). At higher molecular weight and low to moderate charge density, PAM acts by bridging mechanism, while charge neutralization is considered relatively insignificant[62]. Therefore, higher molecular weight polymers can improve the bridging flocculation resulting in larger floc sizes. The anionic polymer with larger floc sizes also resulted in a significantly greater nanoplastic removal at short settling time of 30 s ($p = 0.004$) as well as longer settling time of 3 min (although not statistically significant; $p = 0.065$) (Fig. 4.5). This finding reveals that floc size can play a critical role in removal of nanosized contaminants during the coagulation and flocculation process. The role of floc size in nanoplastic removal was also seen in a recent coagulation and flocculation study where screening was used for floc separation[63]. Using the smallest mesh size of 1000 μm, nanoplastic removal in jar tests performed with only alum and flocculant (mean floc size= 520 ± 50 μm; 82% nanoplastic removal) was significantly lower than jar tests performed with super-bridging fibers (mean floc size >3930 μm; 94% nanoplastic removal). This finding further confirms the critical role that floc size plays in improving nanoplastic removal during coagulation particularly through enhancing removal via sweep flocculation.

Cationic polyacrylamides, regardless of charge density, showed lower overall removal compared to both anionic polyacrylamides for samples taken after 30 s of settling. Cationic polyacrylamides do not result in strong bridging mechanisms since the electrostatic interaction between the flocculants and the colloids results in strong adsorption and consequently smaller floc sizes[28]. These smaller flocs require longer settling times which explains the lower nanoplastic removal seen after only 30 s of settling. As noted above, the larger floc sizes of aPAM2 resulted in a greater nanoplastic removal compared to aPAM1 after 3 min of settling. Even though cPAM1 and cPAM2 also had a smaller floc size distribution compared to aPAM2, the cationic flocculants no longer show a significant difference in nanoplastic removal compared to anionic flocculants at the longer settling time of 3 min ($p>0.05$). Given sufficiently long settling time, the cationic flocculants can compensate for the smaller flocs produced. It is likely that the improved attachment efficiency due to the enhanced destabilization of the negatively charged nanoplastics by the cationic flocculants can compensate for lower collision rates of the smaller flocs. Interestingly, increasing the charge density of the cationic flocculant from ~7% (cPAM1) to ~20% (cPAM2) did not result in a significant change in nanoplastic removal at either 30 s or 3 min settling times. This finding suggests that sufficient cationic sites were already provided by the cPAM with 7% charge density to allow nanoplastic aggregation.

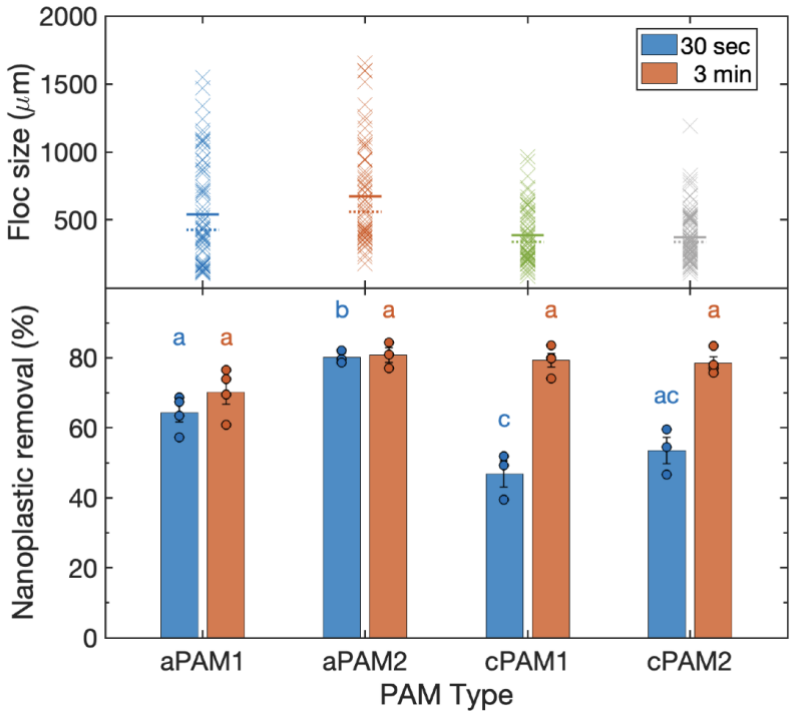

Figure 4.5. Floc size distribution of flocs formed with varying flocculant molecular weight and charge density. Solid line shows the mean size and the dashed line represents the median. Nanoplastic removal after 30 s of settling and 3 min of settling. 5.45 mg Al/L of coagulant; aPAM1, aPAM2, CPAM1 or CPAM2 as flocculant (0.4 mg PAM/L); 2 min of coagulation and 2 min of flocculation at 110 rpm with a final pH between 7 ± 0.2. Legend: aPAM1: very low anionic charge density, high molecular weight; aPAM2: very low anionic charge density, very high molecular weight; cPAM1: very low cationic charge density, high molecular weight; cPAM2: low cationic charge density, high molecular weight. Statistical significance is shown as $p<0.05$ (two sample *t*-test). The nanoplastic removal results presented above are sourced from the same dataset as Abi Farraj et al.[39].

4.4 Conclusion

In this study, the removal of nanoplastics and microfibers with conventional and alternative aluminum-based coagulants is investigated during physicochemical treatment. Using alum as a coagulant removed 97% of microfibers at an optimal pH of 7, however increasing the pH to 8.6 resulted in a significant decline of removal reaching 85%. Similarly, nanoplastic removal with alum after 30 s of settling decreases from 64% to approximately 0% removal when the pH is increased from 7 to 8.6. This is an important observation as several wastewater treatment plants globally operate at pH > 8 – systematically or occasionally. The addition of cationic species to the coagulant resulted in improved nanoplastic removal after settling (30 s): 10% for

alum alone, 52% for ACH, and 68% for ACH+pDADMAC (pH 7.5–8.5). Similarly, ACH resulted in a greater microfiber removal compared to alum (94% versus 87% average removal for pH>8, respectively). QCM-D results suggest that alum interacts with negatively charged colloids through amorphous $Al(OH)_3$ deposition. The dissipation shift measurements reveal that both ACH and alum formed less rigid films, while the addition of pDADMAC resulted in a highly rigid film deposited on the negatively charged surface. The behaviour of nanoplastic removal during physicochemical treatment was also revealed through this study. After 3 min of settling, there was no observed difference in nanoplastic removal with alum in alkaline conditions (pH > 8) which reveals that longer settling time can compensate for loss of cationic coagulant species when sweep flocculation dominates the coagulation process. Nanoplastic removal with different flocculants further highlights this result where increasing cationic charge density did not lead to significantly greater nanoplastic removal. This study improves our understanding of surface interactions of the coagulants with plastic surfaces in relevant environmental conditions. More importantly, this study offers municipalities new solutions in coagulation to better remove nanosized plastic pollution.

4.5 Acknowledgments

The authors acknowledge the Canada Research Chairs Program, the Natural Sciences and Engineering Research Council of Canada (NSERC), the Killam Research Fellowship, and the Canada Foundation for Innovation. M.L. was supported by a Mitacs Accelerate Fellowship and Kemira Water Solutions Canada Inc, and R.S.K. was supported by NSERC and FRQNT Postdoctoral Fellowships.

4.6 References

1 Anderson, J. C., Park, B. J. & Palace, V. P. Microplastics in aquatic environments: implications for Canadian ecosystems. *Environmental Pollution* **218**, 269-280 (2016).

2 Jung, J.-W. *et al.* Ecological risk assessment of microplastics in coastal, shelf, and deep sea waters with a consideration of environmentally relevant size and shape. *Environmental Pollution* **270**, 116217 (2021).
3 Lima, A. R. A., Barletta, M. & Costa, M. F. Seasonal distribution and interactions between plankton and microplastics in a tropical estuary. *Estuarine, Coastal and Shelf Science* **165**, 213-225 (2015).
4 Free, C. M. *et al.* High-levels of microplastic pollution in a large, remote, mountain lake. *Marine pollution bulletin* **85**, 156-163 (2014).
5 Luo, W. *et al.* Comparison of microplastic pollution in different water bodies from urban creeks to coastal waters. *Environmental Pollution* **246**, 174-182 (2019). https://doi.org:https://doi.org/10.1016/j.envpol.2018.11.081
6 Bertoldi, C. *et al.* First evidence of microplastic contamination in the freshwater of Lake Guaíba, Porto Alegre, Brazil. *Science of The Total Environment* **759**, 143503 (2021).
7 Mintenig, S. M., Löder, M. G. J., Primpke, S. & Gerdts, G. Low numbers of microplastics detected in drinking water from ground water sources. *Science of the total environment* **648**, 631-635 (2019).
8 Sun, J., Dai, X., Wang, Q., van Loosdrecht, M. C. M. & Ni, B.-J. Microplastics in wastewater treatment plants: Detection, occurrence and removal. *Water research* **152**, 21-37 (2019).
9 Andrady, A. L. Microplastics in the marine environment. *Marine pollution bulletin* **62**, 1596-1605 (2011).
10 Browne, M. A. *et al.* Accumulation of microplastic on shorelines woldwide: sources and sinks. *Environmental science & technology* **45**, 9175-9179 (2011).
11 Horton, A. A., Walton, A., Spurgeon, D. J., Lahive, E. & Svendsen, C. Microplastics in freshwater and terrestrial environments: evaluating the current understanding to identify the knowledge gaps and future research priorities. *Science of the total environment* **586**, 127-141 (2017).
12 Pedrotti, M. L. *et al.* Pollution by anthropogenic microfibers in North-West Mediterranean Sea and efficiency of microfiber removal by a wastewater treatment plant. *Science of the Total Environment* **758**, 144195 (2021).
13 Pikuda, O., Lapointe, M., Alimi, O. S., Berk, D. & Tufenkji, N. Fate of microfibres from single-use face masks: Release to the environment and removal during wastewater treatment. *Journal of Hazardous Materials* **438**, 129408 (2022).
14 Boucher, J. & Friot, D. *Primary microplastics in the oceans: a global evaluation of sources*. Vol. 10 (IUCN, 2017).
15 Alimi, O. S. *et al.* Weathering pathways and protocols for environmentally relevant microplastics and nanoplastics: What are we missing? *Journal of Hazardous Materials*, 126955 (2021).
16 Jahnke, A. *et al.* Reducing uncertainty and confronting ignorance about the possible impacts of weathering plastic in the marine environment. *Environmental Science & Technology Letters* **4**, 85-90 (2017).
17 Yang, T., Luo, J. & Nowack, B. Characterization of Nanoplastics, Fibrils, and Microplastics Released during Washing and Abrasion of Polyester Textiles. *Environmental Science & Technology* **55**, 15873-15881 (2021). https://doi.org:10.1021/acs.est.1c04826
18 Gigault, J., Pedrono, B., Maxit, B. & Ter Halle, A. Marine plastic litter: the unanalyzed nano-fraction. *Environmental science: nano* **3**, 346-350 (2016).
19 Ekvall, M. T. *et al.* Nanoplastics formed during the mechanical breakdown of daily-use polystyrene products. *Nanoscale Advances* **1**, 1055-1061 (2019).

20 Hernandez, L. M., Yousefi, N. & Tufenkji, N. Are There Nanoplastics in Your Personal Care Products? *Environmental Science & Technology Letters* **4**, 280-285 (2017). https://doi.org:10.1021/acs.estlett.7b00187
21 Pal, P. in *Industrial Water Treatment Process Technology* (ed Parimal Pal) 243-511 (Butterworth-Heinemann, 2017).
22 Lapointe, M., Farner, J. M., Hernandez, L. M. & Tufenkji, N. Understanding and improving microplastic removal during water treatment: impact of coagulation and flocculation. *Environmental science & technology* **54**, 8719-8727 (2020).
23 Li, J., Dagnew, M. & Ray, M. B. Effect of coagulation on microfibers in laundry wastewater. *Environmental Research* **212**, 113401 (2022).
24 Gong, Y., Bai, Y., Zhao, D. & Wang, Q. Aggregation of carboxyl-modified polystyrene nanoplastics in water with aluminum chloride: Structural characterization and theoretical calculation. *Water Research*, 117884 (2021).
25 Zhang, Y. *et al.* Improving nanoplastic removal by coagulation: Impact mechanism of particle size and water chemical conditions. *Journal of Hazardous Materials*, 127962 (2021). https://doi.org:https://doi.org/10.1016/j.jhazmat.2021.127962
26 Ministère de l'Environnement et de la Lutte contre les changements climatiques. Règlement sur les ouvrages municipaux d'assainissement des eaux usées chapitre Q-2, r. 34.1. (MELCC, 2013).
27 Ma, B. *et al.* Characteristics of microplastic removal via coagulation and ultrafiltration during drinking water treatment. *Chemical Engineering Journal* **359**, 159-167 (2019).
28 Lapointe, M. & Barbeau, B. Understanding the roles and characterizing the intrinsic properties of synthetic vs. natural polymers to improve clarification through interparticle Bridging: A review. *Separation and Purification Technology* **231**, 115893 (2020).
29 Organisation for Economic Cooperation & Development. *Test No. 303: Simulation Test-Aerobic Sewage Treatment--A: Activated Sludge Units; B: Biofilms*. (OECD Publishing, 2001).
30 Lapointe, M. & Barbeau, B. Evaluation of activated starch as an alternative to polyacrylamide polymers for drinking water flocculation. *Journal of Water Supply: Research and Technology-Aqua* **64**, 333-343 (2014). https://doi.org:10.2166/aqua.2014.114
31 Lapointe, M. & Barbeau, B. Dual starch–polyacrylamide polymer system for improved flocculation. *Water Research* **124**, 202-209 (2017). https://doi.org:https://doi.org/10.1016/j.watres.2017.07.044
32 Lapointe, M., Kurusu, R. S., Hernandez, L. M. & Tufenkji, N. Removal of Classical and Emerging Contaminants in Water Treatment Using Super-Bridging Fiber-Based Materials. *ACS ES&T Water* **3**, 377-386 (2023).
33 Kurusu, R. S., Lapointe, M. & Tufenkji, N. Sustainable iron-grafted cellulose fibers enable coagulant recycling and improve contaminant removal in water treatment. *Chemical Engineering Journal* **430**, 132927 (2022).
34 Johnson, C. P., Li, X. & Logan, B. E. Settling velocities of fractal aggregates. *Environmental science & technology* **30**, 1911-1918 (1996).
35 Akanbi, M. O., Hernandez, L. M., Mobarok, M. H., Veinot, J. G. C. & Tufenkji, N. QCM-D and NanoTweezer measurements to characterize the effect of soil cellulase on the deposition of PEG-coated TiO 2 nanoparticles in model subsurface environments. *Environmental Science: Nano* **5**, 2172-2183 (2018).
36 Crittenden, J. C., Trussell, R. R., Hand, D. W., Howe, K. J. & Tchobanoglous, G. *MWH's water treatment: principles and design*. (John Wiley & Sons, 2012).

37 Hayden, P. L. & Rubin, A. J. Systematic Investigation of the Hydrolysis and Precipitation of Aluminum (III). Aqueous Environmental Chemistry of Metal. *AJ Rubin. Ann Arbor*, 318-379 (1974).
38 Yang, Z. L., Gao, B. Y., Yue, Q. Y. & Wang, Y. Effect of pH on the coagulation performance of Al-based coagulants and residual aluminum speciation during the treatment of humic acid–kaolin synthetic water. *Journal of Hazardous Materials* **178**, 596-603 (2010).
39 Abi Farraj, S. *et al.* Targeting nanoplastic and microplastic removal in treated wastewater with a simple indicator. *Nature Water (accepted)* **X**, XXX-XXX (2023).
40 Shahi, N. K., Maeng, M., Kim, D. & Dockko, S. Removal behavior of microplastics using alum coagulant and its enhancement using polyamine-coated sand. *Process Safety and Environmental Protection* **141**, 9-17 (2020).
41 Liu, W. *et al.* A review of the removal of microplastics in global wastewater treatment plants: Characteristics and mechanisms. *Environment International* **146**, 106277 (2021). https://doi.org:https://doi.org/10.1016/j.envint.2020.106277
42 Ter Halle, A. & Ghiglione, J. F. Nanoplastics: A Complex, Polluting Terra Incognita. *Environmental Science & Technology* **55**, 14466-14469 (2021).
43 Gigault, J. *et al.* Nanoplastics are neither microplastics nor engineered nanoparticles. *Nature nanotechnology* **16**, 501-507 (2021).
44 Sahu, O. P. & Chaudhari, P. K. Review on Chemical treatment of Industrial Waste Water. *Journal of Applied Sciences and Environmental Management* **17** (2013). https://doi.org:10.4314/jasem.v17i2.8
45 Lapointe, M., Papineau, I., Peldszus, S., Peleato, N. & Barbeau, B. Identifying the best coagulant for simultaneous water treatment objectives: Interactions of mononuclear and polynuclear aluminum species with different natural organic matter fractions. *Journal of Water Process Engineering* **40**, 101829 (2021). https://doi.org:https://doi.org/10.1016/j.jwpe.2020.101829
46 Chen, Z. *et al.* Evaluation of Al30 polynuclear species in polyaluminum solutions as coagulant for water treatment. *Chemosphere* **64**, 912-918 (2006). https://doi.org:https://doi.org/10.1016/j.chemosphere.2006.01.038
47 Aguilar, M. I., Saez, J., Llorens, M., Soler, A. & Ortuno, J. F. Nutrient removal and sludge production in the coagulation–flocculation process. *Water research* **36**, 2910-2919 (2002).
48 Georgantas, D. A. & Grigoropoulou, H. P. Orthophosphate and metaphosphate ion removal from aqueous solution using alum and aluminum hydroxide. *Journal of Colloid and Interface Science* **315**, 70-79 (2007).
49 Wu, B., Wan, J., Zhang, Y., Pan, B. & Lo, I. M. C. Selective phosphate removal from water and wastewater using sorption: process fundamentals and removal mechanisms. *Environmental science & technology* **54**, 50-66 (2019).
50 Mancuso, C., Jamison, M., Zaporski, J. & Yang, Z. Effects of coagulant morphology and chemical properties on soluble reactive phosphate removal in corn ethanol wastewater. *Water Environment Research* **93**, 2589-2597 (2021).
51 Zhang, T., Ding, L., Ren, H., Guo, Z. & Tan, J. Thermodynamic modeling of ferric phosphate precipitation for phosphorus removal and recovery from wastewater. *Journal of Hazardous materials* **176**, 444-450 (2010).
52 Zhang, Y. *et al.* Deposition behavior of residual aluminum in drinking water distribution system: Effect of aluminum speciation. *Journal of Environmental Sciences* **42**, 142-151 (2016).

53 Wu, W., Ma, J., Xu, J. & Wang, Z. Mechanistic insights into chemical conditioning by polyacrylamide with different charge densities and its impacts on sludge dewaterability. *Chemical Engineering Journal* **410**, 128425 (2021).
54 Chen, Q., Xu, S., Liu, Q., Masliyah, J. & Xu, Z. QCM-D study of nanoparticle interactions. *Advances in colloid and interface science* **233**, 94-114 (2016).
55 Liu, G. & Zhang, G. in *QCM-D Studies on Polymer Behavior at Interfaces* 1-8 (Springer, 2013).
56 Quevedo, I. R. & Tufenkji, N. Influence of solution chemistry on the deposition and detachment kinetics of a CdTe quantum dot examined using a quartz crystal microbalance. *Environmental science & technology* **43**, 3176-3182 (2009).
57 Li, W., Liu, D., Wu, J., Kim, C. & Fortner, J. D. Aqueous aggregation and surface deposition processes of engineered superparamagnetic iron oxide nanoparticles for environmental applications. *Environmental science & technology* **48**, 11892-11900 (2014).
58 Reviakine, I., Johannsmann, D. & Richter, R. P. (ACS Publications, 2011).
59 Olsson, A. L. J., van der Mei, H. C., Johannsmann, D., Busscher, H. J. & Sharma, P. K. Probing colloid–substratum contact stiffness by acoustic sensing in a liquid phase. *Analytical chemistry* **84**, 4504-4512 (2012).
60 Quevedo, I. R., Olsson, A. L. J., Clark, R. J., Veinot, J. G. C. & Tufenkji, N. Interpreting deposition behavior of polydisperse surface-modified nanoparticles using QCM-D and sand-packed columns. *Environmental Engineering Science* **31**, 326-337 (2014).
61 Nasser, M. S. & James, A. E. The effect of polyacrylamide charge density and molecular weight on the flocculation and sedimentation behaviour of kaolinite suspensions. *Separation and purification technology* **52**, 241-252 (2006).
62 Patience, M., Addai-Menash, J. & Ralston, J. Investigation of the effect of polymer type on flocculation, rheology and dewatering behaviour of kaolinite dispersions. *International Journal of Mineral Processing* **71**, 247-268 (2003).
63 Lapointe, M., Jahandideh, H., Farner, J. M. & Tufenkji, N. Super-bridging fibrous materials for water treatment. *npj Clean Water* **5**, 11 (2022). https://doi.org:10.1038/s41545-022-00155-4

4.7 Supplementary Information

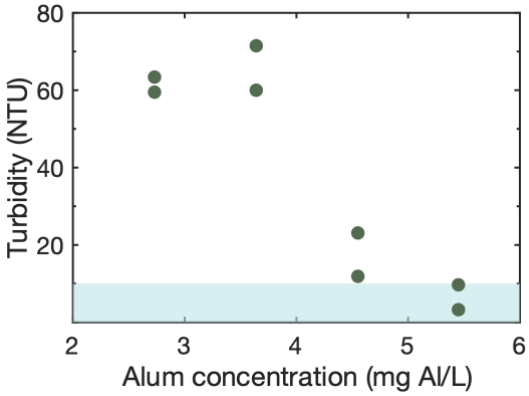

Figure S4.1. Turbidity of treated water as a function of alum concentration for samples collected after 3 min of settling. Conditions: alum used as a coagulant; APAM1 was used as a flocculant (0.4 mg/L); 110 rpm mixing speed; 2 min coagulation; 2 min flocculation. Each data

point represents a single jar test. The blue box shows the maximum acceptable turbidity of 10.0 NTU.

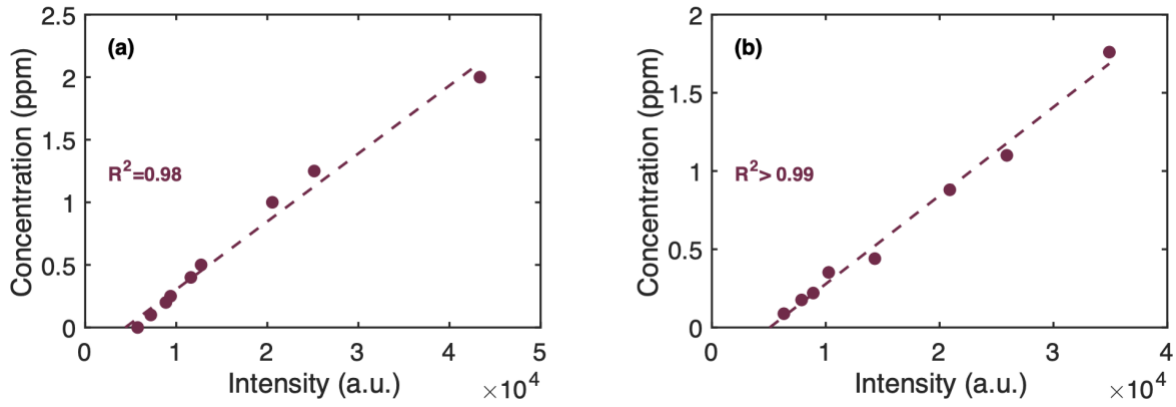

Figure S4.2. Calibration curve of (a) pristine and (b) aged 28 nm polystyrene nanoplastics in synthetic wastewater.

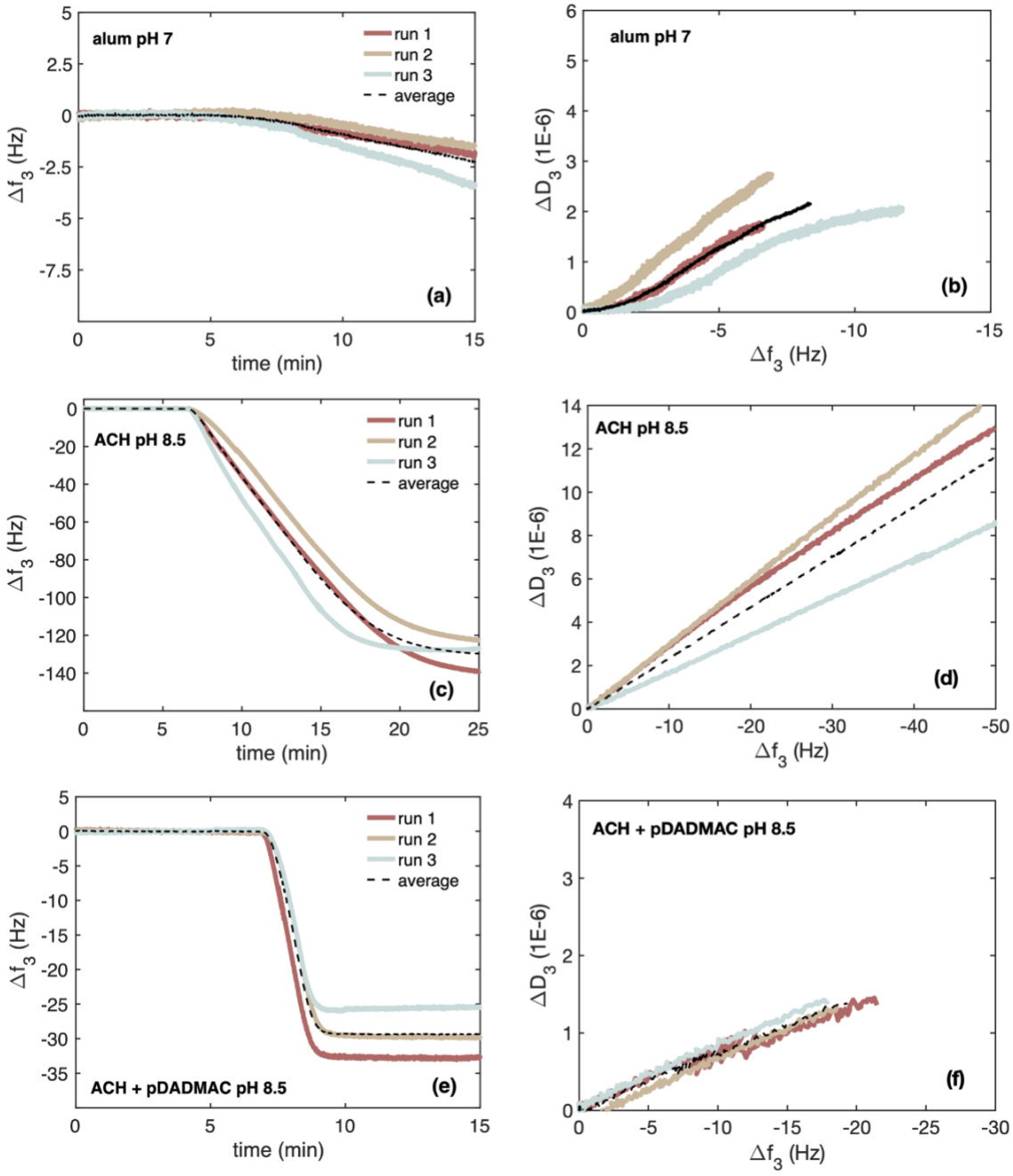

Figure S4.3. Quartz crystal microbalance with dissipation measurements showing three measurements of frequency shift (Δf3) versus time (a,c,e) and change in dissipation (ΔD3) versus frequency shift (Δf3) (b.d.f) for the deposition of alum (pH 7± 0.2), ACH (pH 8.5± 0.2), and ACH+pDADMAC (pH 8.5± 0.2) respectively. A concentration of 5.45 mg Al/L of coagulant was used in each measurement on crystals with silica-coated surfaces. The average of the three measurements is shown in the dashed black line.

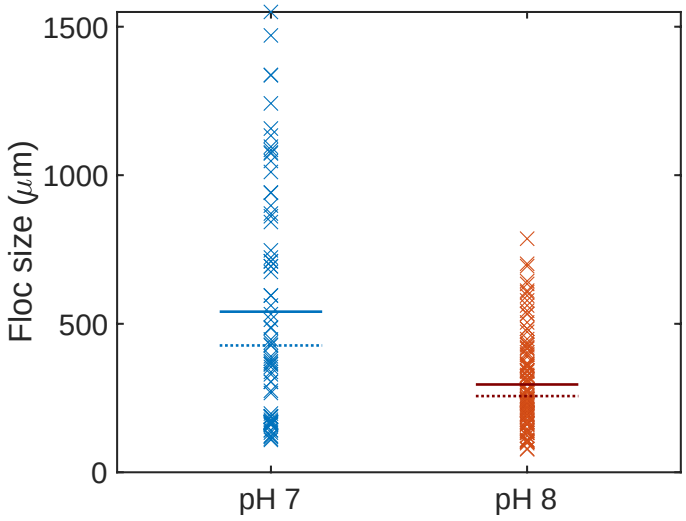

Figure S4.4. Floc size distribution of flocs formed at pH 7± 0.2 and 8± 0.2. Solid line shows the mean size and the dashed line represents the median. Conditions: 5.45 mg Al/L of alum; aPAM1, aPAM2, CPAM1 or CPAM2 as flocculant (0.4 mg PAM/L) as; 2 min of coagulation and 2 min of flocculation at 110 rpm with a final pH between 7 ± 0.2.

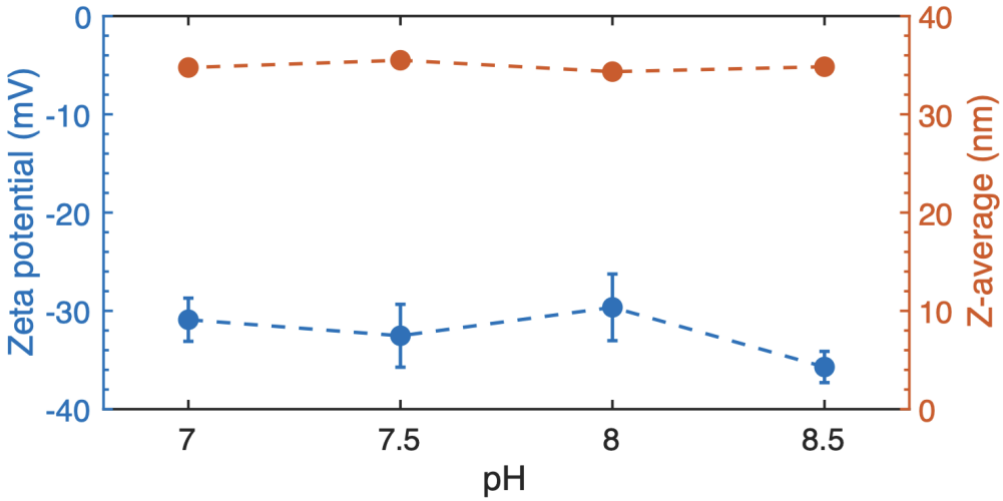

Figure S4.5. Zeta potential and DLS (z-average) measurements of polystyrene nanoplastics (28 nm; carboxylate-functionalized) as a function of pH. Conditions: 0.66 mmol/L ionic strength (NaCl); temperature of 25°C; 100 ppm concentration of nanoplastics. Each data point represents the average of three measurements and error bar shows standard deviation.

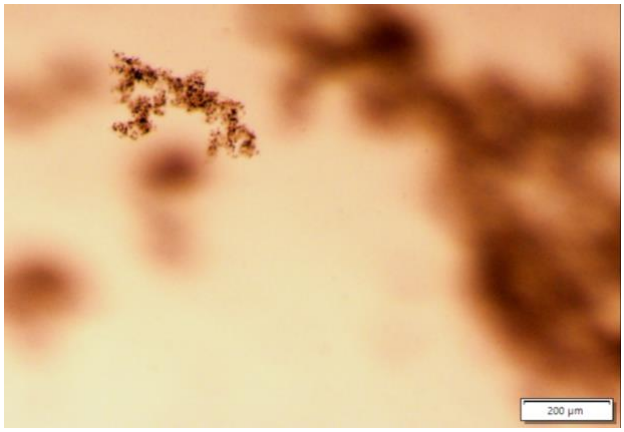

Figure S4.6. Microscope image showing floating flocs formed following 2 min of coagulation with ACH+pDADMAC (5.45 mg Al/L) and 2 min of flocculation with aPAM1 (0.4 mg/L) at a speed of 110 rpm.

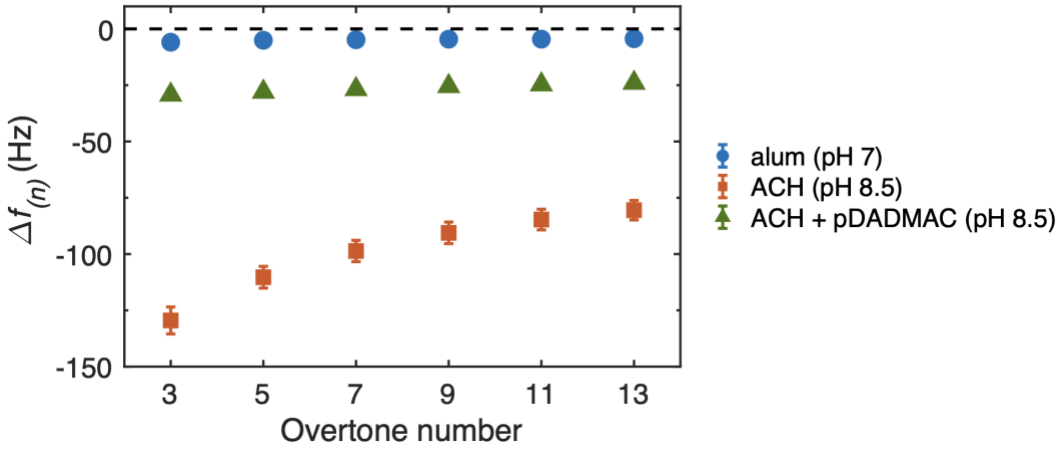

Figure S4.7. Normalized frequency shifts ($\Delta f_{(n)}$) for deposition from QCM-D experiments conducted with alum, ACH and ACH+pDADMAC at different overtones (n= 3, 5, 7, 9, 11, 13).

Chapter 5: Conclusions and future work

5.1 Conclusions

In this study, flocculation kinetic modeling and jar test experiments were conducted to monitor and improve the removal of micro- and nanoplastic contaminants during primary wastewater treatment systems. Mechanisms of plastic contaminant removal during the process were investigated and alternative coagulants were tested to improve plastic removal.

In Chapter 3, a correlation equation between total suspended solids (TSS) and nanoplastic removal was derived based on principles of orthokinetic flocculation. More than 180 experimental jar tests were performed to rigorously validate the proposed correlation tested using 41 various water conditions and 8 different water types including two different municipal wastewater influents, activated sludge-treated water, aerated lagoon water samples and 4 synthetic wastewater matrices. The results of this work show a strong agreement between experimental data and our derived equation with an R^2=0.92 (p=3•10^{-66}) using a large dataset with 117 individual nanoplastic removal measurements. This result is significant as it shows the applicability of our derived correlation regardless of variation in wastewater pH, inorganic type, TSS concentration, separation method, flocculant, and coagulant type as well as nanoplastic type, size, surface charge, aging condition, and initial concentration in wastewater. Based on current TSS regulations in North America, the established model estimates a nanoplastic removal between 39-69% for an influent wastewater with an initial TSS between 60 and 200 mg/L. Microspheres, microfibers, and microfragments were also tested in jar test experiments using synthetic and municipal wastewater samples. The results reveal a microplastic removal greater than 80% for microfibers and microspheres for high TSS removal (>70%). At lower TSS removal, a linear correlation can be used to fit microfiber and TSS removal as well as microsphere and TSS removal (R^2=0.87 and 0.77 respectively). Although

the orthokinetic model was not applicable for microplastic contaminants, the linear correlation revealed the possibility of implementing TSS as an indicator for microplastics as well.

In Chapter 4, alum's ability to remove nanoplastics and microfibers was assessed at varying pH conditions (7.0 to 8.6) in synthetic wastewater. This study confirmed that alum's ability to remove plastic contaminants is impacted in alkaline conditions resulting in significantly lower micro- and nanoplastic removal. To address this challenge, two alternative coagulants—aluminum chlorohydrate (ACH) and aluminum chlorohydrate+polyDADMAC (ACH+pDADMAC)— were investigated. Our work revealed that replacing alum with ACH coagulant improved polyester microfibers removal from 85 ± 3% to 95 ± 1% (pH 8.6). Similarly, replacing alum with ACH+pDADMAC coagulant improved polystyrene nanoplastics removal from 5.8% ± 5% to 71 ± 5% (pH 8.2). Quartz crystal microbalance with dissipation (QCM-D) measurements showed that ACH and ACH+pDADMAC resulted in a faster and more rigid layer deposition compared to alum on the surface of the negatively charged model sensor. Therefore, the alternative coagulants were seen to improve the removal of nanoplastic and microplastic contaminants in conditions that were challenging for alum and offers municipalities alternative chemicals for water treatment.

5.2 Perspectives and future work

Coagulation, flocculation, and settling systems were seen to be effective at removing microplastic and nanoplastic contaminants when operated at optimal treatment conditions. This work revealed that researchers need to consider challenging treatment conditions, including higher pH and presence of organic materials in synthetic wastewater recipes. The interactions between plastic contaminants and colloids present in wastewater also proved to be important during jar test experiments. Future work should consider adding stabilizing agents (e.g., soap, cooking oil/fat) to samples spiked with microfibers and nanoplastics, since microfibers likely

originate from washing machine discharges that contain synthetic textile material.[1-3] In addition, oxidative cleaning products can be included in weathering procedures to oxidize the microplastic and nanoplastic surface and mimic surface modifications that occur after the addition of stain removing products on textiles. The effect of wastewater conditions and plastic aging histories must be taken into account to evaluate the performance of coagulants in removing contaminants of interest. Alternative coagulants and chemicals can therefore emerge as viable options for municipalities to remove contaminants under these challenging conditions.

In addition to conducting jar test experiments in more realistic water types and plastic profiles, researchers need to work towards validating the removal obtained for microplastics and nanoplastics in wastewater effluent streams. Although recent analytical techniques have emerged as tools for nanoplastic detection in wastewater, several economic and technical limitations prevent the accurate measurements of these contaminants.[20] Similarly, the complexity of the wastewater matrix inhibits the continuous monitoring of microplastic contaminants in effluent streams.[18,19] These challenges prevent wastewater treatment operators from validating the plastic contaminant removal and inhibits regulatory bodies from developing viable regulations to control the release of microplastics and nanoplastics.

Through this work, we identified a correlation between nanoplastic removal and TSS removal. This correlation was validated using various water types (synthetic wastewater, municipal effluent, activated sludge-treated water, aerated lagoon water) and plastic conditions (different sizes, surface charge, concentrations, aging process). The high correlation achieved with our model offers the potential for regulating nanoplastic contaminant release from conventional wastewater treatment plants through an inexpensive indicator. Additional experiments are required to validate the model for alternative plastic types (in addition to polystyrene and polyvinyl chloride) as well as nanoplastic fragments. Similarly, the TSS relationship with

microplastic removal will need to be tested with different types of microplastics in addition to polyethylene and polyester. Once validated, this low-cost tool could be the first step to democratize contaminant monitoring globally for industrialized and developing countries in line with the latest recommendations by the UN report on SDG indicator 6.3.1.

References

1 Andrady, A. L. Microplastics in the marine environment. *Marine Pollution Bulletin* **62**, 1596-1605 (2011). https://doi.org:https://doi.org/10.1016/j.marpolbul.2011.05.030

2 Browne, M. A. *et al.* Accumulation of microplastic on shorelines woldwide: sources and sinks. *Environmental Science & Technology* **45**, 9175-9179 (2011). https://doi.org:https://doi.org/10.1021/es201811s

3 Horton, A. A., Walton, A., Spurgeon, D. J., Lahive, E. & Svendsen, C. Microplastics in freshwater and terrestrial environments: Evaluating the current understanding to identify the knowledge gaps and future research priorities. *Science of the Total Environment* **586**, 127-141 (2017). https://doi.org:https://doi.org/10.1016/j.scitotenv.2017.01.190

4 Pedrotti, M. L. *et al.* Pollution by anthropogenic microfibers in North-West Mediterranean Sea and efficiency of microfiber removal by a wastewater treatment plant. *Science of the Total Environment* **758**, 144195 (2021).

5 Alimi, O. S. *et al.* Weathering pathways and protocols for environmentally relevant microplastics and nanoplastics: What are we missing? *Journal of Hazardous Materials*, 126955 (2021). https://doi.org:https://doi.org/10.1016/j.jhazmat.2021.126955

6 Jahnke, A. *et al.* Reducing uncertainty and confronting ignorance about the possible impacts of weathering plastic in the marine environment. *Environmental Science & Technology Letters* **4**, 85-90 (2017). https://doi.org:https://doi.org/10.1021/acs.estlett.7b00008

7 Pal, P. in *Industrial Water Treatment Process Technology* (ed Parimal Pal) Ch. 6, 243-511 (Butterworth-Heinemann, 2017).

8 Boucher, J. & Friot, D. *Primary microplastics in the oceans: a global evaluation of sources*. Vol. 10 (IUCN, 2017).

9 Alimi, O. S., Farner Budarz, J., Hernandez, L. M. & Tufenkji, N. Microplastics and Nanoplastics in Aquatic Environments: Aggregation, Deposition, and Enhanced Contaminant Transport. *Environmental Science & Technology* **52**, 1704-1724 (2018). https://doi.org:https://doi.org/10.1021/acs.est.7b05559

10 Shah, A. A., Hasan, F., Hameed, A. & Ahmed, S. Biological degradation of plastics: A comprehensive review. *Biotechnology Advances* **26**, 246-265 (2008). https://doi.org:https://doi.org/10.1016/j.biotechadv.2007.12.005

11 Cai, L., Wang, J., Peng, J., Wu, Z. & Tan, X. Observation of the degradation of three types of plastic pellets exposed to UV irradiation in three different environments. *Science of The Total Environment* **628-629**, 740-747 (2018). https://doi.org:https://doi.org/10.1016/j.scitotenv.2018.02.079

12 Enfrin, M., Dumée, L. F. & Lee, J. Nano/microplastics in water and wastewater treatment processes–origin, impact and potential solutions. *Water Research* **161**, 621-638 (2019). https://doi.org:https://doi.org/10.1016/j.watres.2019.06.049

13 Ma, B. *et al.* Removal characteristics of microplastics by Fe-based coagulants during drinking water treatment. *Journal of Environmental Sciences* **78**, 267-275 (2019). https://doi.org:https://doi.org/10.1016/j.jes.2018.10.006

14 Ma, B. *et al.* Characteristics of microplastic removal via coagulation and ultrafiltration during drinking water treatment. *Chemical Engineering Journal* **359**, 159-167 (2019). https://doi.org:https://doi.org/10.1016/j.cej.2018.11.155

15 Shahi, N. K., Maeng, M., Kim, D. & Dockko, S. Removal behavior of microplastics using alum coagulant and its enhancement using polyamine-coated sand. *Process Safety and Environmental Protection* **141**, 9-17 (2020). https://doi.org:https://doi.org/10.1016/j.psep.2020.05.020

16 Murray, A. & Örmeci, B. Removal Effectiveness of Nanoplastics (<400 nm) with Separation Processes Used for Water and Wastewater Treatment. *Water* **12** (2020). https://doi.org:10.3390/w12030635

17 Zhang, Y. *et al.* Improving nanoplastic removal by coagulation: Impact mechanism of particle size and water chemical conditions. *Journal of Hazardous Materials*, 127962 (2021). https://doi.org:https://doi.org/10.1016/j.jhazmat.2021.127962

18 Nguyen, B. *et al.* Separation and analysis of microplastics and nanoplastics in complex environmental samples. *Accounts of Chemical Research* **52**, 858-866 (2019). https://doi.org:https://doi.org/10.1021/acs.accounts.8b00602

19 Silva, A. B. *et al.* Microplastics in the environment: Challenges in analytical chemistry-A review. *Analytica Chimica Acta* **1017**, 1-19 (2018). https://doi.org:https://doi.org/10.1016/j.aca.2018.02.043

20 Cai, H. *et al.* Analysis of environmental nanoplastics: Progress and challenges. *Chemical Engineering Journal* **410**, 128208 (2021). https://doi.org:https://doi.org/10.1016/j.cej.2020.128208

21 Gewert, B., Plassmann, M. M. & MacLeod, M. Pathways for degradation of plastic polymers floating in the marine environment. *Environmental Science: Processes & Impacts* **17**, 1513-1521 (2015). https://doi.org:https://doi.org/10.1039/C5EM00207A

22 Niaounakis, M. *Management of marine plastic debris*. (William Andrew, 2017).

23 Andrady, A. L. The plastic in microplastics: A review. *Marine Pollution Bulletin* **119**, 12-22 (2017). https://doi.org:https://doi.org/10.1016/j.marpolbul.2017.01.082

24 Wagner, S. & Reemtsma, T. Things we know and don't know about nanoplastic in the environment. *Nature Nanotechnology* **14**, 300-301 (2019). https://doi.org:https://doi.org/10.1038/s41565-019-0424-z

25 Hernandez, L. M. *et al.* Plastic teabags release billions of microparticles and nanoparticles into tea. *Environmental Science & Technology* **53**, 12300-12310 (2019). https://doi.org:https://doi.org/10.1021/acs.est.9b02540

26 Yang, T., Luo, J. & Nowack, B. Characterization of Nanoplastics, Fibrils, and Microplastics Released during Washing and Abrasion of Polyester Textiles. *Environmental Science & Technology* **55**, 15873-15881 (2021). https://doi.org:10.1021/acs.est.1c04826

27 Hernandez, L. M., Yousefi, N. & Tufenkji, N. Are there nanoplastics in your personal care products? *Environmental Science & Technology Letters* **4**, 280-285 (2017). https://doi.org:https://doi.org/10.1021/acs.estlett.7b00187

28 Lambert, S. & Wagner, M. Characterisation of nanoplastics during the degradation of polystyrene. *Chemosphere* **145**, 265-268 (2016). https://doi.org:https://doi.org/10.1016/j.chemosphere.2015.11.078

29 Lv, X. *et al.* Microplastics in a municipal wastewater treatment plant: Fate, dynamic distribution, removal efficiencies, and control strategies. *Journal of Cleaner Production* **225**, 579-586 (2019). https://doi.org:https://doi.org/10.1016/j.jclepro.2019.03.321

30 Mintenig, S. M., Löder, M. G. J., Primpke, S. & Gerdts, G. Low numbers of microplastics detected in drinking water from ground water sources. *Science of the Total Environment* **648**, 631-635 (2019). https://doi.org:https://doi.org/10.1016/j.scitotenv.2018.08.178

31 Vardar, S., Onay, T. T., Demirel, B. & Kideys, A. E. Evaluation of microplastics removal efficiency at a wastewater treatment plant discharging to the Sea of Marmara. *Environmental Pollution* **289**, 117862 (2021). https://doi.org:https://doi.org/10.1016/j.envpol.2021.117862

32 Mason, S. A. *et al.* Microplastic pollution is widely detected in US municipal wastewater treatment plant effluent. *Environmental Pollution* **218**, 1045-1054 (2016). https://doi.org:https://doi.org/10.1016/j.envpol.2016.08.056

33 Gies, E. A. *et al.* Retention of microplastics in a major secondary wastewater treatment plant in Vancouver, Canada. *Marine Pollution Bulletin* **133**, 553-561 (2018). https://doi.org:https://doi.org/10.1016/j.marpolbul.2018.06.006

34 Prajapati, S., Beal, M., Maley, J. & Brinkmann, M. Qualitative and quantitative analysis of microplastics and microfiber contamination in effluents of the City of Saskatoon wastewater treatment plant. *Environmental Science and Pollution Research*, 1-9 (2021). https://doi.org:https://doi.org/10.1007/s11356-021-12898-7

35 Chae, Y. & An, Y.-J. Effects of micro-and nanoplastics on aquatic ecosystems: Current research trends and perspectives. *Marine pollution bulletin* **124**, 624-632 (2017). https://doi.org:https://doi.org/10.1016/j.marpolbul.2017.01.070

36 Enfrin, M. *et al.* Release of hazardous nanoplastic contaminants due to microplastics fragmentation under shear stress forces. *Journal of Hazardous Materials* **384**, 121393 (2020). https://doi.org:https://doi.org/10.1016/j.jhazmat.2019.121393

37 Liu, W. *et al.* A review of the removal of microplastics in global wastewater treatment plants: Characteristics and mechanisms. *Environment International* **146**, 106277 (2021). https://doi.org:https://doi.org/10.1016/j.envint.2020.106277

38 Enfrin, M., Lee, J., Le-Clech, P. & Dumée, L. F. Kinetic and mechanistic aspects of ultrafiltration membrane fouling by nano- and microplastics. *Journal of Membrane Science* **601** (2020). https://doi.org:https://doi.org/10.1016/j.memsci.2020.117890

39 Pal, P. & Kumar, R. Treatment of Coke Wastewater: A Critical Review for Developing Sustainable Management Strategies. *Separation & Purification Reviews* **43**, 89-123 (2014). https://doi.org:https://doi.org/10.1080/15422119.2012.717161

40 Sahu, O. P. & Chaudhari, P. K. Review on Chemical treatment of Industrial Waste Water. *Journal of Applied Sciences and Environmental Management* **17** (2013). https://doi.org:https://doi.org/10.4314/jasem.v17i2.8

41 Bache D. H., Johnson C., Papavasilopoulos E. & F.J., M. Sweep coagulation: structures, mechanisms, and practice. *Journal of Water SRT-AQUA* **48**, 201-210 (1999).

42 Aguilar, M. I., Saez, J., Llorens, M., Soler, A. & Ortuno, J. F. Nutrient removal and sludge production in the coagulation–flocculation process. *Water research* **36**, 2910-2919 (2002).

43 Bache, D. H. & Gregory, R. *Flocs in water treatment*. (IWA publishing, 2007).

44 Zhang, Y. *et al.* Enhanced removal of polyethylene terephthalate microplastics through polyaluminum chloride coagulation with three typical coagulant aids. *Science of the Total Environment* **800**, 149589 (2021). https://doi.org:https://doi.org/10.1016/j.scitotenv.2021.149589

45 Lapointe, M., Farner, J. M., Hernandez, L. M. & Tufenkji, N. Understanding and improving microplastic removal during water treatment: Impact of coagulation and flocculation. *Environmental Science & Technology* **54**, 8719-8727 (2020). https://doi.org:https://doi.org/10.1021/acs.est.0c00712

46 Desjardins, C., Koudjonou, B. & Desjardins, R. Laboratory study of ballasted flocculation. *Water Research* **36**, 744-754 (2002). https://doi.org:https://doi.org/10.1016/S0043-1354(01)00256-1

47 Zhou, G. *et al.* Removal of polystyrene and polyethylene microplastics using PAC and FeCl3 coagulation: Performance and mechanism. *Science of The Total Environment* **752**, 141837 (2021). https://doi.org:https://doi.org/10.1016/j.scitotenv.2020.141837

48 Chen, Z. *et al.* Evaluation of Al30 polynuclear species in polyaluminum solutions as coagulant for water treatment. *Chemosphere* **64**, 912-918 (2006). https://doi.org:https://doi.org/10.1016/j.chemosphere.2006.01.038

49 Gong, Y., Bai, Y., Zhao, D. & Wang, Q. Aggregation of carboxyl-modified polystyrene nanoplastics in water with aluminum chloride: Structural characterization and theoretical calculation. *Water Research*, 117884 (2021). https://doi.org:https://doi.org/10.1016/j.watres.2021.117884

50 Zhang, Y., Diehl, A., Lewandowski, A., Gopalakrishnan, K. & Baker, T. Removal efficiency of micro-and nanoplastics (180 nm–125 μm) during drinking water treatment. *Science of The Total Environment* **720**, 137383 (2020). https://doi.org:https://doi.org/10.1016/j.scitotenv.2020.137383